UNIVERSITY OF SOUTHAMPTON

Faculty of PHYSICAL AND APPLIED SCIENCE

SCHOOL OF ELECTRONICS AND COMPUTER SCIENCE

Electrodynamic Droplet Actuation for Lab on a Chip System

by

Sara Aghdaei

Thesis for the degree of Doctor of Philosophy

February 2011

UNIVERSITY OF SOUTHAMPTON

Abstract

FACULTY OF PHYSICAL AND APPLIED SCIENCE
SCHOOL OF ELECTRONICS AND COMPUTER SCIENCE

Doctor of Philosophy

Electrodynamic Droplet Actuation for Lab on a Chip System

by Sara Aghdaei

This work presents the development of electrowetting on dielectric and liquid dielectrophoresis as a platform for chemistry, biochemistry and biophysics. These techniques, typically performed on a single planar surface offer flexibility for interfacing with liquid handling instruments and performing biological experimentation with easy access for visualisation. Technology for manipulating and mixing small volumes of liquid in microfluidic devices is also crucially important in chemical and biological protocols and Lab on a Chip devices and systems. The electrodynamic techniques developed here have rapid droplet translation speeds and bring small droplets into contact where inertial dynamics achieve rapid mixing upon coalescence.

In this work materials and fabrication processes for both electrowetting on dielectric and liquid dielectrophoresis technology have been developed and refined. The frequency, voltage and contact angle dependent behaviour of both techniques have been measured using two parallel coplanar electrodes. The frequency dependencies of electrowetting and dielectrophoretic liquid actuation indicate that these effects are high and low-frequency limits, respectively, of a complex set of forces. An electrowetting based particle mixer was developed using a custom made electrode array and the effect of varying voltage and frequency on droplet mixing was examined, with the highest efficiency mixing being achieved at 1 kHz and 110 V in about 0.55 seconds.

A composite electrodynamic technique was used to develop a reliable method for the formation of artificial lipid bilayers within microfluidic platforms for measuring basic biophysical aspects of cell membranes, for biosensing and drug discovery applications. Formation of artificial bilayer lipid membranes (BLMs) was demonstrated at the interface of aqueous droplets submerged in an organic solvent-lipid phase using the liquid dielectrophoresis methods developed in this project to control the droplet movement and bring multiple droplets into contact without coalescence. This technique provides a flexible, reconfigurable method for forming, disassembling and reforming BLMs within a microsystem under simple electronic control. BLM formation was shown to be extremely reliable and the BLMs formed were stable (with lifetimes of up to 20 hours) and therefore were suitable for electrophysiological analysis. This system was used to assess whether nanoparticle-membrane contact leads to perturbation of the membrane structure. The conductance of artificial membranes was monitored following exposure to nanoparticles using this droplet BLM system. It was demonstrated that the presence of nanoparticles with diameters between 50 and 500 nm can damage protein-free membranes at particle concentrations in the femtomolar range. The effects of particle size and surface chemistry were also investigated. It was shown that a large number of nanoparticles can translocate across a membrane, even when the surface coverage is relatively low, indicating that nanoparticles can exhibit significant cytotoxic effects.

Table of Contents

Declaration of Authorship

I, Sara Aghdaei declare that the thesis entitled

Electrodynamic Droplet Actuation for Lab on a Chip System

and the work presented in it are my own. I confirm that:

- this work was done wholly or mainly while in candidature for a research degree at this University;
- where any part of this thesis has previously been submitted for a degree or any other qualification at this University or any other institution, this has been clearly stated;
- where I have consulted the published work of others, this is always clearly attributed;
- where I have quoted from the work of others, the source is always given. With the exception of such quotations, this thesis is entirely my own work;
- I have acknowledged all main sources of help;
- where the thesis is based on work done by myself jointly with others, I have made clear exactly what was done by others and what I have contributed myself;
- parts of this work have been published as:

1. Sara Aghdaei, Mairi E. Sandison, Michele Zagnoni, Nicolas G. Green and Hywel Morgan, "Formation of artificial lipid bilayers using droplet dielectrophoresis", Lab on chip,vol.8, pp 1617-1620,2008.

2. Sara Aghdaei, Nicolas G Green, Thomas B Jones, Hywel Morgan, "Droplet mixer based on electrowetting", Electrostatic 2007, Journal of Physics: Conference Series voll.142, pp. 12071, 2008.

3. S. Aghdaei, T. Heslington, N. Rogers, H. Morgan and M.R.R. de Planque, "Assessment of nanoparticle cytotoxicity with on-chip suspended bilayers", Proceedings of the 14th International Conference on Miniaturized Systems for Chemistry and Life Sciences (MicroTAS 2010), pp. 298-300.

Signed:

Date:

Nomenclature

a	Radius
C	Capacitance
$C_{D.L}$	Double layer capacitance
C_d	Dielectric capacitance
C_w	Capacitance of water droplet
D	Plate spacing
ε_0	Permittivity of free space
ε_1	Relative permittivity of the liquid
ε_d	Dielectric constant of insulator
ε_m	permittivity of the suspending medium
ε^*	Complex permittivity
ε^*_m	Complex permittivity of the suspending medium
ε^*_p	Complex permittivity of the particle
E	Electric field
η	Dimensionless electrowetting number
θ	Contact angle
f_e	Electrical force
f_{CM}	Clausius-Mossotti factor
f	Frequency
f_c	Critical frequency
F_e	Electrostatic force
F_{DEP}	Dielectrophoretic force
G_w	Conductance of water
γ_i	Interfacial energy

γ_{sv}	Solid-vapour interfacial energy
γ_{sl}	Solid-liquid interfacial energy
γ_{lv}	Liquid-vapour interfacial energy
h	Height
h_{cap}	Capillary height of rise
i , j	Imaginary vectors
λ	Lagrangian variable
t	Thickness
v	Vapour
V	Voltage
V'	Volume
Δp	Pressure
ρ_{sl}	Surface charge density
ρ	Density of dipoles in liquid
ρ_m	Mass density
σ	Conductivity
ω	Angular frequency
W'	Co-energy function
w	Width of electrode

Acknowledgments

This project was particularly interesting for me and I have enjoyed the challenges of both the theory and laboratory work. It is difficult to thank sufficiently all the people who have been with me throughout this time for help they have all given me.

First of all, I would like to express my sincere gratitude to Professor Hywel Morgan, for introducing mo to this fascinating area of science and all his support, enthusiasm and encouragement throughout the duration of this project.

Special thanks go to Dr. Nicolas G. Green, for all his valuable discussions, support and sharing his insight in microfluidics. I would also like to thank Dr. Mairi Sandison, Dr. Michele Zagnoni and Dr. Maurits R.R. de Planque for all their valuable advice with my project.

I especially appreciate Dave Sager for all his support and advice through this journey. I would like to acknowledge all the members of the Morgan's Group, both past and present, who have helped me over the years. It has been a pleasure to work with you all.

I am deeply grateful to colleagues in Nano group, in particular Mehdi Banakar, Hossein Nili, Stuart Boden and Ibrahim Sari for their friendly discussion about work and life in general. Thanks for being such great friends.

Last, but not least, I would like to thank my family, especially Mum and Dad for encouraging my education in both arts and sciences, for their unconditional love, support and encouragement to pursue my interests, even when the interests went beyond boundaries of language, field and geography.

1 Introduction

1.1 Method of droplet actuation

There has been growing interest in the past two decades in microsystems that accommodate multiple biological and chemical reactions. Such systems commonly referred to as "Lab-on-a-chip" (LOAC), integrate multiple functional units such as separation, sorting and characterisation systems onto one device. The device should be capable of controllably handling volumes of fluid as small as a fraction of a picolitre. Manipulation and mixing of small volumes of liquid in microfluidic devices has an important potential in chemical and biological protocols and micro total analysis systems [1-3].

Microfluidic systems can be classified into either continuous-flow systems or droplet-based systems. Continuous-flow systems are suitable for certain applications like chemical separation and simple biochemical applications but are not adequate in applications where a high degree of flexibility or complicated fluid manipulation is required. Discrete manipulation of droplets offers flexible and scalable architectures which are fault tolerant and dynamically reconfigurable enabling the displacement, formation, division and mixture of micrometer scale droplets of liquids. In this system droplet actuation can be achieved by using methods such as thermocapillary [4], electrochemical [5], dielectrophoresis [6] and electrowetting on dielectric [7].

Thermocapillary pumping (TCP) has been used to move discrete nanolitre and picolitre sized drops of solution with speeds up to 20 mm/min [4]. In this method the droplet is placed within a microfabricated flow channel etched into a glass substrate. The droplet is heated between 10°C and 70°C at one end to create a surface tension difference between the two ends of the droplet. The difference in surface tension causes a capillary pressure difference between the ends of the drop resulting in droplet motion. Electrochemical positioning of fluids on submillimetre scales has been described by Gallardo [5]. Surfactant species generated at one electrode and consumed at another were used to manipulate the magnitude and direction of gradients in surface tension and guide liquids through simple fluidic networks. Gradients in concentration of molecules can lead to changes in surface tension and can be used to produce fluid motion. These gradients were produced by using electrode surfaces to consume surface-active species. The voltages required to produce the reactions are small, typically less than 1 V.

Aqueous and organic solutions were tested along with solid particles. The liquids can be positioned on unconfined surfaces without the need for channels to guide the liquid [5]. Electrochemical actuation can be used on a planar surface; however it can only be used with certain chemicals due to interaction with solutions being tested. For the case of thermocapillary pumping, the solutions may need to be heated up to 70°C, making it also unsuitable for use in some chemical reactions.

Electrowetting on dielectric (EWOD) and dielectrophoresis (DEP) are two common electrical methods employed for the manipulation of small volumes of liquid. When a non-uniform electric field is applied to the fluid, it can be used to generate droplet movement. Dielectrophoresis (DEP) defines the motion of polarisable particles in non uniform alternating electric fields. The cause of this motion is the polarisation induced by the electric field at the particle interface with the surrounding medium. The particle moves towards regions of low or high electric field strength [6] depending on the relative polarisability of the particle and its suspending medium, defined through the Claussius- Mossotti factor. Electrowetting is defined as the change in solid electrolyte contact angle (wetting) due to an applied potential difference between the solid and the electrolyte. The use of microfabricated electrode array structures has enabled the application of EWOD for dispensing, moving and combining droplets under dynamic electrical fields (kHz-MHz), thereby avoiding the need for pumps, valves and channels and allowing for electronic control of fluid manipulation.

1.1.1 Electrophoresis (EP)

An electric field exerts electrostatic Coulomb force on a charged particle. The particle will move either in the direction of the field or against it, depending on the polarity of the charge on the particle. This effect is known as electrophoresis (EP). The displacement of charged particles within an electric field (EP) was first observed by the Russian physicist F. F. Reus in 1809 [8]. The main application of electrophoresis in the laboratory is the separation of macromolecules such as DNA and proteins under the influence of the applied electric field [9]. The separation technique is based on the mobility of ions in an electric field (positively- charged ions migrate towards a negative electrode and negatively-charged ions migrate toward a positive electrode).

1.1.2 Dielectrophoresis (DEP)

The diagrams in Figure 1-1 show the polarisation of a particle in a non-uniform electric field. By examining the density of electric field lines it is evident that the field strength on one side of the particle is greater than the other. This leads to an imbalance of forces on the induced dipole, resulting in a net force on the particle. This effect is called dielectrophoresis.

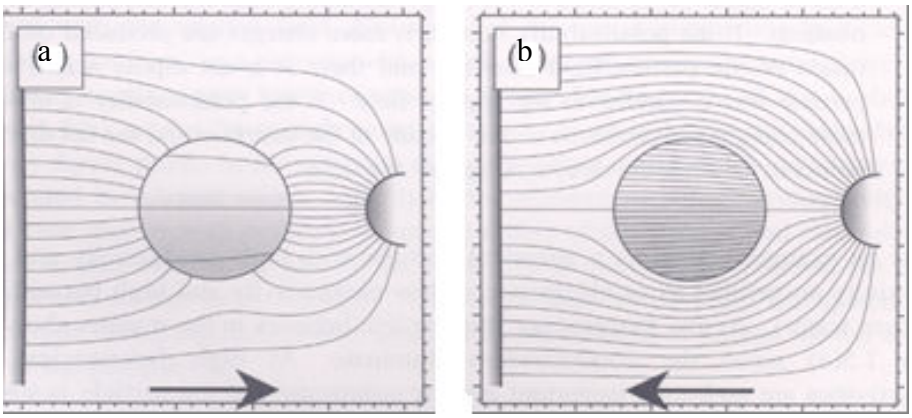

Figure 1-1 a) Positive dielectrophoresis. b) Negative dielectrophoresis. Taken from [9].

Electrophoresis (EP) and dielectrophoresis (DEP) are the major electric forces acting on small particles suspended in a fluid. EP happens when a uniform field is exerted on a particle with a net charge whereas DEP occurs when the non-uniform field is applied [9]. Dielectrophoresis, first explained by Pohl [6], is a remarkable technique compared to the other particle manipulation techniques because it is suitable for manipulating particles that do not have a net intrinsic charge. The polarisation relationship between the particle and the medium define the direction of the induced dipole and DEP force. The DEP force is given by [9]:

$$F_{DEP} = \pi \varepsilon_m a^3 \,\mathrm{Re}(f_{CM}) \nabla \left|E\right|^2 \qquad (1\text{-}1)$$

where, a is the particle radius, ε_m represents the permittivity of the suspending medium, $\mathrm{Re}(f_{CM})$ is the real part of the Clausius-Mossotti factor and E is the peak value of the electric field vector. The Clausius-Mossotti factor is a complex number which describes

the polarisability of the particle and medium. For a homogeneous sphere the CM factor is given by:

$$f_{CM} = \left[\frac{\varepsilon_p^* - \varepsilon_m^*}{\varepsilon_p^* + 2\varepsilon_m^*} \right] \quad (1\text{-}2)$$

where, ε_p^* is the complex permittivity of the particle, and ε_m^* is the complex permittivity of the medium. The complex permittivity of the particle is given by electrical property of a material:

$$\varepsilon^* = \varepsilon - j\frac{\sigma}{\omega} \quad (1\text{-}3)$$

here, ε is the permittivity of the material, ω is the angular frequency of the electric field, σ is the conductivity and j is the imaginary vector.

The direction of the DEP force depends on the relationship between the polarisability of the particle and polarisability of the medium, determined by the real part of the Clausius-Mossotti factor. The particle moves towards high electric field strength regions when the polarisability of the particle is greater than the suspending medium. This phenomenon is called positive DEP. The particles are repelled from the high field strength region, when the polarisability of the particle is less than the suspending medium, this is called negative DEP [9]. Huang and Pethig [10] demonstrated positive and negative DEP using polynomial electrodes for separating yeast cells. Figure 1-2a shows the positive dielectrophoretic effect induced by applying a voltage of 10 V peak to peak at 10 kHz. The conductivity of the medium was 3.61 µS/cm. In this case yeast cells are collected at the electrode edges. In Figure 1-2b the same voltage and frequency has been applied but the conductivity of the medium was 170 µS/cm. In this case negative DEP is induced and yeast cells are repelled from the electrodes and are collected in the centre of the device.

Figure 1-2 a) Positive dielectrophoretic of yeast cells suspended in 280 mM mannitol of conductivity 3.61 μS/cm. b) Negative dielectrophoretic of the same yeast cells suspended in a 280 mM mannitol + 1.4 mM KCI solution of conductivity 170 μS/cm and subjected to a 10 kHz, 10 V peak-peak signal applied to the electrodes. Taken from [10].

1.1.3 Electrowetting-on-dielectric (EWOD)

In 1875 Gabriel Lippmann [11] found that the capillary depression of mercury in contact with electrolyte solutions could be varied by applying a voltage between the mercury and electrolyte. The term electrowetting was first introduced in the paper by G. Beni et al. in 1980, where they reported the application of the phenomenon in a new type of display device [12]. As they reported, the main problem was electrolytic decomposition of water in direct contact with the electrode upon applying voltages beyond a few hundred millivolts. In early 1990s Berge [13] introduced the idea of using a thin insulating layer to separate the conductive liquid from the metallic electrode and eliminate the problem of electrolysis. Nowadays, this concept is known as electrowetting on dielectric (EWOD).

1.1.3.1 Electrowetting definition

Electrowetting is a phenomenon where an electric field can modify the wetting behavior of a droplet in contact with an isolated electrode. If an electric field is applied between a droplet and a horizontal insulated electrode, a surface energy gradient is created that can be used to manipulate the droplet. Electrowetting is also defined as a change in solid-electrolyte contact angle (wetting) due to an applied potential difference between the

solid and the electrolyte [13, 14]. A schematic diagram of this phenomenon is shown in Figure 1-3.

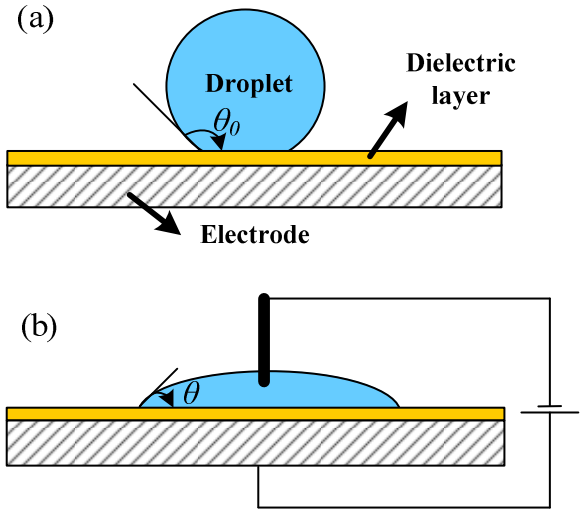

Figure 1-3 Electrowetting effect: a) Sessile droplet placed on a dielectric coated electrode. b) Wetting behaviour of a droplet after applying voltage is changed.

An aqueous droplet initially forms a contact angle θ_0 with a hydrophobic insulator surface as shown in Figure 1-3a. Applying a voltage between a droplet and a counter electrode below the insulator reduces the solid-liquid interfacial energy, leading to a reduction in contact angle and improved wetting of the surface by the droplet (Figure 1-3b).

1.1.3.2 Electrowetting application

1.1.3.2.1 Display technology

Electrowetting technology can be used to create displays [15] that are extremely bright and energy efficient. These two critical features are used for portable devices like mobile phones, MP3 players and cameras. The concept of using an electrowetting-based reflective display is relatively simple, as shown in Figure 1-4. A droplet of oil containing dissolved dye is confined to a square pixel. The bottom of the pixel is coated by a hydrophobic insulator (0.8 μm Teflon AF). The oil is like a continuous layer wetting at zero voltage. Incoming light is absorbed by the dye. Upon applying a voltage, all the oil moves to one side of the pixel that can be predefined by a passive chemical wettability pattern. Therefore the dye covers up only a small part of the pixel in the activated area. This causes an increase in the reflectivity from 2.5% at zero voltage to

35% at the absorption wavelength of the dye at 20 V. The switching speed of the display depends on the pixel size, thickness and the viscosity of the oil film as well as on other geometric parameters [16].

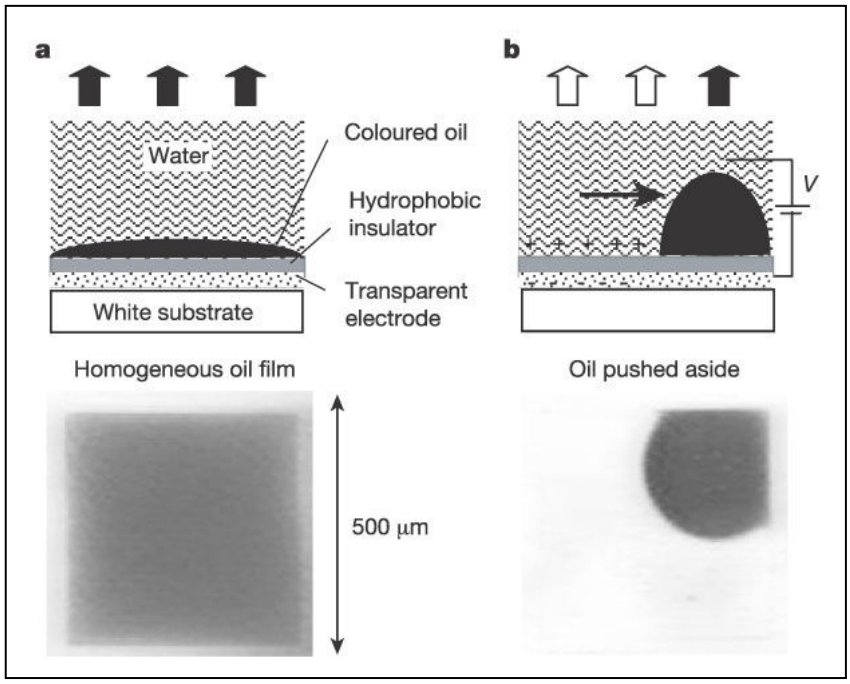

Figure 1-4 Display principle: a) No voltage applied; therefore a coloured homogeneous oil film is present. b) DC voltage applied, causing the oil film to contract. The top row is diagrams and the bottom row is photographs. The photographs show typical oil motion obtained with an homogeneous pixel electrode. Taken from [16].

By splitting each pixel into three subpixels and arranging two oil layers with different dyes in combination with a colour filter on top of each other, Feenstra and Hayes were also able to generate arbitrary colours [15]. The reflectivity of these colour displays was reported to be four times stronger than that of liquid crystal displays [16].

1.1.3.2.2 Variable focal lens

Philips Research has demonstrated a variable-focus lens system called FluidFocus [17]. This system does not use any mechanical moving parts and in principle works like the human eye. The focal length of this fluid lens is adjusted by changing its shape. The FluidFocus lens system consists of two non-mixing fluids, an electrically conducting

aqueous solution and an electrically non-conducting oil. These two immiscible fluids are held in a short tube with visible end caps. The internal surfaces of the tube wall and one of its end caps are coated with a hydrophobic coating. By applying an electric field the hydrophobic layer becomes less hydrophobic and surface tension changes (Figure 1-5). This result in the variation of the radius of curvature of the meniscus between the two fluids and therefore the focal length of the lens will be changed. By increasing the voltage the surface of the initially convex lens can be completely flat or even concave. As a result it is possible to implement a lens with smooth transition from convergent to divergent and back again.

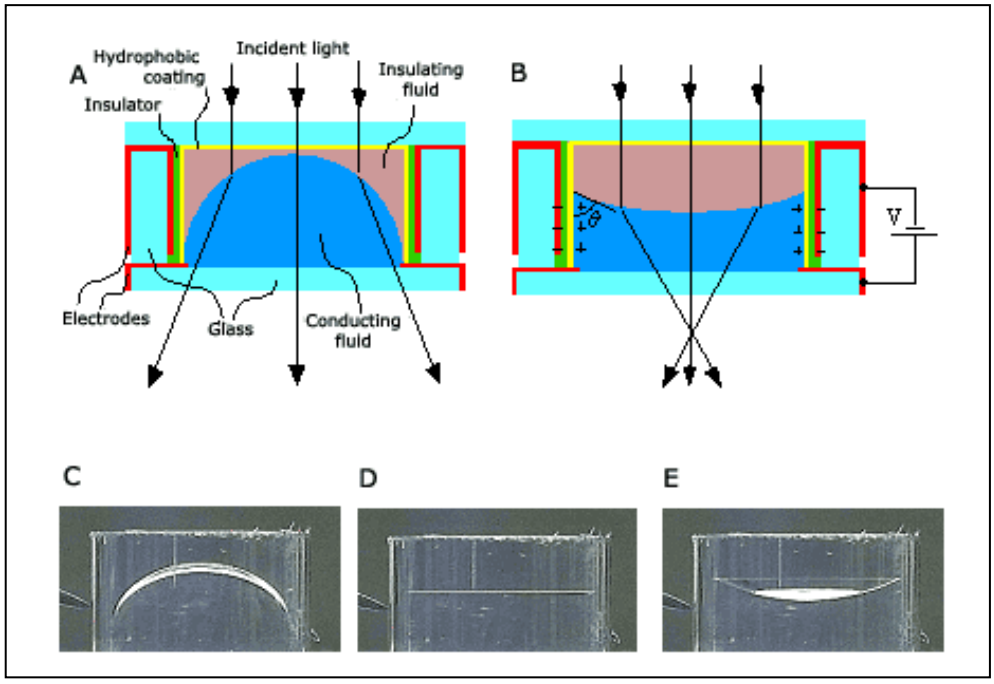

Figure 1-5 A) Schematic of the FluidFocus lens. B) By applying voltage, charges collect in the glass wall electrode and opposite charges collect near the solid/liquid interface in the conducting liquid. (C-E) Formation of 6 mm diameter lens with different convexities using different applied voltages. Taken from [17].

1.1.3.2.3 Lab on a chip

The Lab on a chip is a term used to describe devices that integrate multiple laboratory functions on a single chip. Chip substrates are usually made of glass, polymers or silicon and measure from square millimetres to a few square centimetres. The principal idea of lab on a chip as applied to electrowetting is to provide a substrate with a series

of individually addressable electrodes that make droplet movements possible. Small droplets can be extracted from larger reservoir droplets and transported to specifically designed locations [18]. In practice, the following thoughts should be considered [19]: 1) Electrowetting requires electrical contact to the liquid. 2) In order to allow for reliable droplet actuation, droplet edges must overlap at least two adjacent electrodes. Figure 1-6 shows the four main application of electrowetting: dispensing, moving, splitting and mixing of droplets which have been performed in the lab on a chip system.

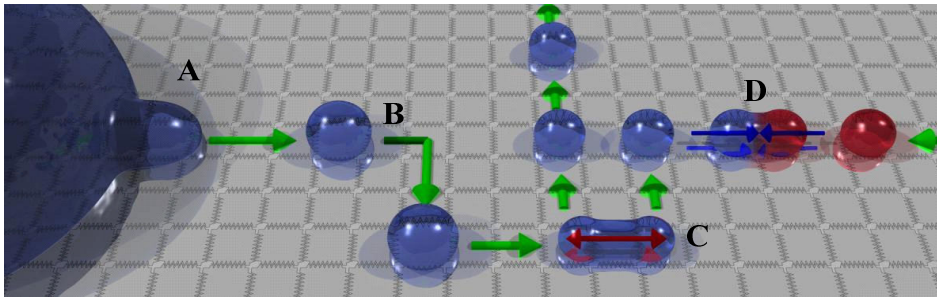

Figure 1-6 Four main operations of a microfluidic electrowetting array in droplet A) generation B) moving C) splitting and D) mixing. Taken from [20].

1.2 Summary and Conclusions

In this chapter, the idea of manipulating fluids as droplets, as opposed to continuous-flow manipulation, was presented. The advantages of, and the challenges facing this method were mentioned and different mechanisms of droplet actuation were presented and discussed. Specifically, the remarkable features of dielectrophoresis (DEP) as a non-invasive technique that can be made compatible with different settings were mentioned. Electrowetting was defined and examples of its application in areas other than lab-on-a-chip, which is the focus of this work, were presented.

From what was presented in this chapter it may be concluded that electrowetting, achieved through any of the several techniques, can enable droplet actuation in flexible, scalable and dynamically configurable structures and thus allow several applications in lab-on-a-chip as well as other areas such as displays and focal lenses.

2 Theory of electrowetting

2.1 Basics of wetting

The contact between a fluid and a surface is known as wetting. If a liquid has a high surface tension a droplet will form whereas a liquid with low surface tension will be flattened over a larger area [21]. Wetting of different fluids is shown in Figure 2-1:

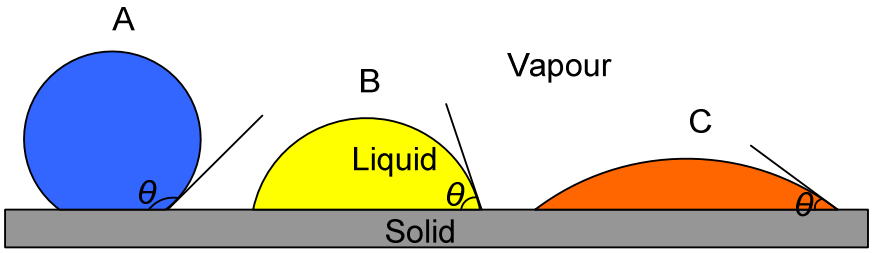

Figure 2-1 Different wetting behaviour of a liquid droplet. The contact angle is closely associated to the liquid-gas interfacial tension; therefore the shape of the liquid-gas interface plays a key role in determining the droplet wetting behaviour. A is a droplet with very high surface tension, while C is a droplet with a low surface tension and more wetting action.

In the above figure droplet A has a high contact angle whereas droplet C has a small contact angle. In the absence of external electric fields, the behavior of the droplet is determined by its surface tension alone. A droplet's free energy F (which is a function of the droplet shape) is obtain from a weighted sum of the areas A_i of the interfaces between three phases; the solid substrate (s), the liquid droplet (l) and the ambient phase, which may be assumed as a vapour (v) for simplicity [19] .

$$F = \sum_i A_i \gamma_i - \lambda \mathrm{V}' \qquad (2\text{-}1)$$

where, γ_i is the interfacial energy (solid-vapour γ_{sv}, solid-liquid γ_{sl} and liquid-vapour γ_{lv}), λ is a Lagrangian variable and equal to the pressure drop Δp across the liquid vapour interface, and V' is the volume of the droplet.

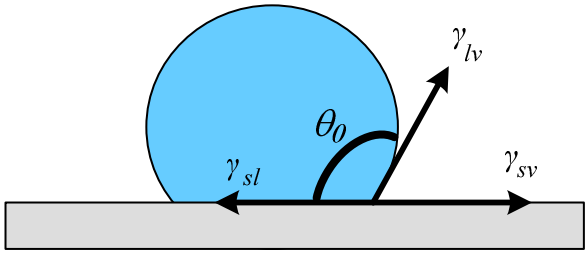

Figure 2-2 Overview of three phase interfacial energy: The contact angle, θ_0, is the angle formed by a liquid at the three phase contact line and it depends on the interfacial tensions between the solid-vapour γ_{sv}, solid-liquid γ_{sl} and liquid-vapour γ_{lv}.

Any equilibrium liquid morphology is satisfied by two essential conditions which are required to minimize the free energy given by equation (2-1) [22, 23]. First is the Laplace equation and the second condition is presented by Young's equation which relates Young's equilibrium contact angle θ_0 to the interfacial energies. This equation is driven by balancing the horizontal component of the forces acting on the three-phase contact line (Figure 2-2):

$$\gamma_{sl} - \gamma_{sv} + \gamma_{lv} \cos\theta_0 = 0 \qquad (2\text{-}2)$$

Young's equilibrium contact angle is then derived as follows:

$$\cos\theta_0 = \frac{\gamma_{sv} - \gamma_{sl}}{\gamma_{lv}} \qquad (2\text{-}3)$$

2.2 The Double Layer

An electrical double layer is a structure formed on a surface when it is placed into a liquid such as water. The local field that surrounds an ion in solution draws water molecules towards it due to their permanent dipole. This creates a cloud of water molecules around each ion [9]. The two layers of the double layer are referred to as the the Stern layer and the diffuse layer as shown in Figure 2-3. Generally, a surface carries a net charge which is due to the dissociation of the chemical group on the surface or by adsorption of ions or molecules from the solution onto the surface.

In the case of electrodes, movement of charge carriers through the circuit and a corresponding charge imbalance on the surface of the electrodes is due to applied

voltage. This electrostatic surface attracts ions of opposite charge (counterions) and repels ion with like charge (co-ions) if immersed in an electrolyte. The region of liquid near to the interface, referred to as the diffuse region, has a higher density of counterions and a lower density of co-ions than the bulk. There is also a layer of tightly associated counterions, referred to as the Stern layer, between the surface and the diffuse layer. The total capacitance of the double layer is the series sum of the Stern layer and diffuse layer capacitance. Since the diffuse layer capacitance depends on the Debye length, the capacitance of the Stern layer is most influential at high ion concentrations [9].

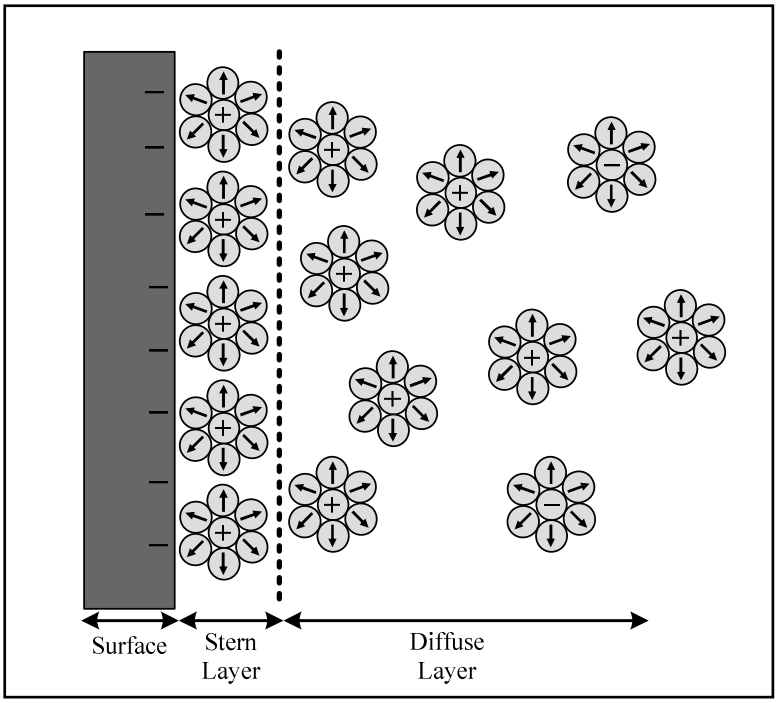

Figure 2-3 In aqueous solutions, counterions are drawn towards a charged surface. An imbalance of ion concentration forms the Stern layer and the diffuse layer around the surface. The ⊖⊕ symbols represent the ions, and ⓓ is the water molecule with the arrow indicating the dipole moment. Adapted from [9].

2.3 Electrowetting: basic equation and contact angle

Lippmann's original experiments were based on direct metal-electrolyte interface [11]. Several tenths of a volt without any current flowing were applied between the metal

(mercury) and the electrolyte. Upon applying an incremental voltage dV, an electric double layer is created at the solid–liquid interface. This double layer is made up of charges on the metal surface and a cloud of oppositely charged counter-ions on the liquid side of the interface. Since the accumulation is a spontaneous process, it leads to a reduction in the (effective) interfacial tension γ_{sl}^{eff} given by [19]:

$$d\gamma_{sl}^{eff} = -\rho_{sl} dV \qquad (2\text{-}4)$$

where ρ_{sl} is the surface charge density of the counter-ions. By integrating equation (2-4), the voltage dependence of γ_{sl}^{eff} is obtained. Mugele and Baret [19] used the Helmholtz model to calculate the integral and assumed that counter-ions are located at a fixed distance $d_{D.L}$ from the surface. In this case, the capacitance of the double layer is a constant and may be calculated as follows [19]:

$$C_{D.L} = \frac{\varepsilon_1 \varepsilon_0}{d_{D.L}} \qquad (2\text{-}5)$$

where ε_1 is the related permittivity of the liquid. Combining equation (2-4) and (2-5):

$$\gamma_{sl}^{eff}(V) = \gamma_{sl} - \int_{V_{pzc}}^{V} \rho_{sl} dV = \gamma_{sl} - \int_{V_{pzc}}^{V} C_{D.L} V dV = \gamma_{sl} - \frac{\varepsilon_1 \varepsilon_0}{2 d_{D.L}} (V - V_{pzc})^2 \qquad (2\text{-}6)$$

Here, V_{pzc} is the potential of zero charge. Note that mercury surfaces — like those of most other materials — acquire a spontaneous charge when immersed into electrolyte solutions at zero voltage. The voltage required to compensate for this spontaneous charging is V_{pzc}. By substituting equation (2-6) into equation (2-3) the contact angle can be calculated for a droplet placed directly on the electrode:

$$\cos\theta = \cos\theta_0 + \frac{\varepsilon_1 \varepsilon_0}{2 d_{D.L} \gamma_{lv}} (V - V_{pzc})^2 \qquad (2\text{-}7)$$

This equation is valid for up to a few hundred millivolts (voltage range must be below the start of electrolysis). However, modern electrowetting avoids this problem by using a thin insulating layer between the droplet and the electrode surface. In EWOD the electric double layer is created at the dielectric-droplet interface. In view of the fact that the dielectric thickness d is much larger than $d_{D.L}$ (Figure 2-4) the total capacitance of

this system is reduced. This system might be described as two capacitors in series [24, 25], which are the double layer at the solid–insulator interface with a capacitance $C_{D.L}$ and the dielectric layer with a capacitance C_d defined as:

$$C_d = \frac{\varepsilon_0 \varepsilon_d}{d} \qquad (2\text{-}8)$$

where ε_d is the dielectric constant of the insulator.

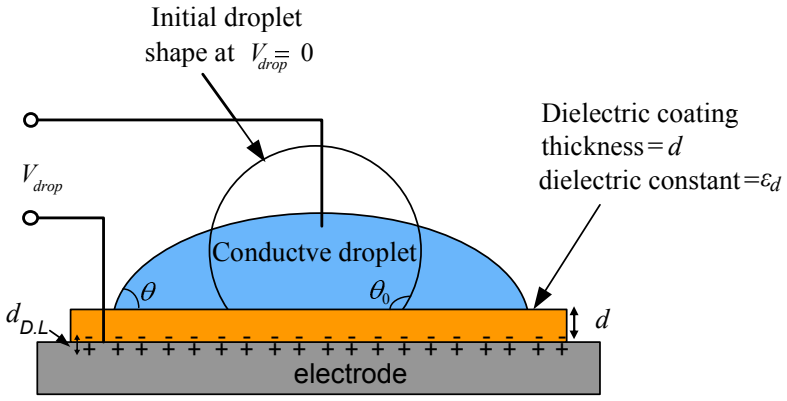

Figure 2-4 Electrowetting behaviour of a sessile conductive liquid droplet. After applying an AC voltage the contact angle of the droplet which is placed on a horizontal dielectric coated electrode is reduced. This change is due to a reduction in the solid-liquid interfacial energy, which leads to a reduction in contact angle and improves the wetting of the surface. Adapted from [27].

Since $C_d << C_{D.L}$ the total capacitance per unit area may be approximated by $C \approx C_d$. With this approximation, the liquid may be treated as a perfect conductor and therefore the electric field penetration into the liquid may be neglected. In this case the voltage drop occurs within the dielectric layer and by assuming $V_{pzc} = 0$, equation (2-6) is reduced to:

$$\gamma_{sl}^{eff}(V) = \gamma_{sl} - \frac{\varepsilon_0 \varepsilon_d}{2d} V^2 \qquad (2\text{-}9)$$

By combining equation (2-9) with equation (2-2), the basic equation for EWOD may be written as follows:

$$\cos\theta = \cos\theta_0 + \frac{\varepsilon_0 \varepsilon_d}{2 d \gamma_{lv}} V^2 \qquad (2\text{-}10)$$

In this equation, θ is the contact angle after applying a voltage and θ_0 is the static contact angle without applying the voltage, ε_0 is the permittivity of free space and γ_{lv} is the liquid/air surface tension. Here, the dimensionless electrowetting number (η) is introduced as:

$$\eta = \frac{\varepsilon_0 \varepsilon_d}{2 d \gamma_{lv}} V^2 \qquad (2\text{-}11)$$

This number is a measure of how the electrostatic energy compares to surface tension [19]. The change in the contact angle of a droplet placed on a horizontal dielectric coated electrode after applying a voltage (EWOD) is illustrated in Figure 2-4.

A conductive liquid has two observable responses to the electric field: (1) change in the apparent contact angle θ made by the liquid with the solid surface and (2) a net electrostatic force producing displacement of the centre of mass (CM) of small liquid volumes [26, 27]. Most authors introducing and describing applications for EWOD often ascribe the second phenomenon to the first. However, one should note that CM motion and contact angle changes are considered as independent observables [26, 27].

2.4 Effect of electrostatic force on contact angle

Kwan Hyoung Kang considered the half plane of the droplet which is placed on an infinite planar dielectric layer in contact with the electrode [28].

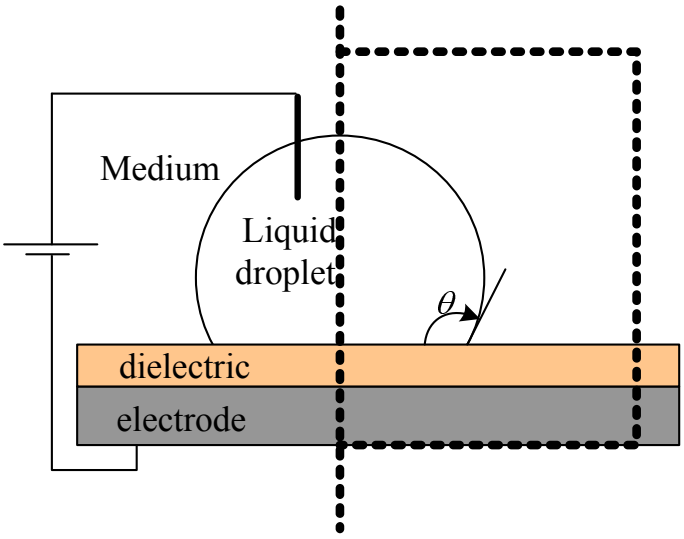

Figure 2-5 Schematic sketch of the domain of interest for analysing an electrostatic force acting on a droplet. Adapted from [28].

The droplet is assumed to be a perfect conductor and is surrounded by an immiscible, perfectly insulating fluid. Within the surrounding fluid and dielectric layer, the net electrostatic force acting on the liquid-medium interfacial surface (Figure 2-5) which is always directed outward with respect to the droplet, may be derived as follows [28]:

$$\overline{F}_e = \frac{\varepsilon V^2}{2d}\cos\theta \qquad (2\text{-}12)$$

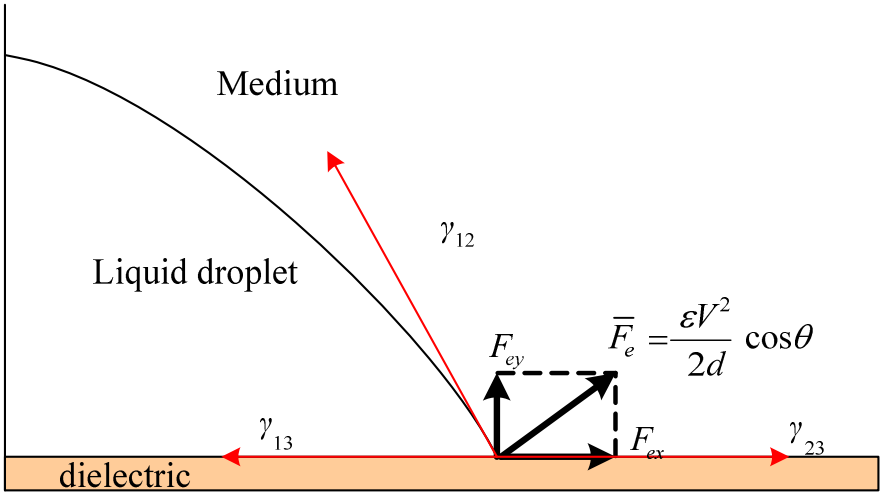

Figure 2-6 Electrostatic force and its influence on the horizontal balance of forces acting on the three-phase contact line. Adapted from [28].

As shown in Figure 2-6, the electrostatic force can be decomposed into horizontal and vertical components which may be expressed by the following equations [28]:

$$F_{ex} = \frac{\varepsilon V^2}{2d} \qquad (2\text{-}13)$$

$$F_{ey} = \frac{\varepsilon V^2}{2d}\cot\theta \qquad (2\text{-}14)$$

The horizontal force component is independent of the contact angle and pulls the three-phase contact line until equilibrium with the surface tension forces is achieved. The reduction in contact angle is due to the overcoming of the vertical force component. As electrowetting is clarified within the framework of classical electrostatics, it should be

considered as an effect which originates from electrostatic pressure rather than a change of apparent interfacial tension at the droplet-dielectric interface. The electric stress exerts an outward normal force at the edge of the contact line and is confined to a small region comparable to the thickness of dielectric layer. The force is responsible for the spreading of a droplet and subsequent change of contact angle [28].

2.5 Pellat experiment and rise of liquid

A nonuniform electric field can influence the hydrostatic equilibrium of a dielectric liquid. In the classical Pellat experiment, when a voltage is applied between parallel electrodes the dielectric liquid rises against the pull of gravity [29]. The original Pellat experiment is shown in Figure 2-7a. If the mass density of the liquid equals ρ_m and the liquid dielectric constant is ε_1 then the expression for height change is [30, 31]:

$$h = \frac{(\varepsilon_1 - 1)\varepsilon_0 E^2}{2\rho_m g} \qquad (2\text{-}15)$$

Here E is the electric field between the electrodes and g is the gravitational acceleration. If the plate spacing D is small enough to provide a uniform field $E = V/D$, then equation (2-14) is precise.

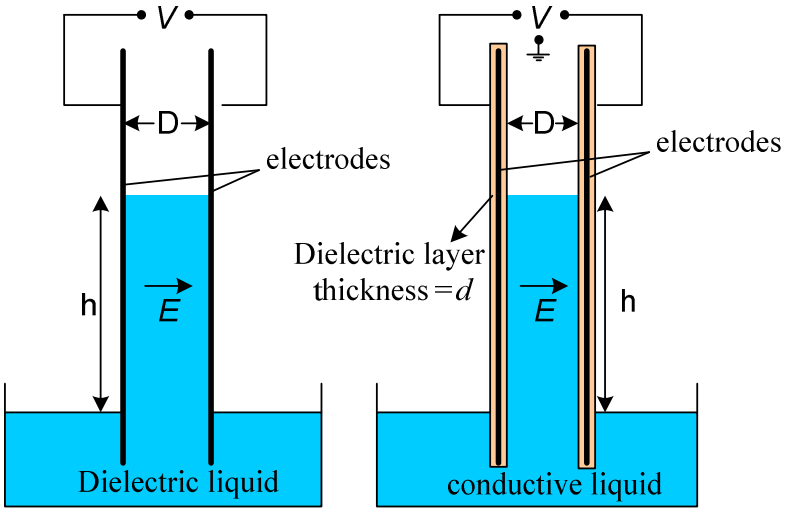

Figure 2-7 a) Pellat's original experiment showing the electromechanical response of a dielectric liquid between parallel electrodes. b) Modified Pellat's experiment involving a conductive liquid between dielectric coated electrodes. The width of the electrodes (w) is greater than the space between them (D). Adapted from [32].

The dipole force acts on the polarised molecules of the liquid in the fringing field region at the bottom of the electrodes. This force can be expressed as $\overline{\rho}.\nabla\overline{E}$, where $\overline{\rho}$ is the vector density of dipoles in the liquid [33] and is non-zero only where the electric field is nonuniform. So in this condition the liquid is lifted up by the electric field.

In 2002 Jones modified Pellat's experiment [32] by using a conductive liquid and insulated electrodes instead of using a dielectric liquid and performed height-of-rise measurements to verify his theoretical model. Two vertical and parallel dielectric coated electrodes are partially immersed into a pool of a conductive liquid such as water (Figure 2-7b). It is assumed that the distance between the two electrodes D is much greater than the thickness of the dielectric, $D >> d$. If $V = 0$, the static capillary height of rise of the liquid column between the electrodes is:

$$h_{cap} = 2\gamma \cos\theta_0 / \rho_m g D \qquad (2\text{-}16)$$

When a voltage V is applied between the two electrodes, the liquid column further rises up to h_{EWOD} and according to the equation (2-10) the contact angle decreases. One way to determine h_{EWOD} is to use a force diagram that balances the net surface tension 'force' per unit length at the contact line against gravity. According to this notion, the voltage-induced decrease in the contact angle pulls the liquid column up by an additional amount proportional to the difference in the cosines of θ and θ_0. By combining equation (2-10) and (2-16) h_{EWDO} is obtained as follows [27]:

$$h_{EWOD} = 2\gamma(\cos\theta - \cos\theta_0) / \rho_m g D = \varepsilon_d \varepsilon_0 V^2 / 4\rho_m g d D \qquad (2\text{-}17)$$

Considering the contact angle model resulting in equation (2-17), h_{EWOD} does not depend on a change in the liquid contact angle. An alternative way to derive h_{EWOD} is using the electromechanical model by direct determination of the force of electrical origin [27]. Since h_{EWOD} is greater than the capillary meniscus height, this approach is insensitive to the profile of the meniscus. The capacitance of the system in Figure 2-7 is a function of the height of the liquid column h [27]:

$$C(h) = \varepsilon_d \varepsilon_0 \frac{wh}{2d} + \text{constant} \qquad (2\text{-}18)$$

where w is the width of the electrodes and $w >>$ D. The upward-directed force of electrical origin is derived by using the co-energy function $W_e' = C(h)V^2/2$ [27].

$$f^e = \frac{\partial W_e'}{\partial h}\Big|_v = \frac{\varepsilon_d \varepsilon_0 w}{4d} V^2 \qquad (2\text{-}19)$$

Equating f^e to the gravitational force exerted on the elevated column of liquid in Figure 2-7 yields the same expression for h_{EWOD} as given by equation (2-17). Therefore, the force of electrical origin resulting in displacement of the centre of mass of a liquid volume does not depend on changes of the liquid contact angle.

2.6 Summary and Conclusion

This chapter presented an overview of the theory underlying electrowetting. In the first section, different forms of wetting giving rise to different contact angles were presented and the behaviour of a droplet in the absence of an applied electric field was discussed.
In the second section, the notion of the electric double layer and how it leads to the accumulation of ions and counter-ions at interfaces was presented. This was followed by a definition of the double layer capacitance, from which the basic equation of electrowetting that gives the contact angle of a droplet in the presence of an applied voltage was derived. The electrostatic force on a droplet subjected to an applied voltage and the corresponding force-balance equations were presented in the fourth section.
The original and modified versions of the Pellat experiment where the fluid confined to two parallel electrodes rises due to an electric force overcoming gravity were discussed and governing equations derived in the final section.

3 Basic experiments on electrowetting on dielectric and liquid dielectrophoresis

3.1 Introduction

Microfluidic systems based on electric fields offer great promise in the laboratory on a chip and other micro total analysis system technologies. Microfabricated electrode structures patterned on a substrate with the application of AC or DC voltages, have the capacity to manipulate and control liquid masses, transport and dispense pico or microlitre droplets, perform liquid mixing and separation without involving any pumps or valves. Of growing interest among these are electrowetting on dielectric and dielectrophoretic methods. These two mechanisms are, respectively, the low and high frequency limits of the electromechanical response of a liquid to an electric field [34]. DEP liquid actuation involves liquid masses instead of particles. It is similar to particulate DEP which in a polarised liquid moves towards a region of higher field intensity. Unlike particulate DEP, the electric field influences the shape of the liquid [35].

At high frequencies (typically between 10 kHz – 200 kHz), applying a non uniform AC electric field induces a dielectrophoretic (DEP) force which can move and manipulate liquids and create linear arrays of very small droplets. These droplets are usually formed on the surface of co-planar electrodes which are coated by an insulating layer. This system of droplet generation has potential applications for microfluidics in lab-on-a-chip technology [36]. The DEP force draws out a liquid finger or rivulet starting from a parent droplet when an AC voltage is applied [37]. Once the voltage is removed, the rivulet breaks up into regularly spaced droplets on the surface.

It is also reported that the translational motion of the droplet in the presence of an AC voltage is very similar to the inch-worm mechanism. During its motion, the droplet elongates and returns to a spherical shape periodically. Throughout the elongation, the advancing side of the droplet shifts forward while the trailing side remains virtually pinned. During the restoring cycle, the trailing side is pulled forward while the advancing side remains virtually pinned. This motion is sustained until the droplet reaches the end of the structure (Figure 3-1) [38].

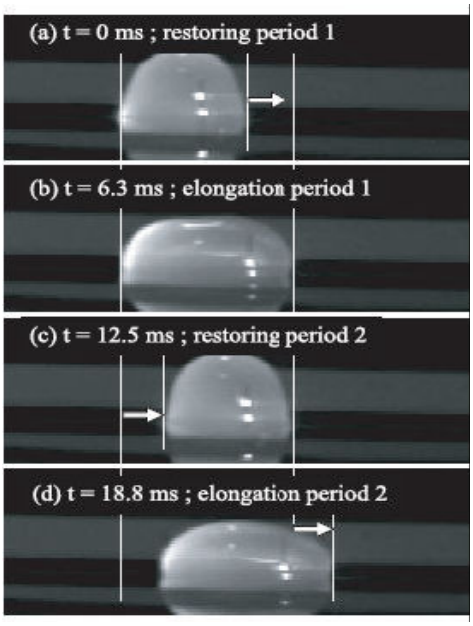

Figure 3-1 The inchworm-like droplet motion. High speed image of droplet motion has been taken by Masahid Gunji and Masao Washizu. f = 80 Hz V = 70 Vrms. Taken from [38].

In this chapter, the frequency dependency of electrowetting and dielectrophoretic liquid actuation using two parallel coplanar electrodes is investigated. It is observed that it is the same basic response of a liquid to an electric field which amounts to the electrowetting and liquid DEP effects are in low and high-frequency limits, respectively. These limits correspond to the use of conducting and insulating liquids.

Additionally, the role of surfactants during electrowetting is analysed. Surfactants (amphiphilic macromolecules with a hydrophobic tail and hydrophilic head) are commonly used in a variety of biotechnological applications. They tend to move towards the interfaces between a liquid and an organic solution. When the surfactants are added to a droplet based system as a medium, they modify the wetting properties of the droplet and this influences the behaviour of the droplet in electrowetting on dielectric. For this purpose, the classical electrowetting set-up was used. The surfactant used in this work is asolectin lipid which is dissolved in an organic solvent (decane).

3.2 Fabrication of dielectric layers

The photoresists used in this project is SU-8. The dielectric constant of SU-8 is around 3, and is independent of processing condition. The thinnest available grade of SU-8 (MicroChem SU-8 2000.5, 14% in cyclopentanone) was used to coat the electrodes. TI Prime was used as an adhesion promoter to improve resist adhesion. In the first step the substrate was cleaned with acetone and isopropyl, baked on a hotplate at a temperature of 150°C for 15 minutes to remove absorbed water from the device surface. The device was then spincoated with TI Prime at 3000 rpm for 20 seconds and baked at 120°C for 2 minutes on the hotplate. After that SU-8.2000.5 was deposited by spin coating at 500 rpm for 5 second then 6000 rpm for 30 seconds followed by soft-baking on a hot plate at 105°C for 1 min. The device was then exposed to UV light for 1 minute and post-baked at 125°C for 60 seconds. Then it was developed in ethyl lactate (Shipley Microposit EC Solvent-11) for 30 seconds, rinsed with isopropyl alcohol (IPA) and blow-dried with nitrogen gas. This produced a 0.7 μm thick SU-8 layer. Finally a 0.25 μm film of Cytop (Asahi Glass Co (AGC)) was spin-coated onto the device at 2000 rpm for 20 seconds before hard-baking at 80°C to provide a hydrophobic surface.

3.3 Conventional electrowetting

3.3.1 Experimental set up

The conventional experimental setup for the electrowetting experiment is demonstrated in Figure 3-2. A 2 μl water droplet is placed on a planar (insulated) aluminium electrode by a micropipette. A thin gold wire is inserted into the droplet as an external electrode. On the electrode surface, 0.7 μm thick SU8 is spincoated as an insulating layer. On top of that, a Cytop layer is deposited to make the surface hydrophobic. The initial contact angle and the diameter of the droplet are about 110° and 1 mm, respectively. A sinusoidal AC signal is generated by a function generator and then amplified by a high voltage amplifier. The amplified electrical signal is applied to the droplet. The droplet shape is observed using a CCD camera and the image is recorded on a computer. Care was taken in all experiments conducted in air to keep the evaporation effect to a

minimum. A glass reservoir was also glued around the electrode and filled with different medium solutions.

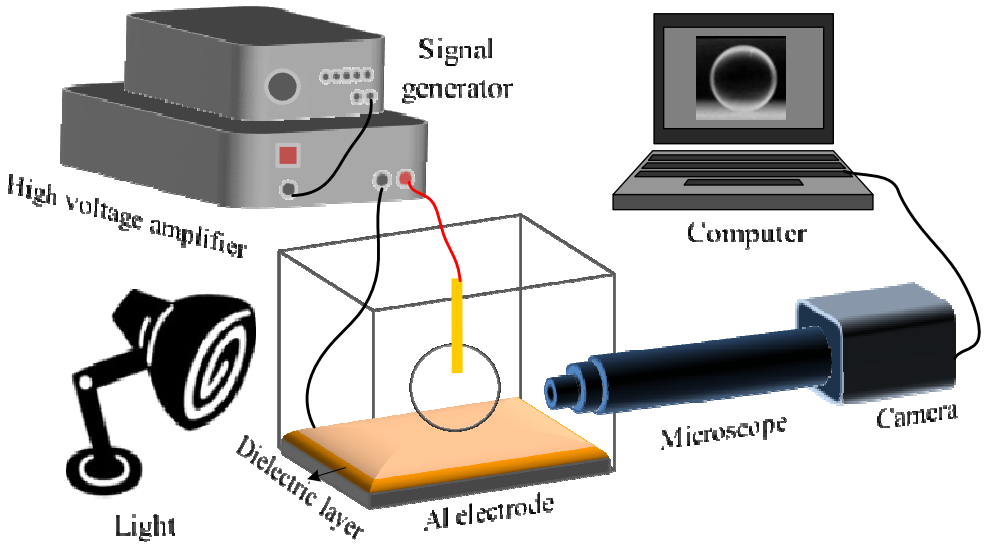

Figure 3-2 Schematic diagram of the classical electrowetting experimental setup. An AC signal is generated using the signal generator and amplified to a high voltage. All the experiments are observed through the horizontal microscope and recorded by the camera.

In the experiment, the change in contact angle of a DI water droplet is measured at the electric field frequency of 2 kHz. The contact angle is obtained by using the drop-analysis program provided by the Biomedical Imaging group in EPFL. The method is based on a Java plugin for ImageJ software [39].

3.3.2 Effect of surfactant on electrowetting

To analyse the effect of surfactants on the droplet contact angle in electrowetting, experiments were conducted using an organic solvent (decane), asolectin lipid and also no medium (air). In order for the droplet shape to stabilise sufficiently, measurements were made 2 minutes after placing the droplets. The voltage was then applied and increased in 5 V increments. Figure 3-3a shows variations of the cosine of the contact angle with the square of the voltage (V^2) in different media.

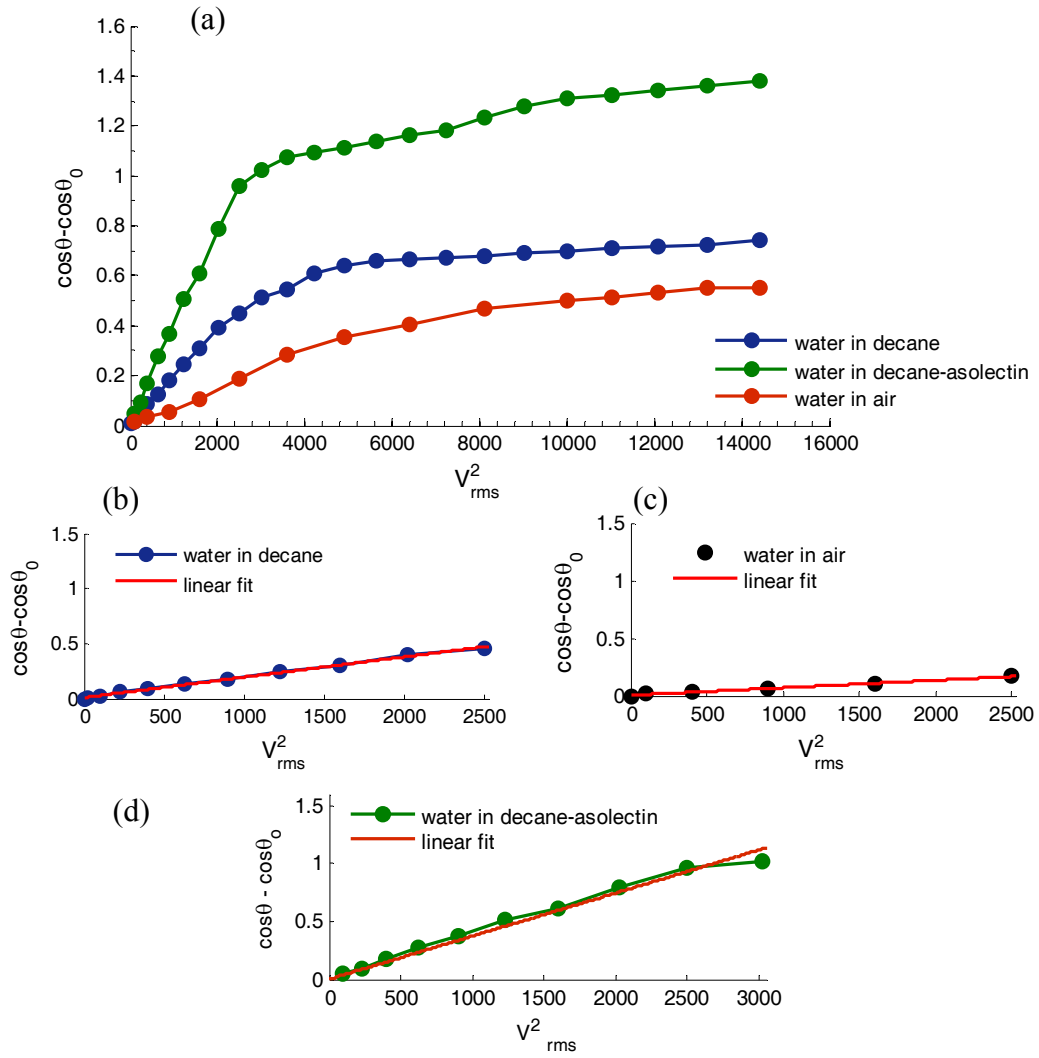

Figure 3-3 a) Variations of V^2 with the cosine of the contact angle when a 2 µl DI water droplet is exposed to air, decane and asolectin-decane. (b-d) Linear fit to experimental values at lower voltages when a 2 µl DI water droplet is exposed to b) decane, c) air and d) asolectin-decane. The surface tension of water from electrowetting measurements is estimated at 74.31 mN/m, 38.2 mN/m, and 26.11 mN/m in air, decane and asolectin/decane respectively. The capacitance of the system was 20.89 μFm^{-2}.

According to the Lippmann-Young law, these changes should follow a linear trend. As can be seen from Figure 3-3b-d, such a linear relationship is observed for lower voltages (about > 50 V). However, beyond a certain voltage the contact angle reached a lower limit. This behaviour is in contrast with equation (2-10) that predicts complete wetting at a certain voltage value. This phenomenon is known as contact angle saturation, the origins of which are not yet fully understood [40, 41]. It is reported that the associated mechanism eventually depends on the dielectric material used to isolate the electrodes

and also on the thickness of the dielectric. Without surfactants, the Lippman-Young relation predicts a linear dependence of the cosine of the contact angle on the square of the electric potential at low voltages. The slope, $C/2\gamma$, is constant due to the surface tension being constant. C is the capacitance per surface area and given by [42]:

$$C = \frac{\varepsilon_0}{\frac{d_{su8}}{\varepsilon_{su8}} + \frac{d_{cytop}}{\varepsilon_{cytop}}} \qquad (3\text{-}1)$$

In the set up described earlier $C = 20.89\ \mu Fm^{-2}$.

Figure 3-3d indicates that in the case of using asolectin as a medium where surfactants are present, the linearity is still observed, indicating that $C/2\gamma$ is still constant. Experimental values at lower voltages are then fitted linearly and the value of the surface tension of water in the air, decane, and asolectin-decane solution is estimated at 74.31 mN/m, 38.2 mN/m and 26.11 mN/m respectively. The results obtained for the surface tension of water in air and decane are similar to published data (72 mN/m and 34.42 mN/m [43]), the difference being attributed to the ambient temperature compared to the published work. Note that the lipid concentration in decane is 10 mg/ml at room temperature and that the value of the surface tension might vary for different lipid concentrations. Raccurt et al [42] have also examined different surfactants. The result they have obtained with Tween 20 at 0.05% is similar to the results in this work obtained with asolectin lipid.

Over several experiments in decane, an average hysteresis of 4±1 between the receding and advancing curves was observed. Figure 3-4a shows a typical electrowetting graph with variations of the contact angle versus applied voltage. The maximum hysteresis in this experiment was about 5^o. In the presence of the surfactant, asolectin lipid, no contact angle hysteresis was observed and the only change in droplet, between the voltage ramps up and down, was a slight increase in the diameter and the corresponding contact area. Figure 3-4b illustrates the change in contact area of a 2 µl water droplet submerged in an asolectin-decane solution.

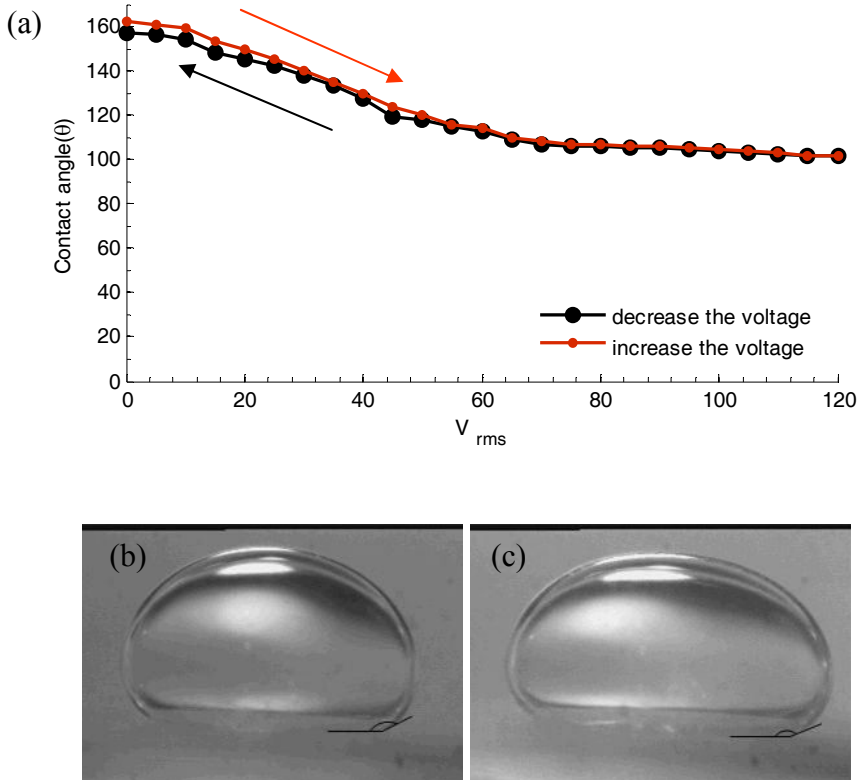

Figure 3-4 a) Contact angle variations with voltage of the 2 µl water droplet in decane in two successive experiments: increasing the voltage up to 120 V (0-120 V) and then bringing it back to 0 V (120-0 V). b) The 2 µl water droplet dispensed in an asolectin-decane solution and left to stabilise for 5 min. c) The droplet after the voltage ramps up to 80 V then down to 0 V.

On a more general note, oil and surfactant environments reduce the contact angle hysteresis in EWOD, while smoother dielectric surface and chemical homogeneity is also effective [44].

The resulting threshold voltages for wetting the droplet in air, decane and lipid environment was observed at 15 V, 5 V and 2 V respectively. Recently, Jong Chang and his colleague [45] fabricated a new device that has atomic-layer-deposited aluminium oxide (Al_2O_3) as the dielectric layer for lowering the driving voltage. They reported that the threshold voltage of only 3 V was needed to move a 2 µl droplet by means of EWOD in the presence of air without using any oil or surfactant.

3.4 Characterising of the parallel planar electrodes

The conventional electrowetting setup is most suitable for describing the wetting behaviour of a droplet in the presence of an electric field while an external electrode is submerged inside the droplet. However, movement of a small volume of liquid in excess of several centimetres has attracted considerable interest in electrowetting. As the classic setup has a limitation for observing droplet motion, a pair of planar electrodes on a small chip is used instead. The structure of the device differs based on the specific application. To understand the concept of electrowetting and liquid dielectrophoresis, we used two devices consisting of two parallel electrodes with 1.5 mm width and 10 mm length which are separated with a constant gap of either 500 µm or 50 µm. Figure 3-5 shows these structures of on chip electrowetting devices. Each device consists of a pair of individually addressable electrodes that is used to produce the desired electric field.

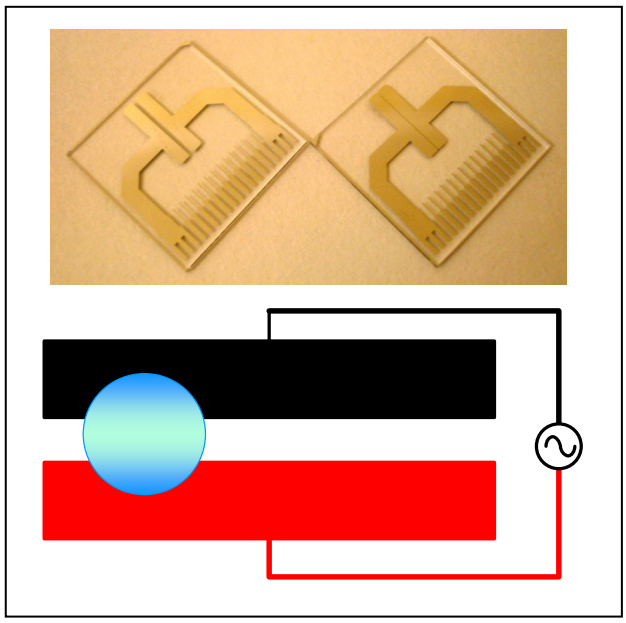

Figure 3-5 Overview of two parallel planar electrodes separated by 500 µm or 50 µm. To analyse the behaviour of the water droplet in the presence of a non-uniform electric field, the electrodes are connected to an AC voltage.

3.4.1 Experimental setup

The electrode arrays were fabricated in layers of titanium and platinum (10/200 nm) using photolithography and ion beam milling. The devices were then coated with 0.7 µm-thicks SU8 as a dielectric layer and a thin layer of Cytop to make the surface hydrophobic. A 2 µl droplet of deionised water was placed at one end of the electrodes. An AC signal with different RMS values at different frequencies was applied to the electrodes. The schematic of the setup is presented in Figure 3-6. The electrodes were connected to an AC generator and high voltage amplifier (KH Krohn-Hite Corporation) via an electronic switching circuit. The experiments were observed using a standard camera.

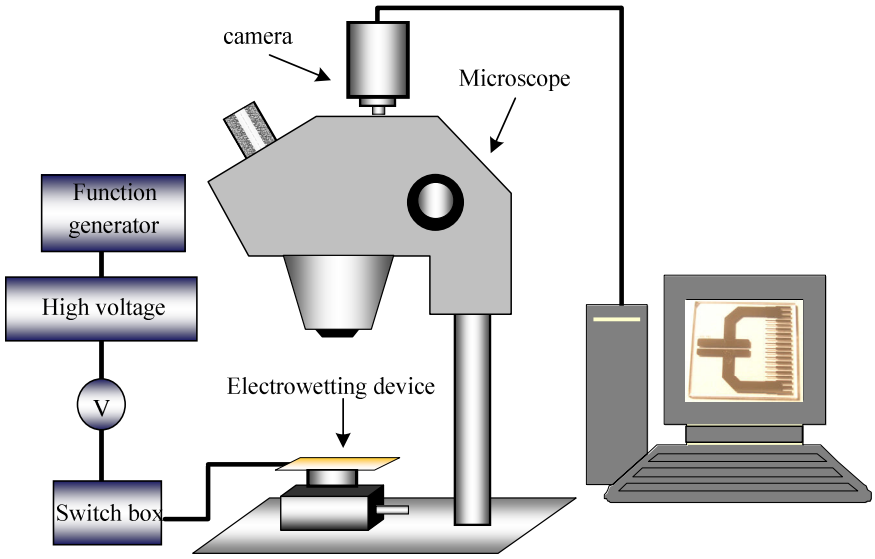

Figure 3-6 Schematic diagram of electrowetting experimental setup. An AC signal is generated using the function generator, amplified to a high voltage and then transferred to the switch box which is connected to the chip holder. Turning on/off and controlling the polarity of the electrodes is possible through the switch box. The results are monitored and saved by a PC.

3.4.2 Electrowetting and dielectrophoretic behaviour of a droplet in AC electric field

As mentioned previously, two devices with different gaps between the electrodes (50 µm, 500 µm) were used. Electrowetting and liquid dielectrophoretic (DEP) effects were investigated and discussed. In another set of experiments the 'self-propulsion' phenomenon noted by Gunji and Washizu [38] was observed.

Generally, at electric field frequencies above the hydrodynamic response of the droplet, the liquid response should only depend on the average time of the applied voltage so the RMS value should be used in equation (2-10). This statement is however only true as long as the assumptions in deriving the Lippmann equation are valid. One of the assumptions, that the liquid be a perfect conductor, is violated at high frequencies. Beyond a critical frequency f_c, the dissolved ions can no longer screen the applied field from the interior of the liquid and therefore the liquid can no longer be treated as a perfect conductor. The liquid behaves as a perfect conductor in frequencies below f_c. However in frequencies above f_c its behaviour tends towards a dielectric [19].

It is the capacitive coupling of the planar electrodes to water that gives rise to the frequency dependence of the liquid profile. The RC circuit model in Figure 3-7 helps quantify such dependence [35].

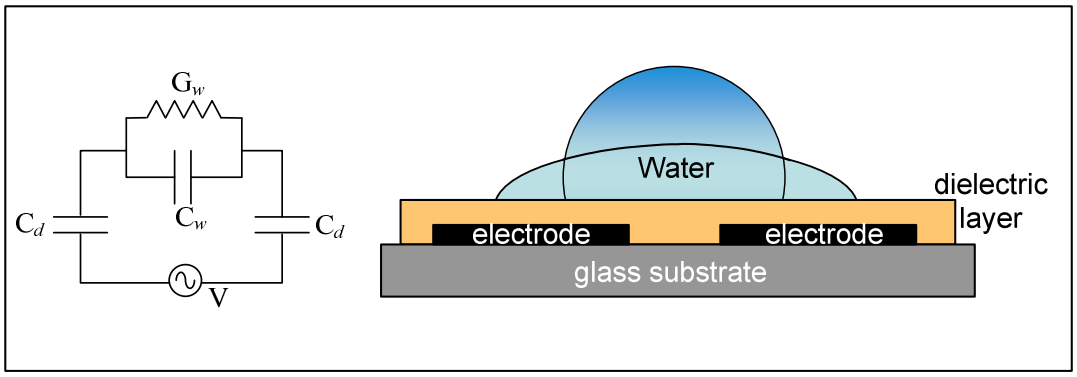

Figure 3-7 The RC equivalent model and cross section of the experimental setup. At low frequencies the voltage drops mainly across the dielectric layer and electrowetting takes place whereas at high frequencies the voltage drops mainly across the liquid, giving rise to a strong non-uniform electric field that gives the liquid a compact semicircular shape. Adapted from [35].

In Figure 3-7 the dielectric coating is modelled by the series capacitors C_d, and the ohmic conductance and capacitance of water are represented by G_w and C_w, respectively. The critical frequency f_c is given by [35]:

$$f_c = \frac{G_w}{2\pi(C_d/2 + C_w)} \qquad (3\text{-}2)$$

For frequencies far below f_c, the bulk of the applied voltage drops across the dielectric layer, making the water an equipotential body with zero electric field inside. At

frequencies far beyond f_c, almost all the voltage drops across the water, thereby creating a strong non-uniform field that gives the liquid a compact semicircular profile.

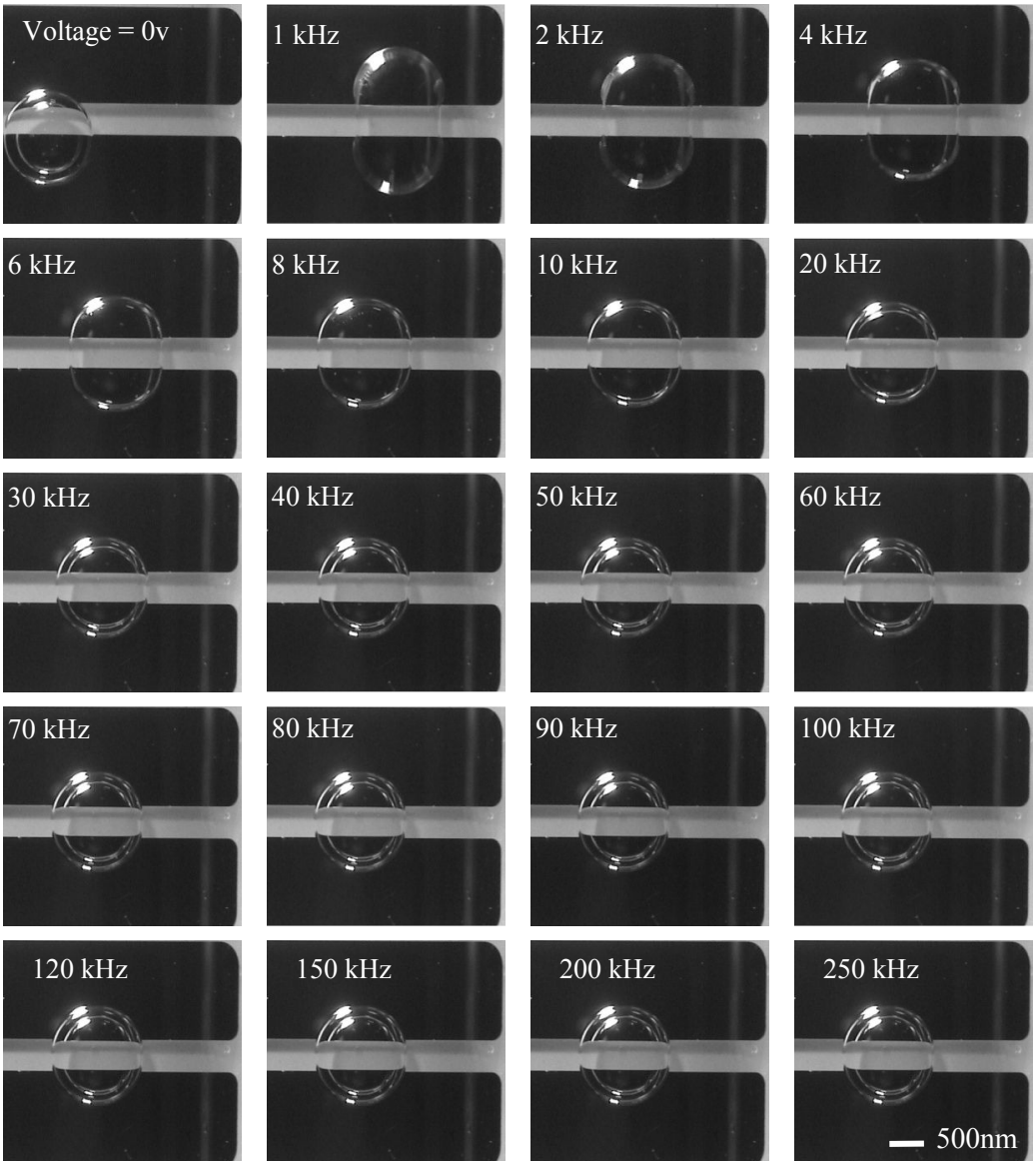

Figure 3-8 Droplet deformation and the electrowetting behaviour from low to high frequency (top view) at V_{rms} = 100 V; 1 kHz ≤ f ≤ 250 kHz; droplet conductivity: 10^{-4} S/m; diameter: approximately 1 mm; ambient medium: decane; the gap between the coplanar electrodes: g = 500 μm.

In the experiments, a droplet of 2 μl DI water was dispensed at one end of the electrodes with decane as the medium. An AC voltage in the frequency range of 1 kHz - 250 kHz was gradually applied. Figure 3-8 and Figure 3-9 show droplet deformation in the device (top/plan view) with 500 μm gap for applied voltages of 100 V and 150 V respectively. Equation (3-2) predicts a critical frequency of 6.8 kHz for this setting. For frequencies less than this critical frequency, the effect of electrowetting is conspicuous in Figure 3-8

and 3-9. By further increasing the frequency, at a certain voltage, the influence of electrowetting becomes less pronounced. Figure 3-10 shows the change in contact area against frequency at three different voltages (50 V, 100 V and 150 V), quantifying the frequency dependent deformations discussed above, and indicating the continuous nature of the transition from conductive to dielectric behaviour as a function of frequency. At lower frequencies, the large contact areas demonstrate the most significant deformation of the droplet. This deformation is reduced by the increase in frequency. By further increasing the frequency, electrowetting eventually breaks down. This breakdown frequency changes in different voltages and it is observed at frequencies 20 kHz, 30 kHz and 200 kHz for voltages 50 V, 100 V and 150 V respectively.

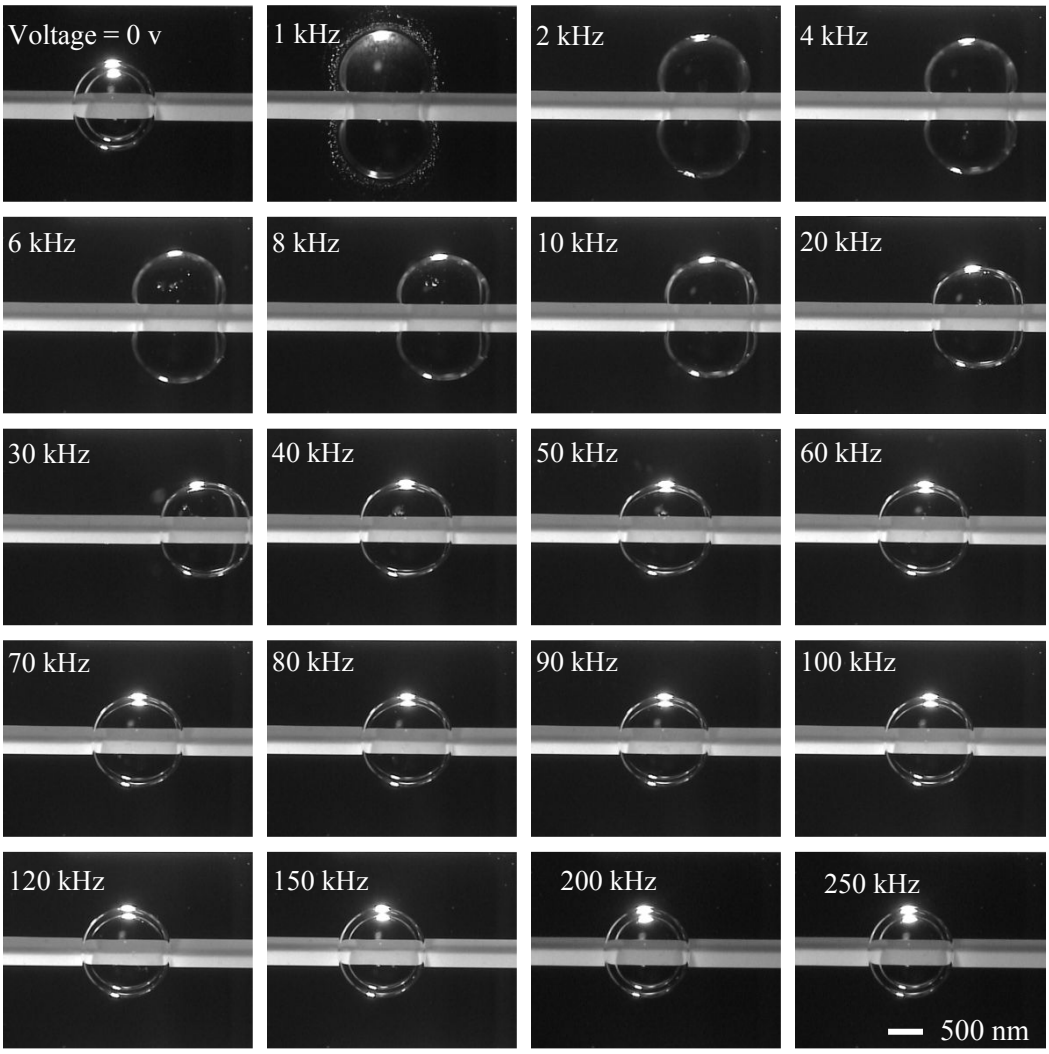

Figure 3-9 Droplet deformation and the electrowetting behaviour from low to high frequency (top view) at V_{rms} = 150 V; 1 kHz ≤ f ≤ 250 kHz; droplet conductivity: 10^{-4} S/m; diameter: approximately 1 mm; ambient medium: decane; the gap between the coplanar electrodes: g = 500 μm.

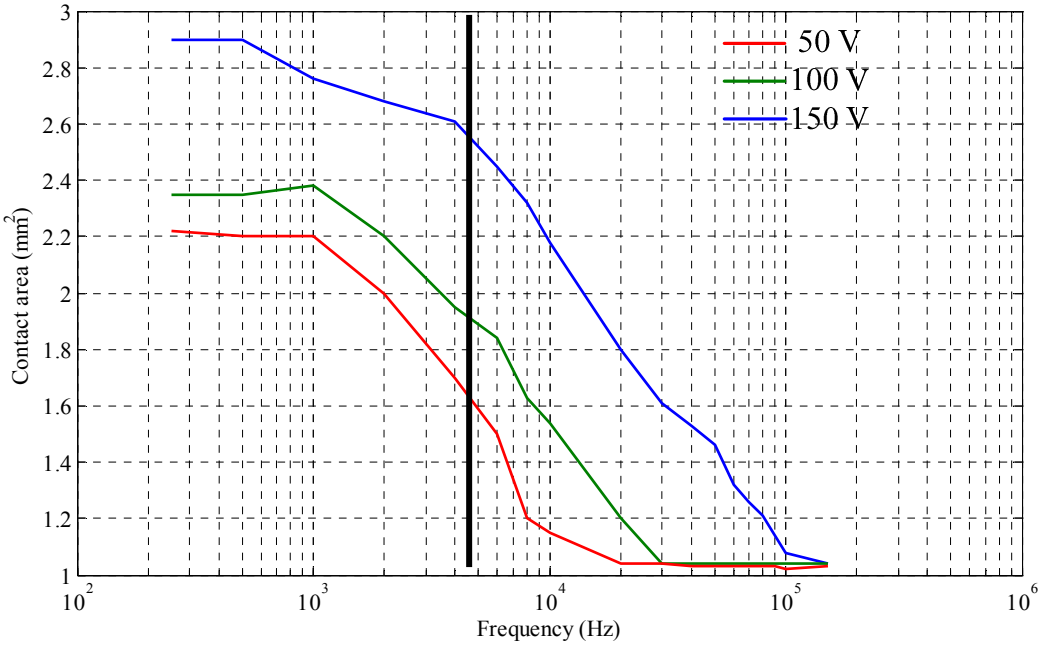

Figure 3-10 Contact area versus frequency for the experiments shown in Figure 3-8 (V_{rms} = 100 V) Figure 3-9 (V_{rms} = 150 V) and an additional experiment with V_{rms} = 50 V. The critical frequency for the setup is estimated at f_c = 6.8 kHz (highlighted in the graph). For frequencies lower than f_c the electrowetting behaviour is strong but decreases with increasing frequency.

With further increasing the frequency beyond the breakdown point for electrowetting the dominant force affecting the profile of the droplet is liquid DEP. The basis of the DEP force is the interaction of a non-uniform electric field with charges due to polarisation of the droplet and it can be described as the tendency of a dielectric liquid in a non-uniform electrical field to move towards regions of high electric field intensity. Figure 3-11 shows the top view of a 2 µl droplet of DI water submerged in decane where the gap between the electrodes is 50 µm. In this, the voltage is kept constant at 100 V and the frequency is increased from 2 kHz to 250 kHz. In this setup the critical frequency is 15 kHz and electrowetting can be observed for frequencies below this value while liquid DEP occurs at much higher frequencies.

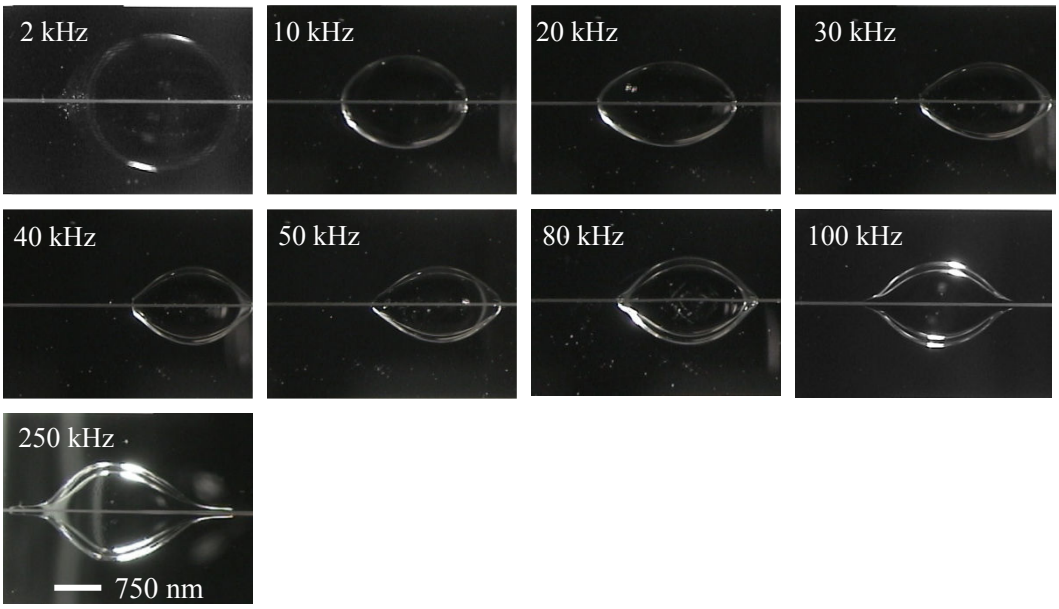

Figure 3-11 Electrowetting and liquid dielectrophoretic behaviours at different frequencies; V_{rms} = 100 V; 2 kHz ≤ f ≤ 250 kHz; droplet conductivity: 10^{-4} S/m; diameter: approximately 1 mm; ambient medium: decane and the gap between the coplanar electrodes, g = 50 μm.

The DEP force acts against the surface tension. Higher voltages increase the intensity of the DEP force. When the DEP force overcomes surface tension, it stretches the liquid in the form of a rivulet. Therefore a minimum voltage must be surpassed to observe the liquid finger formation which can be seen in Figure 3-11 at f = 250 kHz. In the previous setting where g = 500 μm, the required voltage to enable the finger formation was larger than the voltage that could be supplied by our high voltage amplifier. Therefore g was decreased to 50 μm, in which case the liquid finger was observed at V_{rms} = 170 V and f = 100 kHz, as shown in Figure 3-12. If a higher frequency is used, a lower voltage can be applied to achieve similar behaviour (see Figure 3-13 where V_{rms} = 155 V and f = 250 kHz). The liquid finger ruptures into approximately uniform, sessile droplets due to capillary instability if the voltage is removed.

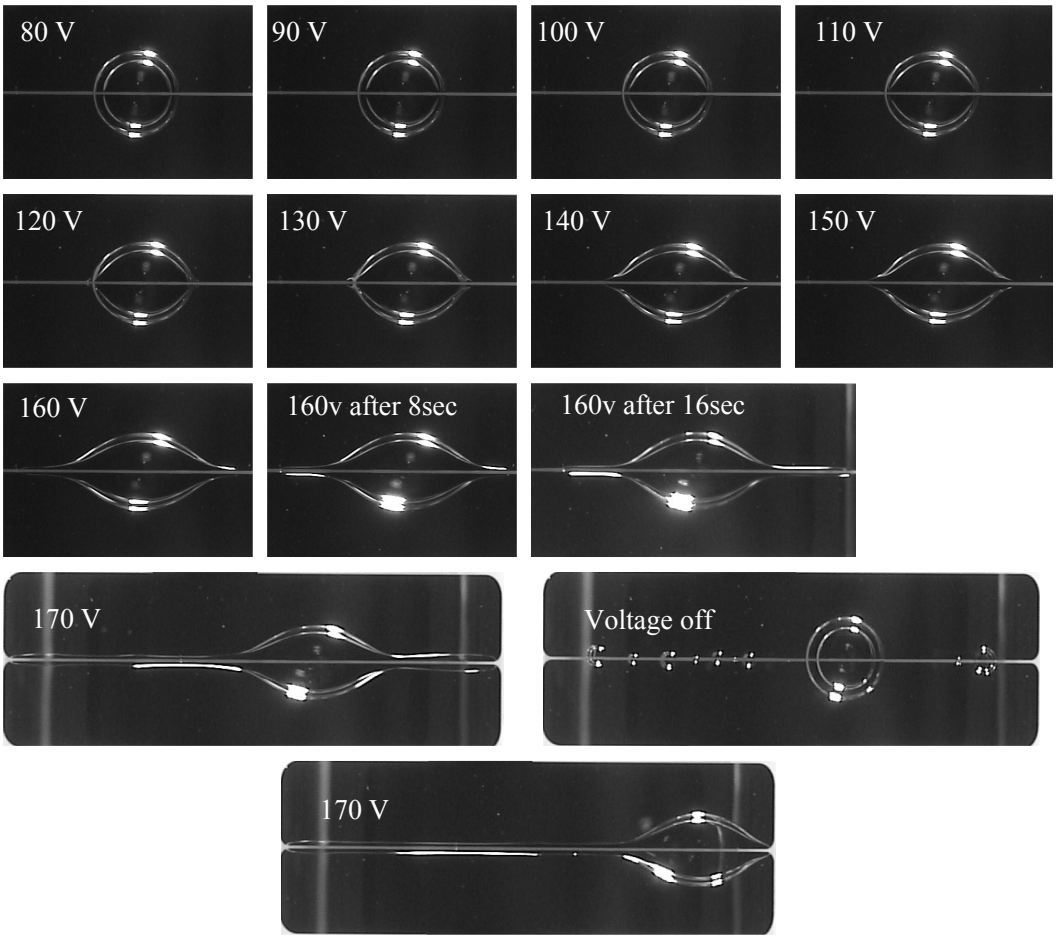

Figure 3-12 Liquid dielectrophoretic behaviours at different voltages f = 100 kHz; 80 V ≤ V_{rms} ≤ 170 V; droplet conductivity: 10^{-4} S/m; diameter: approximately 1 mm; ambient medium: decane and the gap between the coplanar electrodes, g = 50 µm. The finger reached to the end of the structure by applying 170 V.

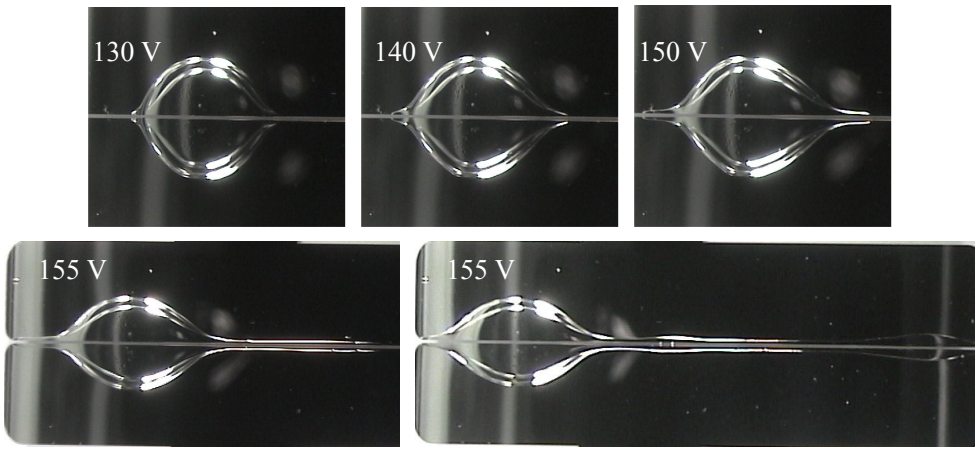

Figure 3-13 Liquid dielectrophoretic behaviours at different voltages f = 250 kHz; 130 V ≤ V_{rms} ≤ 155 V; droplet conductivity: 10^{-4} S/m; diameter: approximately 1 mm; ambient medium: decane and the gap between the coplanar electrodes, g = 50 µm. At this frequency the finger reached to the end of the structure by increasing the voltage to 155 V.

3.4.3 Numerical simulations

In order to understand the behaviour of the droplet, one has to calculate the forces that are acting upon it. The force $\overline{F}$ exerted at any point in the droplet by the established electric field $\overline{E}$ can be calculated by the Kortewig-Hemholtz formula [32, 34]

$$\overline{F} = \rho_v \overline{E} - \frac{1}{2} E^2 \nabla \varepsilon \qquad (3\text{-}3)$$

Where, ρ_v is the volume charge density. The term accounting for electrostriction is ignored due to incompressibility of water. It can be shown that the same force may be expressed in terms of the Maxwell stress tensor $\overline{T}$ as follows:

$$\overline{F} = \nabla . \overline{T} \qquad (3\text{-}4)$$

The components of the tensor $\overline{T}$ are given as [32, 34]:

$$T_{ij} = \varepsilon E_i E_j - \frac{1}{2} \varepsilon E^2 \delta_{ij} \qquad for\ i, j = 1,2,3 \qquad (3\text{-}5)$$

δ_{ij} is the Kronecker delta (a function of two variables which is 1 if $i = j$ and 0 if $i \neq j$). The resultant force may be calculated by integrating the above mentioned force over the volume v_D of the droplet.

$$\overline{F} = \iiint_{v_D} \nabla . \overline{T} dv \qquad (3\text{-}6)$$

Applying the divergence theorem to the above equation yields:

$$\overline{F} = \oiint_{\Sigma} \overline{n} . \overline{T} dS \qquad (3\text{-}7)$$

where $\sum$ is any surface enclosing the droplet.

This result shows that using the Maxwell stress tensor one can obtain the resultant force exerted on the droplet by calculating the surface integral on the surface of the droplet.

Basically, the Maxwell stress tensor is an entity that, at any point on the droplet surface, relates the force vector to the outward normal vector.

Calculating the components of the Maxwell stress tensor on the xy, xz and yz planes gives quantitative indication of the forces normal to these planes and hence an indication of the way the droplet tends to deform.

Three-dimensional (3D) numerical simulations were run in COMSOL 3.5 to calculate the components of the Maxwell stress tensor on a water droplet (1 mm diameter) on the xz plane.

The droplet was defined as a semisphere placed on parallel electrodes (1.55 mm width, 10 mm length) separated by 50 μm. The surface of the electrodes was insulated with a dielectric layer. The environment of the droplet was defined to be decane. The relative permittivities of the dielectric layer and decane were attributed values of 3 and 2, respectively. The droplet was simulated as a rigid body in order to extract information about the electric stress tensor that is produced on the droplet interface. As boundary conditions, an AC electric potential of 150 V was set for the actuation electrode and 0 V for the ground electrode. All external boundaries were set to have an electrical insulation. Figure 3-14 shows a typical 3D simulation of the Maxwell stress tensor at the interface of a water droplet and decane for the two parallel planar electrodes. In this simulation the frequency was kept at 2 kHz.

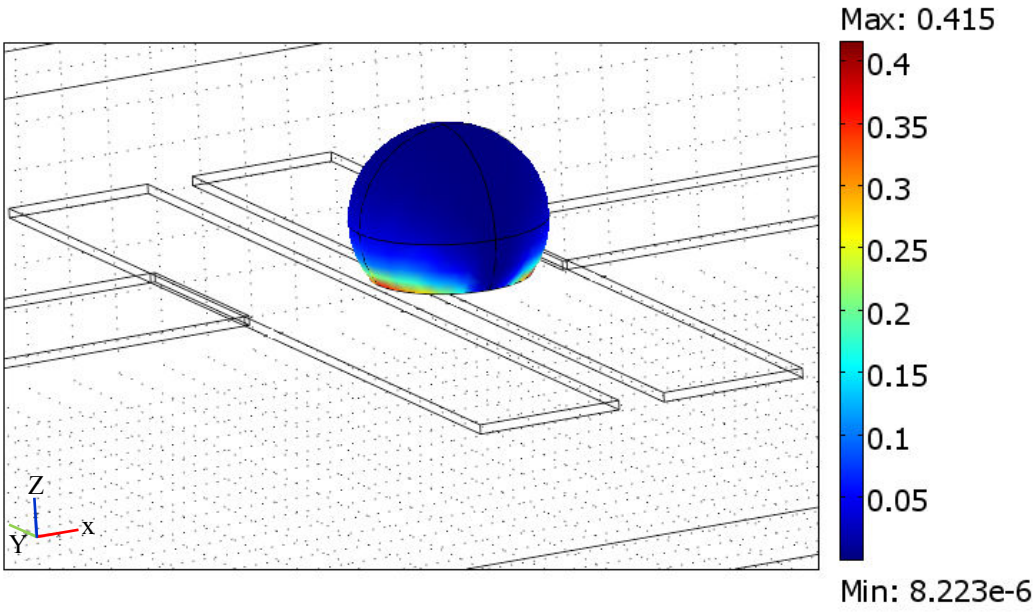

Figure 3-14 3D simulation of the Maxwell stress tensor at the interface of a water droplet and decane, placed on the two parallel planar electrodes (V = 150 V, f = 2 kHz). Colours represent the magnitude of the electric stress tensor. The unit on the colour bar is Pascal.

Running the simulation at a fixed voltage (150 V) and applying a frequency range of 2 kHz – 250 kHz resulted in changes in the magnitude of the stress on droplet surface that tends to deform it along the electrodes.

Figure 3-15 shows these changes and indicates that by increasing the frequency the resultant force on the droplet is along the y direction where the liquid starts to form a rivulet.

	Stress tensor on xz-plane at x direction	Stress tensor on xz-plane at y direction	Stress tensor on xz-plane at z direction
2 kHz	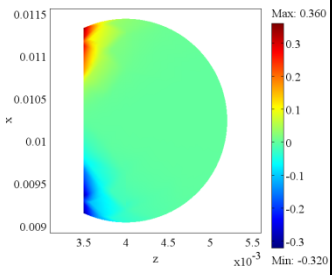	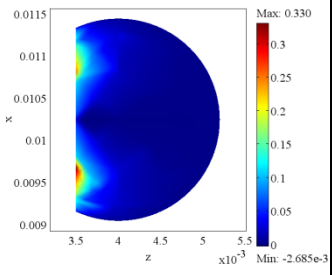	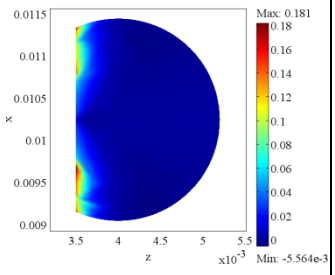
10 kHz	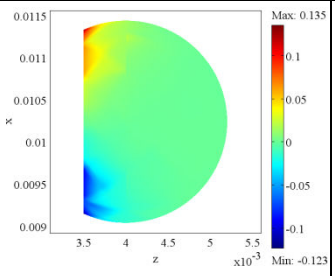	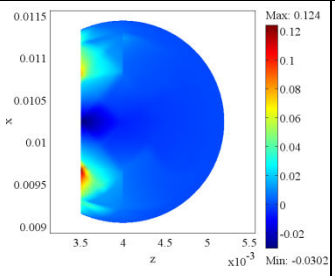	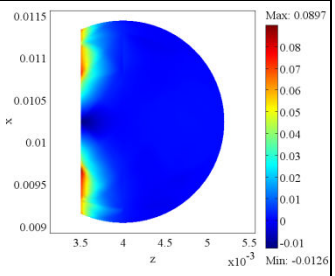
20 kHz	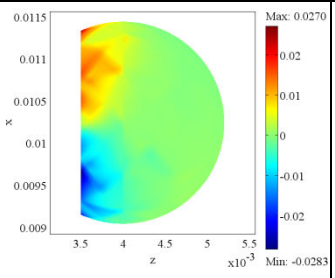	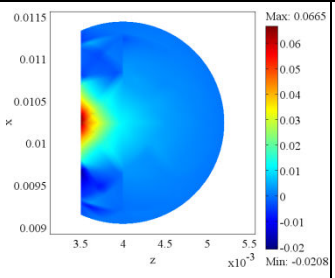	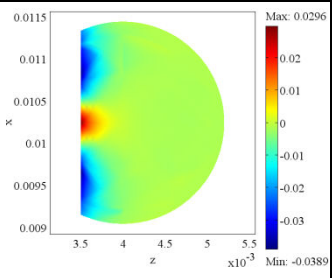
30 kHz	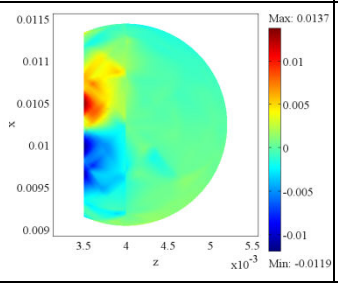	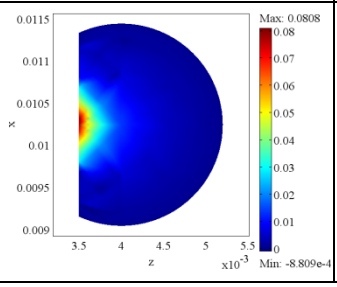	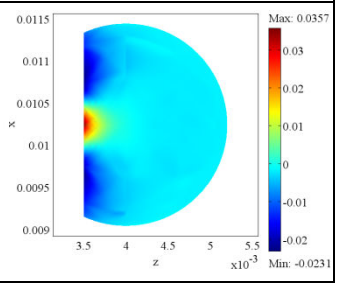

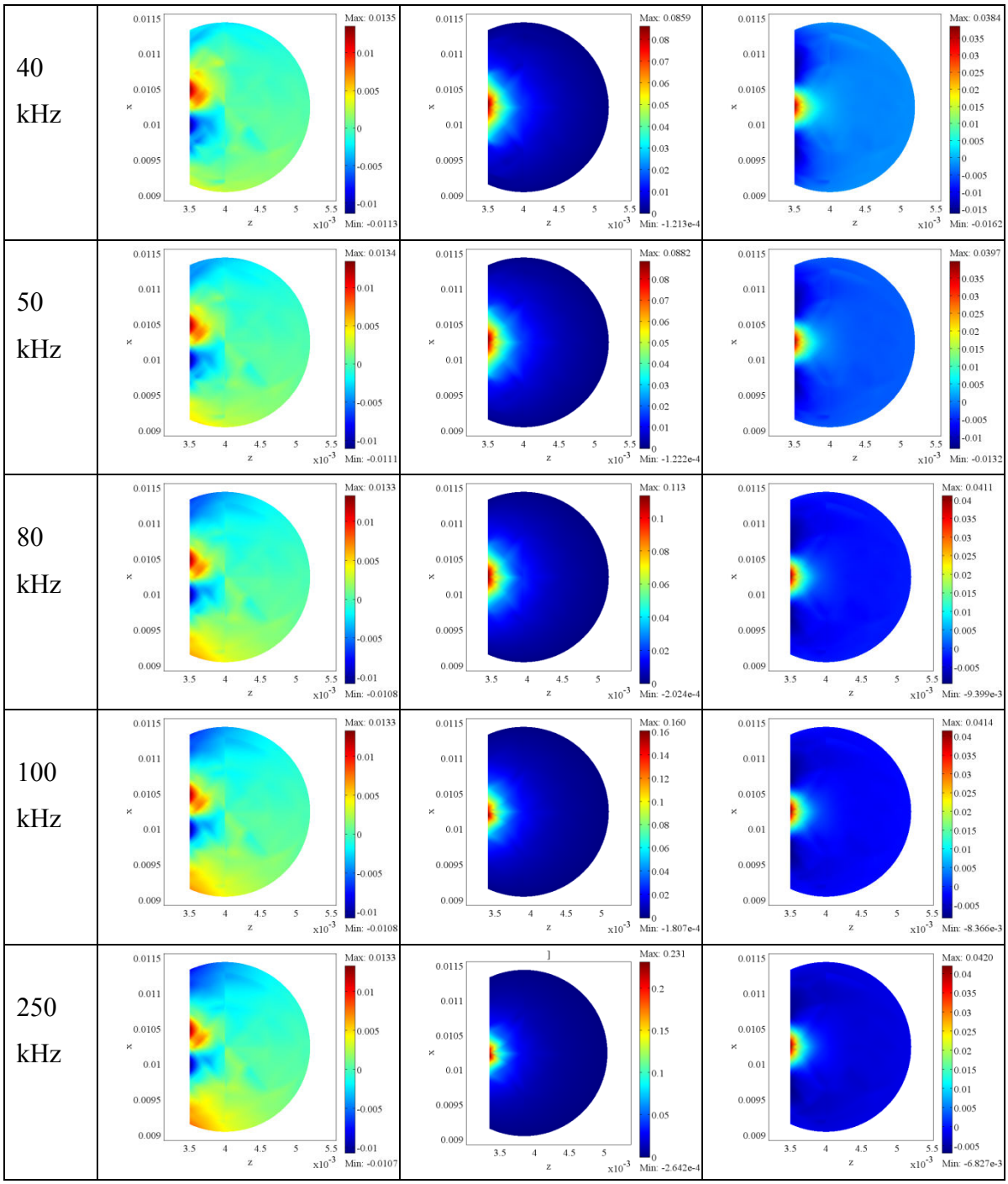

Figure 3-15 Changes in the magnitude of the stress on the xz plane, indicating that at a certain voltage by increasing the frequency the force on the droplet which is tending to deform it along the x and z direction is reduced while it is increased in the y direction where in the experiment the liquid starts to form a rivulet.

3.4.4 Self-propulsion motion

Figure 3-16 shows the motion of a water droplet on parallel electrodes with 500 μm gap. Based on electromechanical theory, the droplet should move to minimise the total electrostatic energy of the system. Thus, it would stop when the energy is minimised. To continue the motion the field pattern must be altered. It is observed that at low frequencies (350 Hz – 2 kHz) when an AC voltage in the range of (30 V – 50 V) is applied, the droplet slightly flattens but it is stationary which denotes that the energy of the system is minimized. However, after a delay the droplet starts to move. This observation seems to contradict the expected behaviour of the droplet based on electromechanical theory.

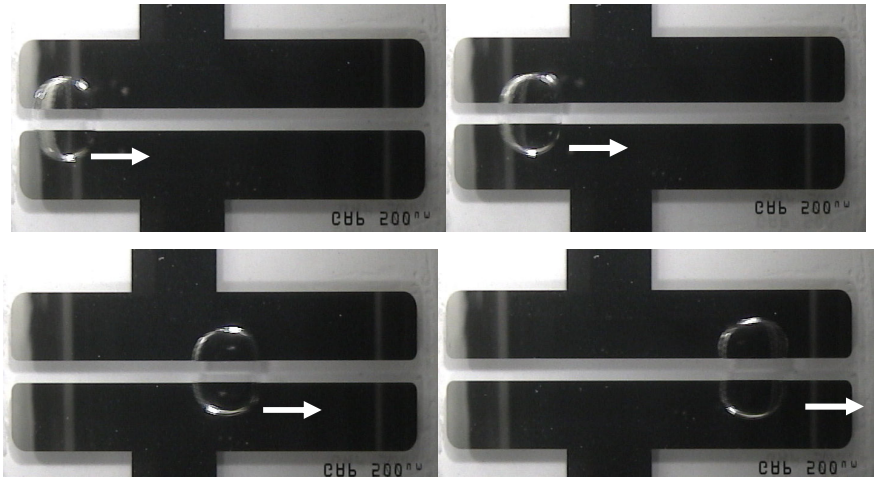

Figure 3-16 Water droplet motion on the parallel electrodes with 500 μm gap, while the droplet was submerged in decane and the applied voltage was 40 V_{rms} at 2 kHz.

.

Gunji and Washizu [38] observed similar behaviour in an air medium and discussed possible reasons for this phenomenon. They noted that the initial direction of the droplet motion is unpredictable, but once started the droplet leaves behind a moisture layer on the surface, which reduces the electric field on the droplet's trailing side. Thus the field on the advancing side is stronger than that on the trailing side, which pushes the droplet forward.

3.5 Summary and Conclusion

The main point of this chapter was to understand and analyse the behaviour of a droplet in the presence of an AC electric field. For this, first the contact angle of a DI water droplet placed on SU8-and Cytop-covered electrodes were measured as a function of applied voltage. Experiments were conducted using an organic solvent (decane), asolectin lipid and also using no medium (air). The voltage was increased in 5 V increments. Then the capacitances of the system were estimated. For this aim an accurate measurement of the thickness of the SU-8 and Cytop layers were needed which were measured by the step profiler.

It is found that by adding the surfactants (asolectin) to the droplet-based system as a medium, they modify the wetting properties of the droplet and this influences the behaviour of the droplet in electrowetting on dielectric. The presence of surfactants reduced the threshold voltages of the wetting as well as contact angle hysteresis. Using this system, the value of the surface tension at the interface of water and asolectin-decane solution was estimated at 26.11 mN/m (the lipid concentration in decane was 10 mg/ml).

By replacing the classical setup with two parallel coplanar electrodes, the phenomena of electrowetting and liquid dielectrophoresis were analysed. It was observed that it is the same basic response of a liquid to an electric field which amounts to the electrowetting and liquid DEP effects in high and low-frequency limits, respectively. These limits correspond to the use of conducting and insulating liquids. In order to understand the behaviour of the droplet, the components of the Maxwell stress tensor on the xz planes were simulated in COMSOL. It gave the forces normal to the planes and hence an indication of the way that the droplet tends to deform with changing the applied voltage and frequency.

4 Mixing

4.1 Introduction

Manipulation and mixing of small volumes of liquids in microfluidic devices has an important potential in chemical and biological protocols and micro total analysis systems (lab-on-a-chip). In these systems mixing could be used for preprocessing, dilution or reaction between samples and reagents in particular ratios. Mixing in the sub-nanolitre regime is difficult to achieve in reasonable time scales. Improved mixing depends on two principles:

1. The ability to create turbulent flow at such small scales.
2. The ability to increase the interfacial region between streams to obtain fast mixing by diffusion

Turbulent flow would require the liquids to move at high velocities or use an external source to apply energy into the flow, therefore most researchers have been focusing on the second principle. In both categories of microfluidic system (continous-flow and droplet-based) mixing can be achieved with two methods. Passive mixing, which is mediated through diffusion without any external energy for the mixing and active mixing, in which external energy is used to create either dispersed multilaminates or turbulence in the liquid [1-3]. Mixing can be completed without transporting droplets by electrowetting where a sustained droplet oscillation is triggered. To understand the self-excited droplet oscillation assumes that a wire is dipped into a droplet (Figure 4-1). At the beginning the voltage is zero and the distance between the wire and substrate is d [1].

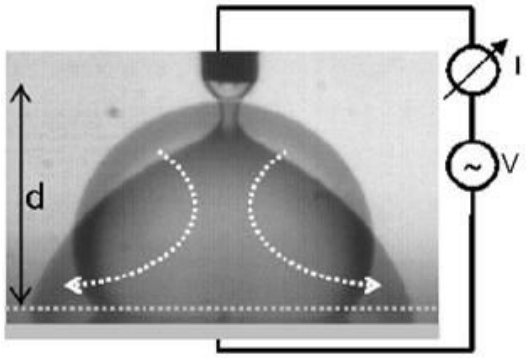

Figure 4-1 The image of maximum and minimum foot print areas during droplet oscillation. The horizontal dash shows the insulating layer and the solid horizontal grey line represents substrate electrode. Taken from [1].

Applying a voltage V, the contact angle between droplet and substrate θ decrease and the droplet becomes flatter. At some point a capillary neck between the wire and droplet is formed. The capillary neck breaks when V is increased beyond a certain threshold voltage V_t. After the break the droplet is completely discharged so the droplet-substrate voltage is zero and θ switches back to $\theta_d \sim \theta_0$ (θ_d is a dynamic contact angle which is smaller than θ_0). Consequently the drop relaxes back towards a spherical cap with $\theta = \theta_0$ until it contacts the wire and the cycle will start again. The droplet starts self-excited oscillation between attached and detached morphologies. The arrows in Figure 4-1 show the net displacement of liquid throughout droplet spreading [1]. The droplet oscillation depends on the values of V and d. Also two requirements must be considered for oscillation to happen:

1. The droplet must detach from the wire through stretching.
2. The droplet must touch the wire again through relaxation.

Figure 4-2 shows the result of mixing by self-excited oscillation of two droplets of the same size (water and glycerol).

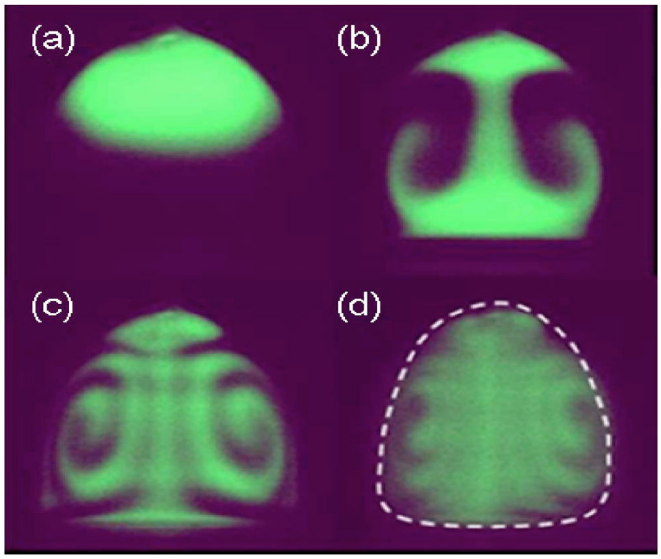

Figure 4-2 Mixing of 1mm water-glycerol drops in 81 Hz oscillation frequency. Taken from [1].

The top droplet is stained with fluorescent dye while the bottom drop remained dark under epifluorescence observation. By choosing d and V in the oscillation region and immersing the wire in the droplets, mixing happens in 45 cycles (approximately 0.55 second). In this method the two droplets are completely mixed within 100–2000 oscillation cycles for low and high viscosities respectively [1].

4.2 Mixing by electrowetting using planar electrodes

Here we present a microfabricated actuator that can be used to perform microfluidic transport and mixing. The operating principle for droplet transport is based on electrowetting and dielectrophoretic. A liquid droplet mixer enables the mixing of samples and reagents for chemical and biological analysis in micro total analysis systems (μTAS). The ability to mix liquids rapidly utilizing minimum area greatly improves the throughput of these systems. For this purpose a system was designed to mix two aqueous droplets. An electrowetting based mixer was developed to improve the speed of droplet mixing. The principle was demonstrated with droplets containing ink. A droplet of deionised water and a staining drop containing black ink was used and the mixing process recorded by a high speed camera.

4.2.1 Device principle

Mixing two droplets, located at positions A and B at a centre point O (Figure 4-3), requires two consecutive steps; first, they need to be moved, dielectrophoretically, to a common point (O in Figure 4-3). Next, the actual mixing of the two droplets takes place.

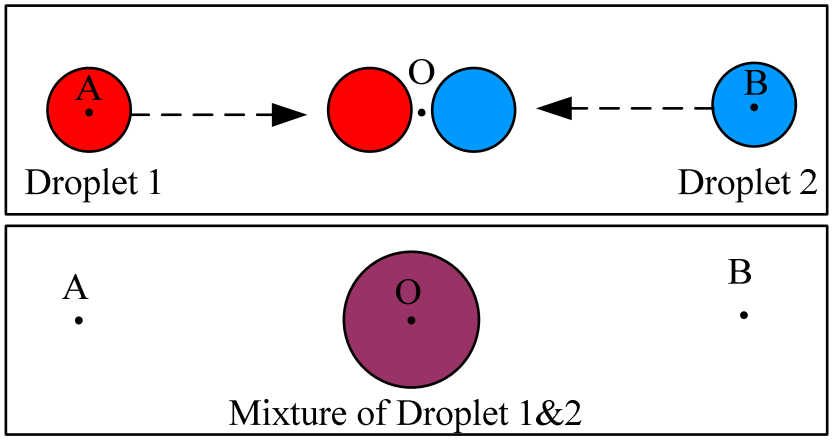

Figure 4-3 Two droplets placed at initial points A and B. After moving them to the mixing point, they will join in one droplet and the active mixing can take a place

For droplets A and B to move to mixing point O through DEP, field gradients need to be generated between both A-O and B-O. In the initial design for mixing two droplets

shown in Figure 4-4, the field gradient was generated by a gradient in capacitance between points A-B and A´-B´.

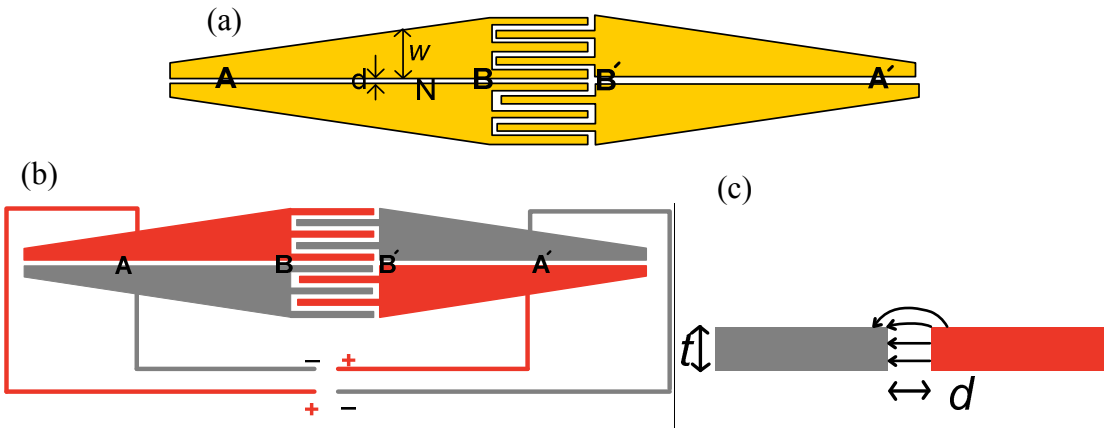

Figure 4-4 a) The initial design of electrowetting chip for mixing of two water droplets. On either side are two pairs of microelectrodes which are separated by a constant gap *d*. In the centre of device the structure of electrodes is broken to interdigitated region for purpose of mixing. Point A and A´ indicate the initial position of the droplets. The gradient capacitance and magnitude of electric field are increased only by increasing the width of electrodes *w*. The droplets are predicted to move from position A to B (or A´ to B´) under the application of an electric potential between the pair of electrodes as indicated in configuration (b). c) Cross section of the device showing the constant thickness of the electrodes and electrical field lines due to applying a potential.

In this device, the capacitance per unit length at an arbitrary point N is given by:

$$C = \varepsilon_0 \varepsilon_r \frac{t}{d} \qquad (4\text{-}1)$$

Here ε_r is permittivity of the dielectric and as can be seen in Figure 4-4, *d* is the distance between the two electrodes and *t* is the thickness of the electrodes (dimension of the electrodes into the page at point N). According to equation (4-1), the capacitance does not change from point A to B (or A´ to B´) as both electrode thickness *t*, and separation *d* remain unchanged. It must be noted, however, that equation (4-1) does not account for fringing at electrode edges. The correction factor to equation (4-1), i.e. the fringe capacitance, is given by [46]:

$$C_{fringe} \approx \left(\frac{w}{d}\right)^{0.5} \qquad (4\text{-}2)$$

where, *w* is the width of the electrodes. In contrast to equation (4-1), equation (4-2) does predict a change in capacitance from point A to B (or A´ to B´). However, as the width of the electrode does not change significantly along the electrode, and due to the 0.5

power, the change in capacitance is expected to be very small. Based on this theory the device presented in Figure 4-5 was designed. In this design, equation (4-1) predicts an increase in capacitance from point A to B (or A´ to B´) due to the decreasing value of *d*. Also, according to equation (4-2), the fringing capacitance should increase from point A to B (or A´ to B´) due to a decreasing *d* and an increasing *w*. Therefore, both the normal and fringing capacitances contribute to an overall notable increase in the value of the capacitance from points A to B (or A´ to B´) hence a more significant increase in magnitude of the electric field.

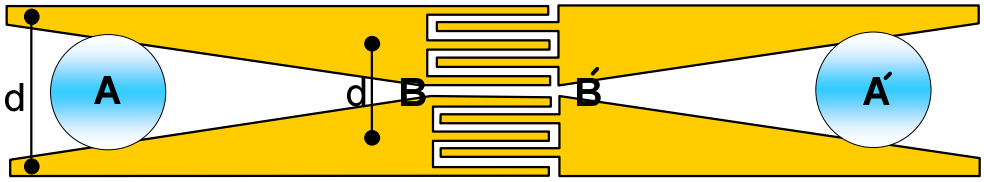

Figure 4-5 Schematic diagram of the assembled electrowetting chip for mixing. On either side are a pair of microelectrodes, the separation of which decreases towards the centre of the chip. In the central area, the structure of the electrodes is broken into a region of interdigitated fingers for mixing. The gradient capacitance and magnitude of electric field are increased by increasing the thickness of electrodes and decrease of electrodes distance d. Point A and A´ are indicating the initial position of the droplets.

Figure 4-6 illustrates the principle of operation during the application of AC electrical potentials. A droplet is placed at point A on either side of the device and a signal is applied between the pair of electrodes on the upper and lower side. The triangular shape of the electrodes produces an increasing capacitance per unit length towards the centre of the chip, since the width of the electrode increases and the separation between the electrodes decreases. One way of considering electrowetting is to consider the fluid as moving up gradients in capacitance since the energy in the system then decreases as a result. Therefore, by placing the droplet at point A and applying the voltage, the droplet will move toward point B. At this point the droplet will be held at point B due to the induction force from interdigitated and both left and right pairs of electrodes (Figure 4-6a). When the phase of, for example, the upper pair is then switched, strong electric fields are then generated in the interdigitated area, rapidly pulling both droplets into the centre, where they will mix.

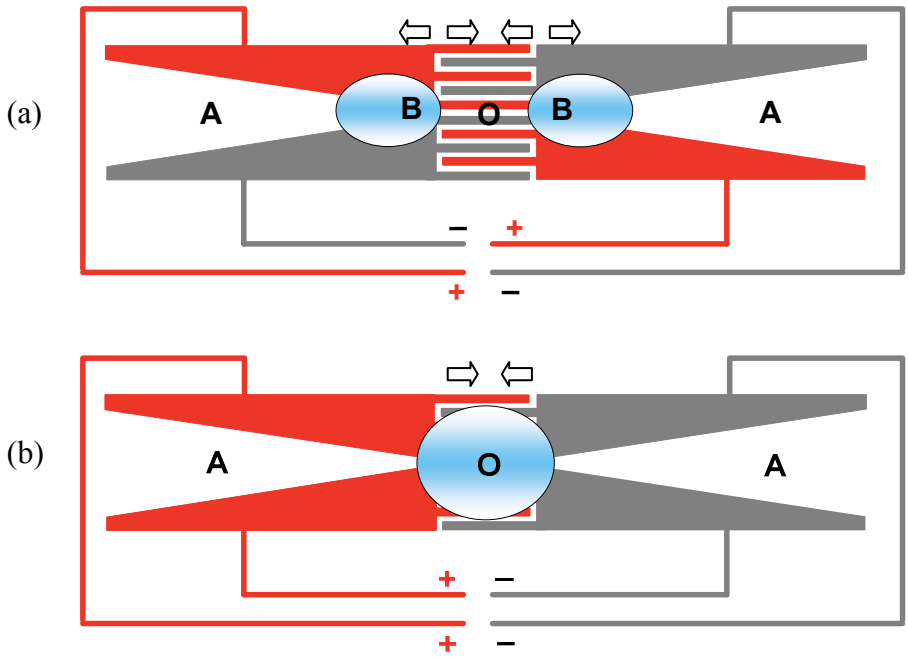

Figure 4-6 The droplets move from position A to B under the application of an electrical potential between the pair of electrodes on the upper and lower side, as indicated by the schematic power supplies. The droplets can be held at point B due to the induction force from interdigitated, left and right pairs electrodes (configuration a). Switching the lower or upper pairs result in removing the induction force and left and right pairs to be in phase (configuration b) then pulls the droplets into the central interdigitated area for mixing.

4.2.2 Fabrication of the dielectric layer

The electrode arrays were fabricated in layers of titanium and platinum by Philips at M.Plaza. The insulating dielectric layer was deposited using a combination of two different materials: two thin layers of SU-8 2000.5 which were produced a 0.7 µm thick dielectric layer and a thin layer of Cytop (0.25 µm) to provide a hydrophobic surface. The details of the coating are explained in chapter 2.

4.2.3 Experimental set up

The experimental setup is shown in Figure 3-6. The signals were applied to the electrodes using a signal generator and broadband amplifier. The signals were routed through a switched multiplexor which allowed up to nine pairs of individual electrodes to be powered as well as handling the inverting of the phases. A programme was developed in Labview to control the polarity and timing of the electrodes throughout the

experiment (see appendix). The experiments were observed using a black and white Fast-Vision-13 high speed camera since the velocities in electrowetting experiments are too fast to be observed using standard cameras. Liquid droplets of deionised water (DI water) and black ink solution with a pH = 7.2 and conductivity σ = 5.4 mS/m were positioned on the electrowetting chip using pipette dispensers.

4.2.4 Result

After coating the chip with SU-8 and Cytop, two droplets of deionised water (DI water) were positioned on the electrowetting chip using pipette dispensers. Points A and B in Figure 4-7 show the positions in which the droplets were placed. A voltage of 50 V at 1.5 kHz was applied. Polarity of electrodes 9 and 4′ were positive and polarity of electrodes 9′ and 4 were negative (see Figure 4-4). After applying the voltage as Figure 4-7 shows, the droplet experienced a decrease in contact angle so that it spread, indicating that electrowetting is the only factor that affects droplet behaviour in this device. No DEP movement of the droplet was observed even by increasing the voltage to 180 V.

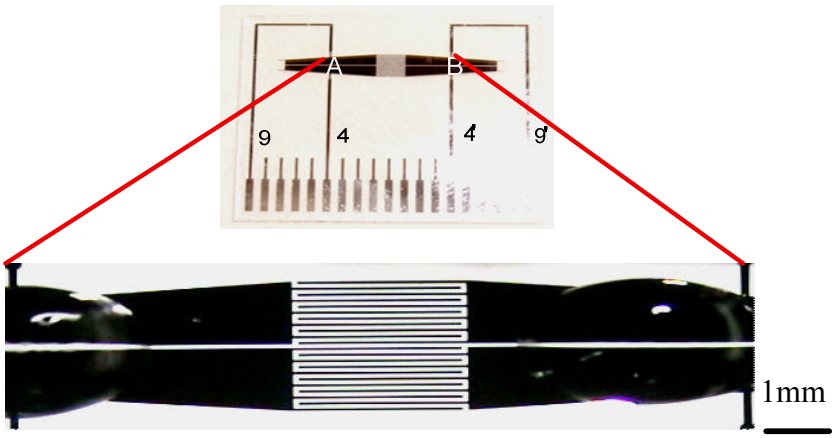

Figure 4-7 The initial design of the electrowetting chip for the mixing of two water droplets. On either side are two pairs of microelectrodes which are separated by a constant gap. In the centre of device the structure of electrodes is broken to interdigitated region for mixing. Points A and B indicate the positions of the droplet. Using this structure, resulted in two droplets just elongating by means of electrowetting.

It is clear from experimental results obtained with the chip explained above that for the droplets to move dielectrophoretically from either of the two points A and B to the

centre of the device, an increase in field gradient and hence an increase in capacitance gradient is required between the start points and the end point. The second design in Figure 4-5 was used to accomplish mixing of the two droplets. The experimental results obtained are in agreement with the principle explained earlier.

Figure 4-8 shows a captured video frame following the application of an electrical potential. The volume of the dispensed droplets was approximately 2µl, with a black ink droplet (pH = 7.2 and σ = 54 µS/cm) placed at position A and a water (DI water) droplet at B. Droplets are in contact with a thin layer of Cytop. The measured contact angle of the droplet is roughly 105° (Figure 4-9).

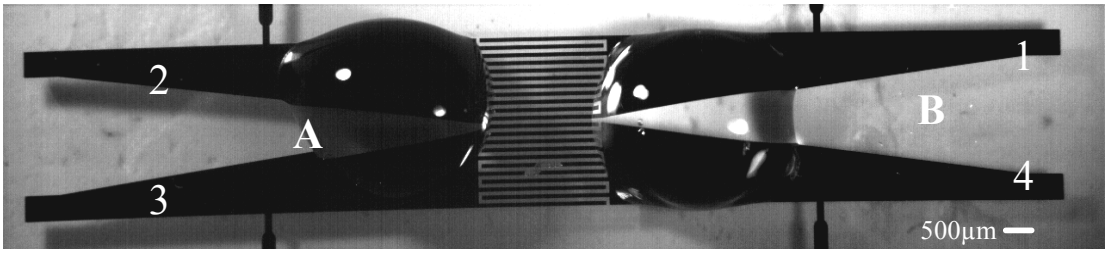

Figure 4-8 Water and ink drops are moving from point A and B toward the centre of the device. Polarity of electrodes 2 and 4 were positive and polarity of electrodes 1 and 3 were negative. Due to field opposition and force balance at the end of wedge shape electrodes and interdigitated electrodes droplets movements are stopped. To remove the induced force from the wedge shape electrodes it is required to change the polarity of either electrodes 1and 2 or 3 and 4.

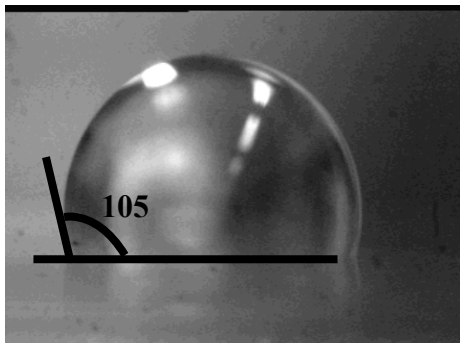

Figure 4-9 Side view of 1 µl water droplet placed on a thin film coated substrate with Cytop (0.25 µm) for the purpose of measuring the hydrophobicity of the Cytop. Water droplets on Cytop coated surface exhibit a high contact angle of 105°.

The effect of varying voltage and frequency on droplet mixing was investigated. For each case the volume of the ink and water droplets were adjusted to maintain a constant droplet diameter. The initial applied voltage was 60 V between the two electrode pairs,

1&2 and 3&4, with electrodes 1 and 2 out phase, similarly 3 and 4 (see configuration (a) Figure 4-6). After the voltage was applied, the contact angle of two droplets decreased and the droplets spread across the electrode pair at points A and B. This voltage, however, was not sufficient to induce a lateral movement. Increasing the voltage to 80 V resulted in the two droplets moving to the edges of the interdigitated electrodes which had a maximum electric field and higher capacitance. As depicted in Figure 4-8 this position was stable and due to field opposition and force balance at the end of wedge shape electrodes and interdigitated electrodes droplets movement stopped. To remove the induced force from the wedge shape electrodes it is required to change the polarity of either electrodes 1 and 2 or 3 and 4. Therefore by changing the polarity of electrodes 1 and 2 and increasing the voltage to 110 V droplets move toward the centre of the device and the two drops start to coalesce.

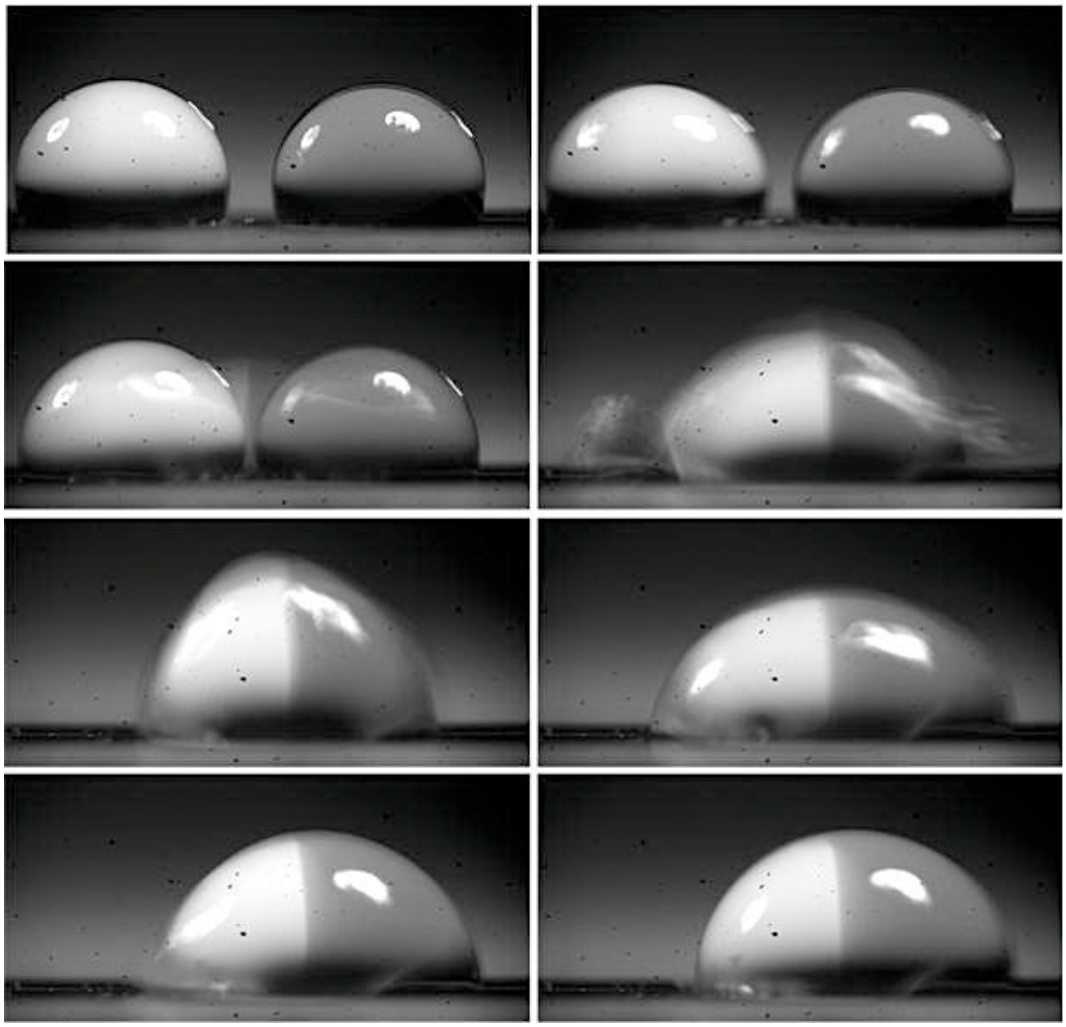

Figure 4-10 Side view of 2 µl ink and water droplets which are brought into contact for mixing by applying 110 V at 1 kHz. Two droplets formed into one within 0.014 seconds.

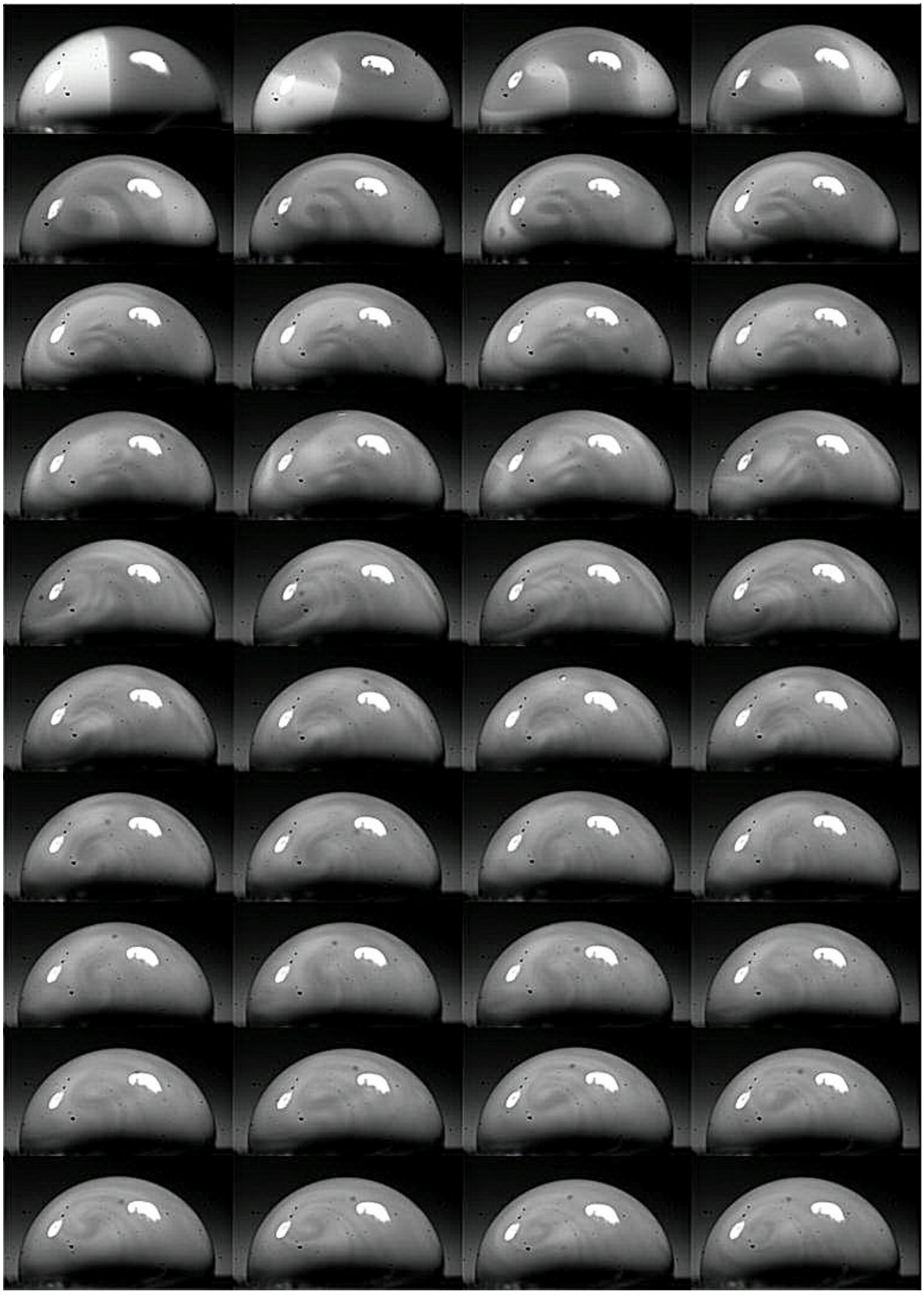

Figure 4-11 Series of images with 0.02 second intervals showing the internal diffusion of the ink and movement of the two droplets under an applied voltage of 110 V at 1 kHz.

To obtain an objective estimation of mixing time, we calculate the standard deviation of dye intensity within the droplet and normalised the data such that it decreases from maximum of 1 at the beginning of experiment to zero in the final state (Figure 4-13a-c). Droplet mixing was visualised via high speed imaging over frequency ranging from 500 Hz to 10 kHz. The most efficiency mixing achieved was at 1 kHz and 110 V. Figure 4-11 shows a series of mixing images at 1 kHz captured over a 1 second period. Droplet merging was observed to occur in 0.014 seconds, within the first 7 frames of the high speed camera (Figure 4-10). Following merging, internal rotational flow and mixing by diffusion was observed until a uniform distribution of the ink was observed.

We assumed droplets are mixed when the normalised standard deviation intensity dropped to 10% of its initial value. To determine this point the experimental data were fitted to an exponential curve. Figure 4-13a shows the mixing time at 1 kHz and 110 V is 0.55 seconds, but if the voltage is decreased to 80 V the mixing time is increased to about 1 sec (Figure 4-13b). The actual speed of the droplet increases with increasing voltage. However, it was found that increasing the voltage to more than 120 V caused insulator damage due to charging and Joule heating. For frequencies higher than 1 kHz, we observed the absence of vortex flow pattern. As shown in Figure 4-13c the estimated mixing time at 10 kHz increased to 6.5 seconds. Figure 4-12 shows a captured video frame of the experiment at 10 kHz and 110 V with vertical flow motion of droplet (flow from the top to the bottom of the droplet) which from fully circulating resulted in worse mixing time. The image was taken 2.5 seconds after coalescence.

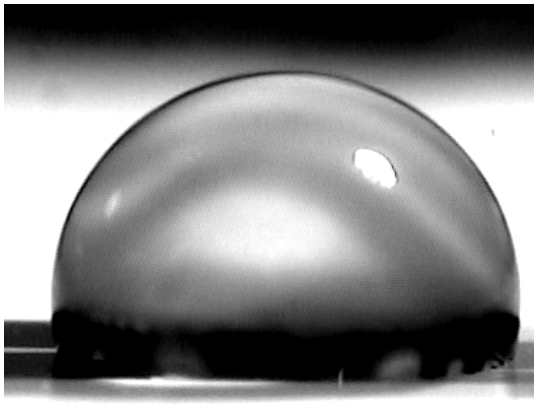

Figure 4-12 Side view of droplet mixing under applied 10 KHz frequency and 110 V. Mixing occurred with a vertical flow (flow from the top to the bottom of the droplet) which lead to delay in mixing time increasing it to 6.5 seconds.

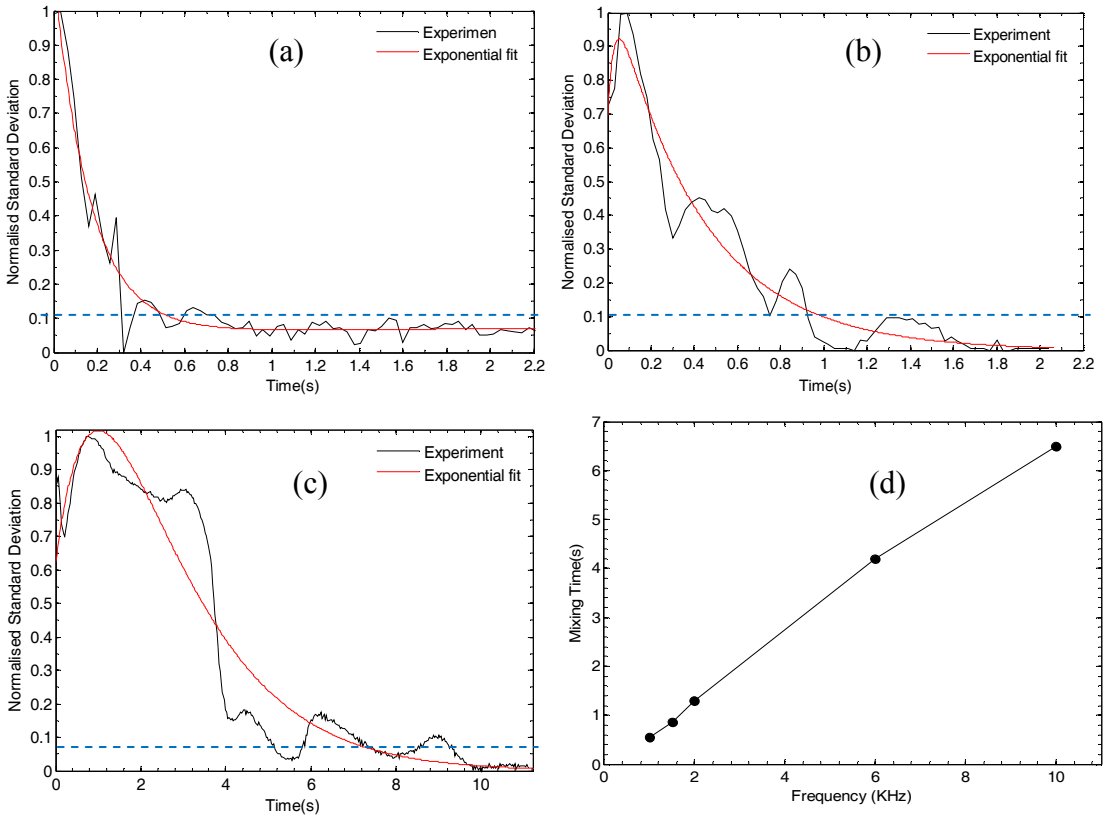

Figure 4-13 Normalised standard deviation of dye intensity variation versus time: a) 1 kHz – 110 V, b) 1 kHz – 80 V, c) 10 kHz – 110 V. The experimental results were fitted to an exponential. The dashed line indicates the mixing time. d) Performance of mixing at different frequencies.

In the low frequency region around 500 Hz, high rotating flow motion and droplet self oscillation was observed. This phenomenon at high voltage (110 V) stopped the droplet movement to the mixing area. In addition, with the voltage on continuously, bubbles were created inside the droplets and insulation break down occurred. This could possibly be caused by Joule heating. To avoid Joule heating an aluminium sheet was placed under the device and the gap between the device and aluminium sheet filled by heat sink compound to cool down the electrodes. However, this did not eliminate the problem at low frequency and high voltage. In addition parts of the insulating layer started to delaminate, it was observed as a cyclic stream within the droplet.

Figure 4-14 shows a frame with ink and water droplets which were spin rotating at 500 Hz. After applying the voltage, bubbles first appear in the ink droplet. It was found that the only way to move the droplet was by reducing the voltage, which helps to

reduce droplet spinning and further movement. However, the electric field and electrowetting force is reduced and as a result this affects the mixing process and the mixing time increases.

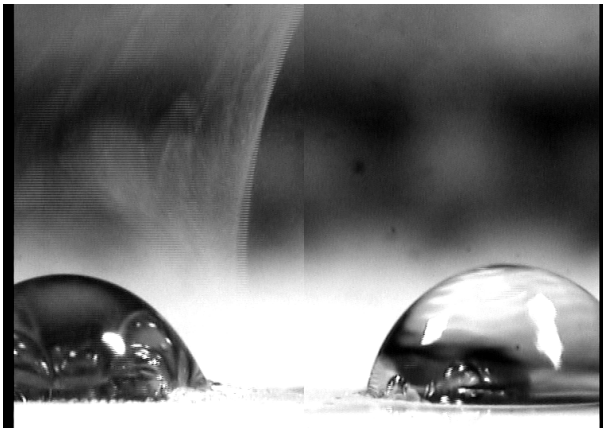

Figure 4-14 High rotating flow motion and droplet oscillation due to the application of low frequency (500 Hz). This phenomenon at high voltage (110 V) stopped droplet movement to the interdigitated region where the mixing is taking a place. With the voltage on continuously, bubbles were created inside the droplets and insulated breakdown occurred.

To determine the diffusive mixing time the passive mixing experiment was done using the same volume of water and ink droplets. Droplets were pushed together without applying a potential and the result shows mixing occurred in 16 seconds.

In conventional electrowetting as reported by Pollack and Fair (2000), droplets positioned between a grounded electrode plate and the array of individually controllable electrodes are patterned in the bottom substrate. Using this method required the solution to be confined between electrodes making it complicated to integrate into other systems and increasing the fabrication cost. In addition using this kind of set up for mixing two droplets the aspect ratio of gap height between two parallel plates and electrode size has an affect on mixing time. However, the planar electrode that is used in our experiment has few limitations on solutions that can be used but it is a simple design and has quick actuation of droplets. It is proposed that electric fields are used to guide droplets instead of using channels in the substrate and due to its planar design, could easily be combined with a wide range of microanalysis systems.

Since, EWOD is a method for manipulation of contact angle of a liquid droplet placed on insulated electrodes, the emergence of contact line manipulation of small scale droplets by EWOD is the way to create an oscillation of sessile drops induced by

contact angle change. This type of oscillatory motion has the unique capability of inducing small and large amplitude oscillations of a droplet resting on a solid surface without any additional requirements, e.g., second fluid, vibration of the solid wall etc. Some groups have used this property of the electrowetting to enhance the mixing time but it is necessary to switch the electrodes on and off sequencely in a period of time, but in our device the interdigitated electrodes were used for active mixing and to excite oscillations of droplets. It was observed that in low frequency droplets behave as a self-oscillator, therefore there is no need to turn the electrodes on and off to provide the oscillation in the droplets and enhance the mixing time.

4.3 Conclusion

A chip was designed and fabricated for droplet mixing based on electrowetting. To apply the appropriate voltage to the four independent electrodes of the chip, a control programme was developed in Labview. To investigate the performance of the chip, a droplet of deionised water and a drop containing black ink were used. The movement of the droplets in a controlled manner from the dispensing position to the centre of the device was demonstrated. The mixing process was recorded by a high speed camera. After applying a voltage, two droplets moved toward the interdigitated electrodes. However, field opposition stopped the droplets from moving to the centre. By changing the polarity of the electrodes, droplets were moved toward the centre of the device and coalescence started. The results presented show that mixing by electrowetting can be greatly speeded up through active manipulation of the droplets. The effect of varying voltage and frequency on droplet mixing was examined. The most efficient mixing was at 1 kHz and 110 V, and the results indicate that the fastest mixing of two 2 µl droplets is about 0.55 seconds.

5 Bilayer Lipid Membrane

5.1 Introduction

5.1.1 Cell membrane structure

Cell membranes (also called plasma membrane) are fundamental to the life of the cell. The plasma membrane surrounds the cell and defines its boundaries. All biological membranes include a wide range of biological molecules, proteins and lipids which are involved in a large array of cellular processes, for example cell adhesion, ion channel conductance and cell signalling. Cell membranes are dynamic, fluid structures and most of their molecules are able to move about in the plane of the membrane. The lipid molecules are arranged as a continuous double layer about 5 nm thick and surround all cells providing the cell membrane structure. The basic structure of the membrane is lipid bilayer and it works as a relatively impermeable barrier to the passage of most water-soluble molecules. Figure 5-1 shows nanoscale components in cell membrane [47].

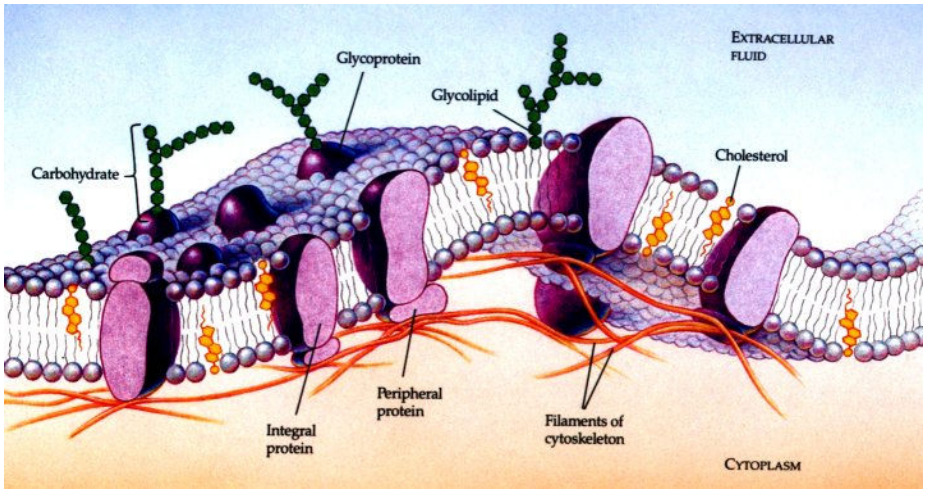

Figure 5-1 A schematic of cell membrane. The membrane is made of a self organising lipid bilayer. Taken from [48].

5.1.2 Lipid Bilayer

The lipid bilayer structure is attributable to the special properties of the lipid molecules which cause them to assemble spontaneously into bilayers even in simple artificial

condition [47]. All of the lipid molecules in cell membrane are amphipathic. The cell membranes have three classes of amphipathic lipids: phospholipids, glycolipids and steroids. However, in the majority of cases phospholipids are the most abundant [49]. Each lipid molecule has a hydrophilic (polar) head and hydrophobic (non polar) tail. The hydrophilic region is attracted to aqueous conditions while the hydrophobic region is repelled from such conditions. The phospholipid molecules polar head contains a phosphate group and two hydrophobic tails are usually fatty acids that can be different in length [47, 50]. Figure 5-2 shows the shape and the parts of a phospholipid molecule.

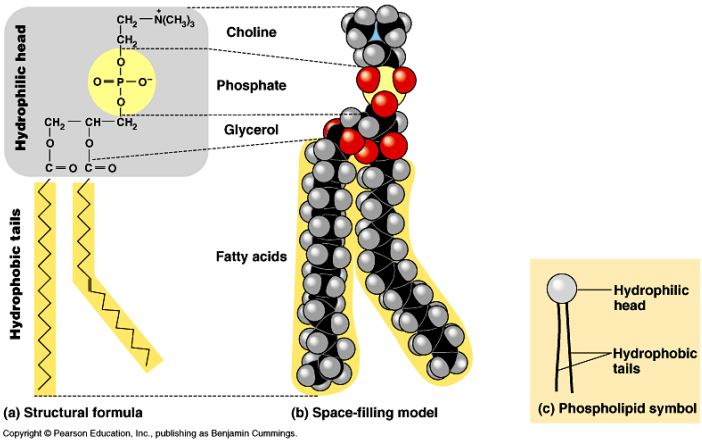

Figure 5-2 Structure of a phospholipid molecule. Taken from [51].

The shape and amphipathic nature of the lipid molecules causes them to form bilayers spontaneously in aqueous solution. When lipid molecules are surrounded by water, they tend to aggregate. Their hydrophobic tails are buried in the interior and their hydrophilic heads are exposed to water. Depending on their shape they can do it in two ways: 1) form a spherical micelle with the inner tails, 2) form a biomolecular sheet (planar bilayers), with the hydrophobic tails sandwiched between the hydrophilic head groups. This organisation is spontaneous and the process does not require energy. A lipid bilayer has other characteristics such as fluidity which is important to many membrane functions [47].

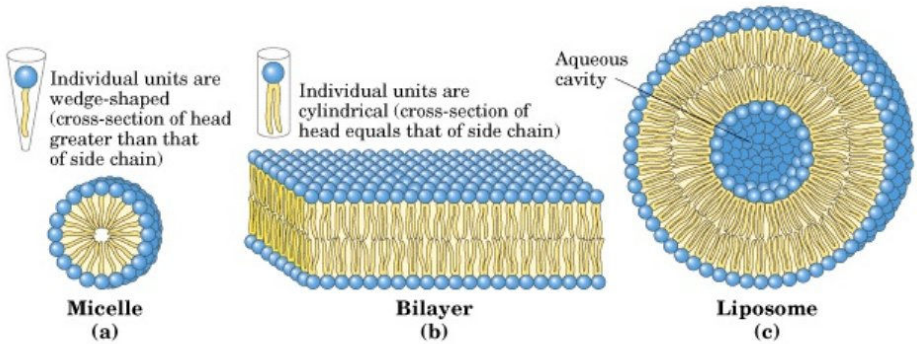

Figure 5-3 Cross section of a) Micelle (Individual units of lipid micelle are wedge shape). b) Bilayer (Individual units of lipid micelle are cylindrical shape). c) Liposome. Taken from [52].

In experimental studies, two types of artificial bilayer have been useful 1) bilayer made in the form of spherical vesicles, called liposomes, 2) planar lipid bilayers, called black lipid membrane (BLM) [47]. Three types of lipid bilayers are illustrated in Figure 5-3.

5.1.3 Artificial Lipid Bilayer

5.1.3.1 Painting Method

In 1962 Mueller-Rudin introduced a method to form an artificial planar lipid bilayer, known as a painting method [53, 54]. By using this method a bilayer is formed over a tiny aperture that connects a two sided chamber. It is possible to acquire most bilayer supplies including cup and chamber system from commercial sources. In this way, the aperture is pre-drilled in a cup then the cup fits into a chamber and is separated into two chambers with equal volume. Painted bilayers are formed by placing a small amount of lipid over the surface of the aperture the solution level is lowered by pumping out below the aperture and then raised above. It takes a few minutes for the excess solvent in the lipids covering the aperture to drain into the aqueous solution thus forming a stable bilayer [55].

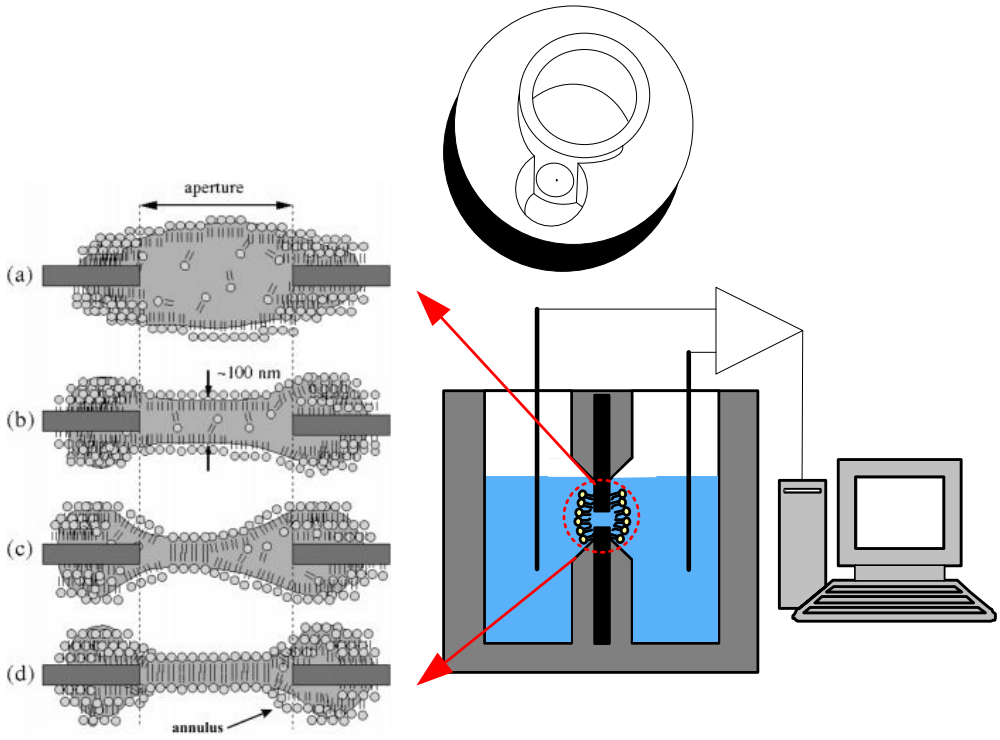

Figure 5-4 Schematic diagram of the cups using for formation of artificial lipid bilayer through the painting method. Cross section of the set up and mechanism of lipid bilayer formation, (a-d) taken from [56].

Mechanism of lipid bilayer formation assumed by Tien and Dawidowicz [56, 57] is illustrated in Figure 5-4. A thick lipid-solvent plug surrounds the aperture. Aqueous solution is on both sides of the aperture and a lipid monolayer is at the phase boundaries. If this film thins to a thickness of around 100 nm as a result of solvent drainage, random fluctuations as a result of thermal motion or mechanical vibrations can bring lipid molecules close enough for acting van der Waals forces upon them. So, by holding these molecules together, van der Waals forces act upon adjacent molecules, results thinning of a lipid bilayer [56, 58].

5.1.3.2 Folding method

In 1972 Montal-Mueller formed the bilayer by spreading lipids on the surface of the aqueous phase of each chamber while the buffer is below the level of the aperture. By rising the buffer level above the aperture, lipid monolayers from each side of the chamber form a planar lipid bilayer across the aperture [59]. Formation of the bilayer using this method is shown in Figure 5-5. The Schindler technique is basically the same

as the folding technique, except that lipids are added to the chamber in the form of liposomes [60]. The advantage of the Schindler technique is that the liposome preparation and the resulting bilayer contain minimal amounts of organic solvent.

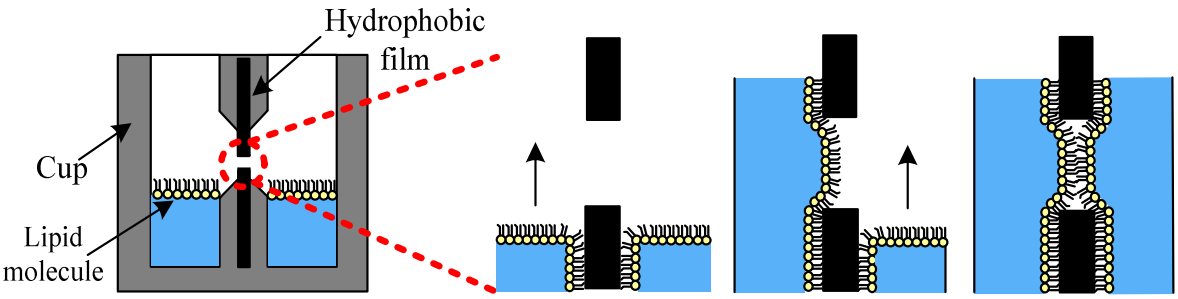

Figure 5-5 Formation of the lipid bilayer from two monolayers across the aperture, through the folding method.

5.1.3.3 Lipid bilayer on chip

Artificial bilayer lipid membrane (BLMs) techniques are important for electrophysiological studies of membrane proteins [61]. In order to combine the many benefits of microfluidics with the sensitivity and selectivity of BLM approaches, several research groups have begun developing devices and methods for forming artificial BLMs within microsystems [56, 62-71]. Initially, the majority of microdevices for BLM formation were produced using silicon micromachining techniques [63, 66-68] and the BLMs within them were created manually (e.g. by "painting" the BLM across an aperture). As there are noise problems associated with the use of silicon structures and the fabrication is time-consuming and expensive, various groups have developed alternative microdevices, including structures with apertures formed through SU8-gold layers [64] and thinned glass substrates [65]. More recently the use of polymer microfluidic BLM devices, which can be rapidly fabricated and are electrically insulating [9, 10] have been investigated. Using these devices reproducible and potentially automatable methods for forming on-chip BLMs have been developed [1], with Zagnoni et al. demonstrating that these platforms are suitable for the study of trans-membrane proteins [56, 72]. All these approaches however are similar to the classical

BLM method, in that a BLM is formed across an aperture that is surrounded by aqueous solution.

5.1.3.4 Droplet interface bilayer

An alternative approach has recently been described independently by both Holden et al. and Funakoshi et al. [73, 74]. When water droplets are immersed in a lipid-alkane solution, lipid monolayers will form at the alkane-water interface. If the two droplets are then brought into contact, a bilayer will form at the interface.

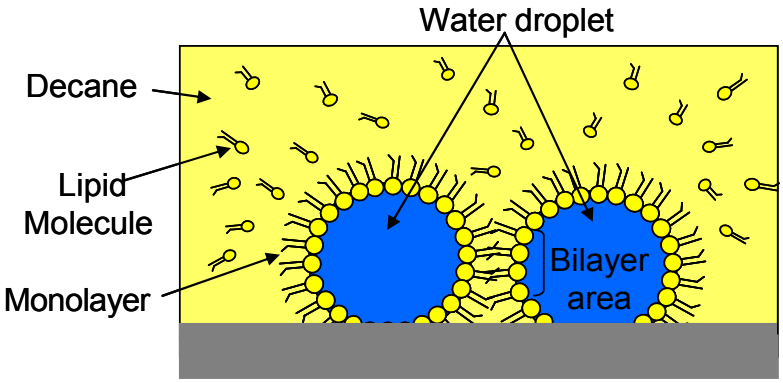

Figure 5-6 Conceptual diagram of lipid bilayer formation by contacting two lipid monolayers**.**

In 2006 Funakoshi et al. introduced this new approach by designing the double well chip [73]. The schematic of the devices is shown in Figure 5-7. Two wells, 4 mm in diameter and 2 mm in depth, were machined into a 5 mm-thick PMMA plastic plate with an overlapped area, where the width of the intersectional plane is 2 mm. The chamber is filled with 15 μL of lipid solution. Then two droplets of electrolyte (15 μL in volume), were injected into each chamber. As a result interfaces of two droplets made contact at the intersection of two wells and a bilayer formed spontaneously.

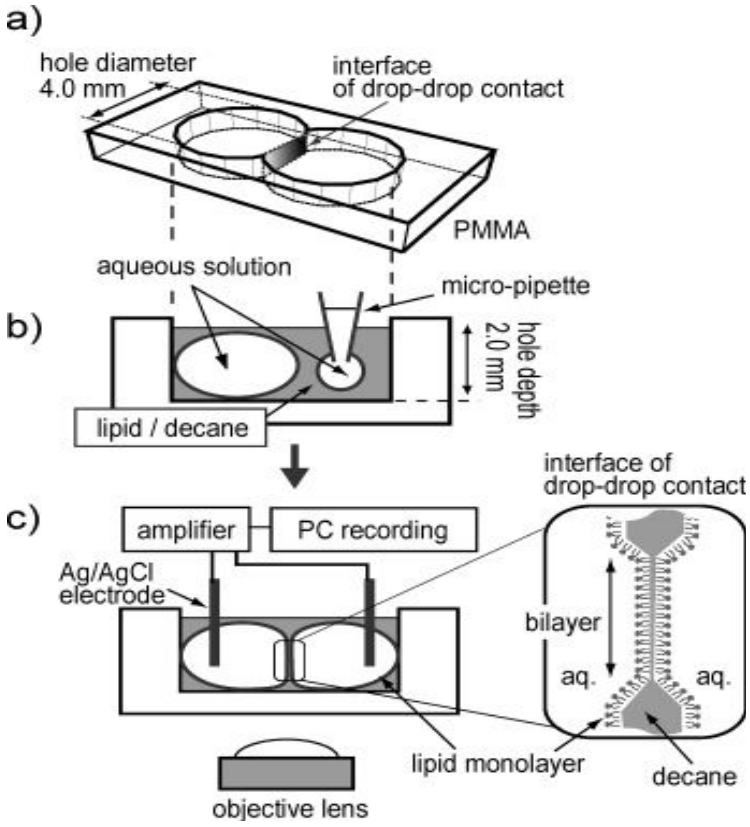

Figure 5-7 a) Outline of the double well chip. b) Two aqueous droplets are injected in each chamber filled with lipid solution; a water/ipid solution/water interface is formed at the intersection. c) Ag/AgCl electrodes are inserted in each droplet. Taken from [73].

They used coloured and non-coloured droplets (Figure 5-8) and found that these droplets stayed unmixed for a long period of time (more than 1 hour) and this system is stable for formation of multiple membranes. After contacting the two droplets using the double well chip at t = 0 the capacitive transient current increased to reach the stable value (t =150 seconds). The capacitance at this time was reported to be 25 nF. The observation of the functions of the membrane proteins incorporated into the bilayer is one way to prove that the bilayer had been formed, so reconstitution of the peptide ion channel, α-HL, which passes ions and small molecules was used. The current steps that corresponded to the incorporation of single α-HL pores into the lipid bilayer are shown in Figure 5-8.

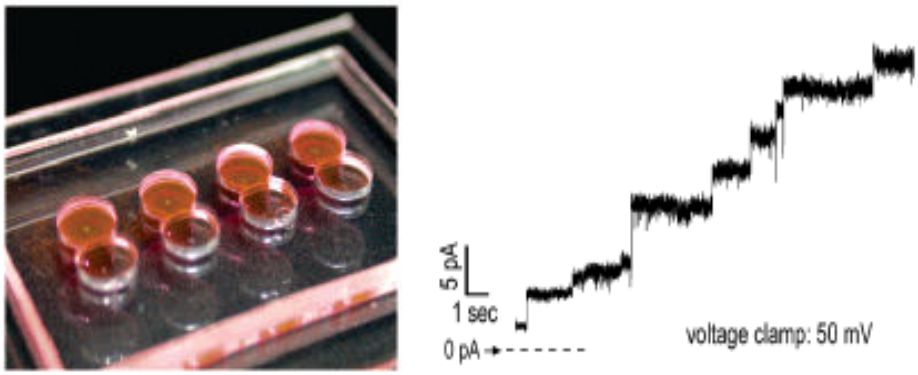

Figure 5-8 Single channel current through α-hemolysin nanopores incorporated into the lipid bilayer formed in the double well chip. Ion current across the membrane was recorded at 50 mV. Taken from [73].

Additionally, Funakoshi et al. used the idea of the formation of the lipid bilayer by contacting two lipid monolayers to make a "cross-channel chip" [73]. By using this device the two interfaces are brought together at the cross section of two microchannels by controlling via syringe pumps. The schematic of the cross-channel is shown in Figure 5-9. For formation of the lipid bilayer the aqueous solution was injected via two opposite inlets of one channel then lipid solution was injected into the crossing channel. The interface between the water and lipid solution was contacted by pushing opposing electrolytes.

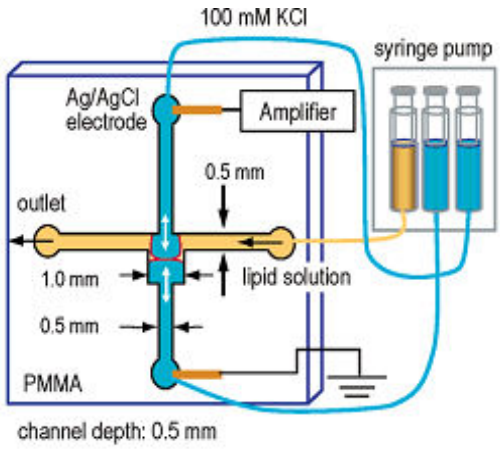

Figure 5-9 Schematic of the cross-channel chip. Two opposing inlet ports were connected to syringes containing electrolyte and one port in the crossing channel was connected to that with lipid solution Two aqueous solutions with lipid solution in between made contact at the cross section to form a BLM. Taken from [73].

During 2007 Holden et al. found that when two 200 nL water droplets were placed under the lipid solution and brought immediately into contact, they fused into a single droplet in less than 1 minute. therefore in their first approach they kept two droplets separated under the lipid bath for 30 minutes before bringing them into contact.

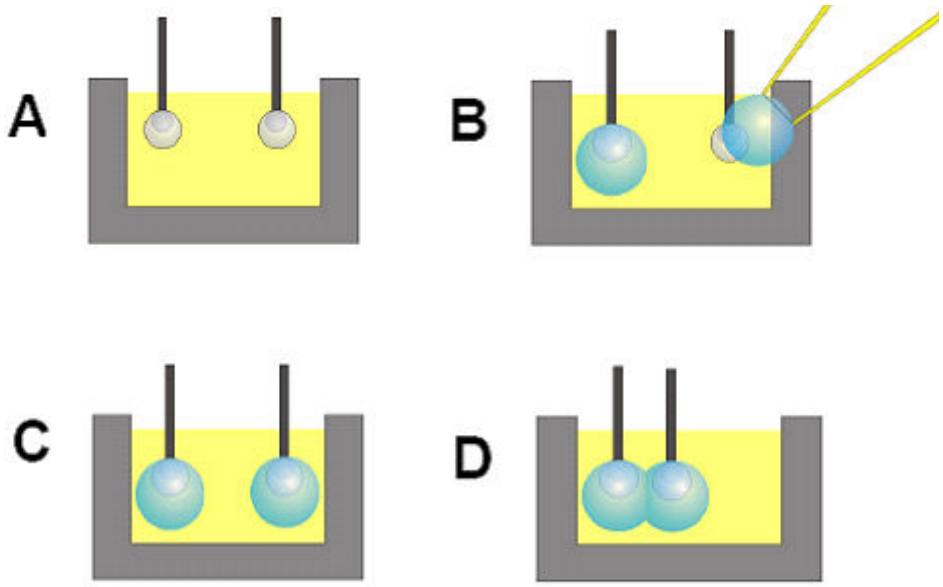

Figure 5-10 a) Two Ag/AgCl electrodes were coated with agarose gel at the tip and then submerged under lipid bath. b) A 200 nL aqueous droplet was hung from each electrode. c) The droplets were stabilised in the oil for thirty minutes. d) The two droplets were brought in contact by using a micromanipulator and a bilayer spontaneously formed. Taken from [74].

Figure 5-10 shows the process of formation of droplet interface bilayer by hanging two aqueous droplets from Ag/AgCl electrodes whose ends were coated with 5% agarose gel and submerged under lipid solution [74]. In this experiment the droplets were brought into contact after 30 minutes, by using micromanipulator and a bilayer formed at the interface of two droplets and it was monitored by measuring the capacitance. By using a specific capacitance of 0.65 $\mu F/cm^2$, they estimated the contact area between droplets to be 450 μm^2. Recording through proteins in single droplet interface bilayer is shown in Figure 5-11. The left-hand droplet contained α-hemolysin while the right hand droplet contained γ-cyclodextrin (γCD) in the same buffer as the other droplet. The (γCD) binds to the α-HL pore and acts as a reversible blocker. Current levels 0, 1, and 2 in Figure 5-11 shows the ionic current recording at 0 mV, through the pore with γCD bound and through the open pore at -50 mV respectively.

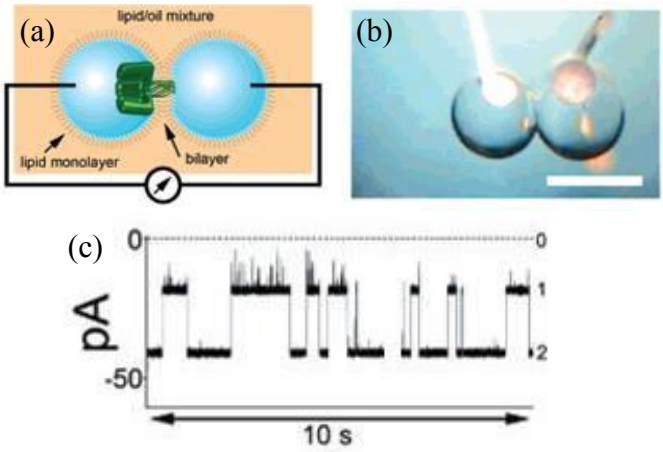

Figure 5-11 a) Single bilayers were formed by hanging a pair of droplets from electrodes under an oil/lipid mixture. b) The droplets brought into contact using a micromanipulator after 30 minutes the α-HL pores inserted into the DIB and electrical measurements were made. c) Ionic current recording. Taken from [74].

In addition Holden et al. used this new technique to form a lipid bilayer to create a multiple bilayer in a network of droplets. For this purpose they used a Perspex surface with a square array of micromachined dimples (egg-crate). As is shown in Figure 5-12 the first drop was deposited on an Ag/AgCl electrode which was placed on the bottom of the device by using a pipette. Then a 20 cm long tube is filled with DPhPC in hexadecane. Droplets were added into the top. As the droplet approached the bottom, the tube was inverted and the tip placed into the lipid bath. Droplets fall into the dimples below and this sequence was repeated to place all the droplets into the device. The last droplet connects the rest of the network to the droplet containing the fixed electrode.

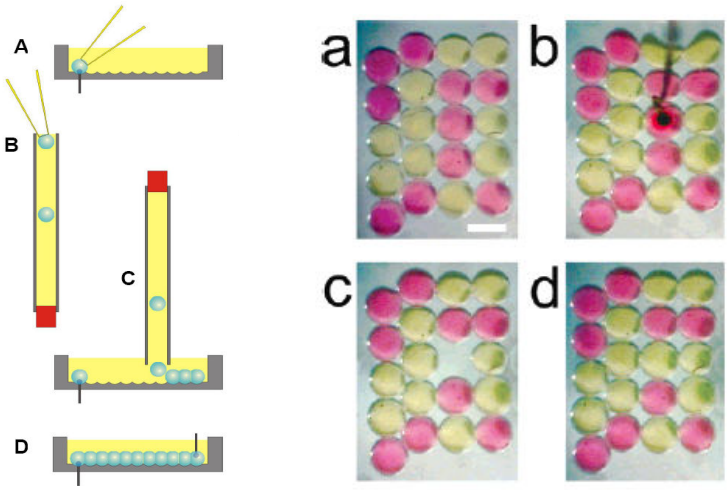

Figure 5-12 Schematic of the formation of a droplet interface network. Droplets were stabilized separately and then transferred one-at-a-time to form a network (A-D). Droplet interface bilayer network (a-d). Twenty droplets were arranged on a Perspex surface with a square array of indentations under lipid/oil mixture. Taken from [74].

When a droplet was added, it connected to its neighbours. The interface between the droplets was stable to mechanical perturbation. Extracting any droplet from the network through an agarose gel coated Ag/AgCl electrode controlled by micromanipulator was possible. Further, a missing droplet could be easily replaced by another stabilising droplet. The new droplet spontaneously integrated into the network. Formation of the droplet interface bilayer network has applications to the creation of biosensors. By using a network of three droplets a biobattery was formed.

In 2010 Stanley et al. introduced a new method of automatic formation of BLMs at the interface of the droplet. In this method water in oil droplets were pumped into polytetrafluoroethylene tubing. The device included four tubes to create uniform flow through the channel. The schematic of the setup is demonstrated in Figure 5-13. By using this system the complex networks of droplet interface bilayer formed in three dimensions for the first time [75].

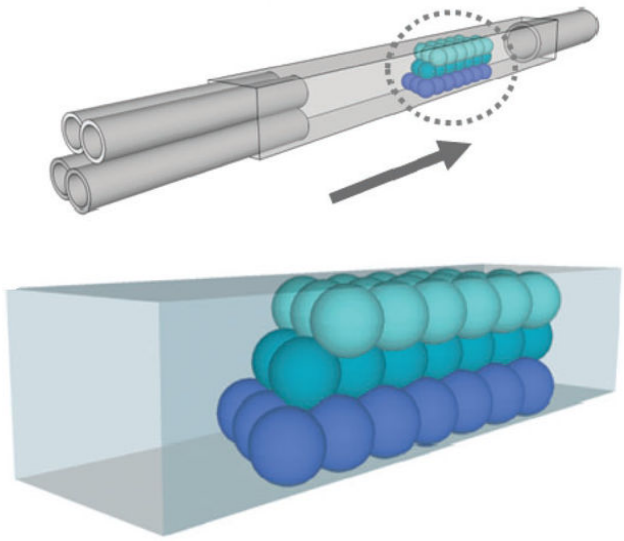

Figure 5-13 A Schematic diagram of the set up for formation of droplet interface network in 3D. Droplets uniformly pumped into the channel, when the droplets come into contact a bilayer forms at the interface of the droplets. Taken from [75].

5.2 Formation of Artificial Lipid Bilayer using Electrodynamic techniques

A number of experiments have been performed in order to investigate the formation of artificial BLMs at the interface of aqueous droplets that are manipulated manually. Here we developed the new method to manipulate the droplets in the presence of an electric

field. The droplets were submerged in an organic solvent-lipid phase and the movement of the aqueous droplets was controlled by EWOD chip which was previously designed and fabricated for mixing of droplets. This method of droplet manipulation is simple, amenable to automation and integration with other fluidic functions. First the behaviour of a droplet in lipid organic solvent in the absence of an electric field was investigated, then droplet manipulation via applying a potential in respect of voltage and frequency was studied and finally formation of droplet bilayer interface was achieved. By incorporating peptides into the droplet buffer, single channel recordings across the droplet-interface bilayer were acquired for both gramicidin and α-hemolysin. In addition we demonstrated that by using this approach a series of droplets can be manipulated to form a BLM network.

5.2.1 Study of the contact angle and surfactant behaviour

To determine the behavior of an aqueous droplet in contact with different surfaces, whilst immersed in an organic phase, contact angle measurements were performed using three different surfaces (glass, Cytop and SU8). Two organic phases were tested, n-decane and an asolectin-decane solution (20 mg/ml).

5.2.1.1 Contact angle measurement set up

The microscope for measuring the contact angle contains a 7X precision zoom lens which are high quality modular video lenses that provide high resolution and large depth of field. The complete optical system consists of TV tube, upper zoom module and lower module. The focusable lower modules allow for 10 mm of internal focus. The camera is attached to the set up and software is installed to create a contact angle measurement instrument. The contact angle is obtained by using ImageJ software

5.2.1.2 Result

For a pure decane solution the water droplet behaved as expected with respect to the surface: on a hydrophobic surface, such as the fluoropolymer Cytop, the droplet did not wet the surface, whilst on hydrophilic surface such as glass, wetting was clearly observed (Figure 5-14). In both cases no variation in contact angle was measured over a period of 600 seconds from the dispensing time.

Time (sec)	Cytop Decane	Glass Decane
t = 15 sec	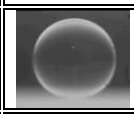	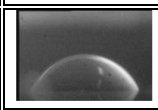
t = 30 sec	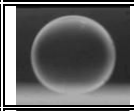	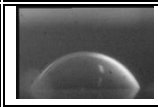
t = 45 sec	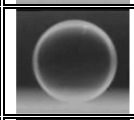	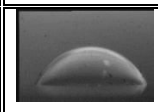
t = 60 sec	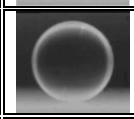	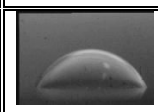
t = 120 sec	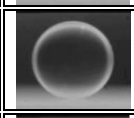	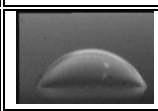
t = 600 sec	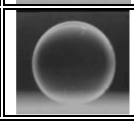	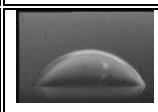

Figure 5-14 Behavior of 0.5 µl droplet of water in contact with hydrophobic and hydrophilic surface in decane alone.

However when using an asolectin-decane solution, the following points were observed: 1) irrespective of the type of surface used (hydrophobic or hydrophilic) the droplet does not wet the surface. 2) The contact angle changes with time. 3) Maximum variation in the contact angle occurs within the first 90 seconds from the time the droplet is released. 4) The more hydrophilic the surface, the more the difference between the initial and final contact angles. The initial contact angle θ_0 and the final contact angle θ_F are the values of θ at t = 15 seconds and t = 900 seconds respectively. 5) Three different surfaces were used and it was observed that the initial and final contact angle correlate with the hydrophobicities of the surfaces. In other words:

$$\theta_0 \text{ (Cytop)} > \theta_0 \text{ (SU8)} > \theta_0 \text{ (Glass)}$$

and

$$\theta_F \text{ (Cytop)} > \theta_F \text{ (SU8)} > \theta_F \text{ (Glass)}$$

The quantity $\Delta\theta = \theta_F - \theta_0$ follows the same pattern:

$$\Delta\theta \text{ (Cytop)} > \Delta\theta \text{ (SU8)} > \Delta\theta \text{ (Glass)}$$

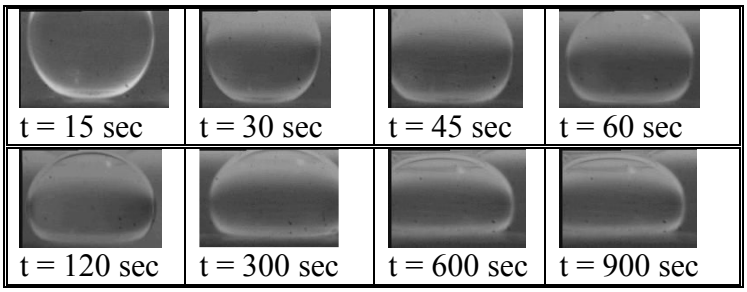

Time (sec)	Contact angle (degree)
15	158
30	160
45	163
60	164
120	165
300	167
600	168
900	168

Figure 5-15 The contact angle and shape of a 2 µl droplet of water in contact with Cytop in lipid and decane solution 900 seconds after dispensing.

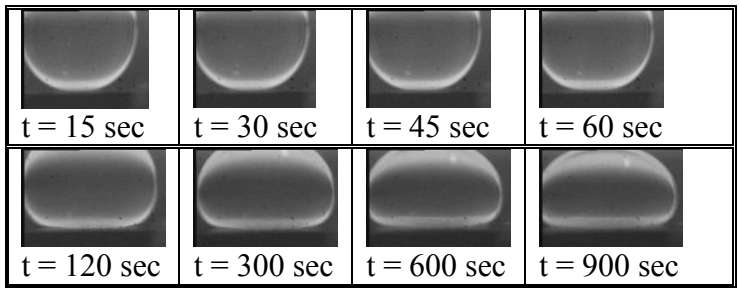

Time (sec)	Contact angle (degree)
15	152
30	156
45	159
60	159
120	165
300	167
600	167
900	167

Figure 5-16 Behaviour of a 2 µl droplet of water in contact with SU8 in lipid and decane solution over 900 seconds after dispensing.

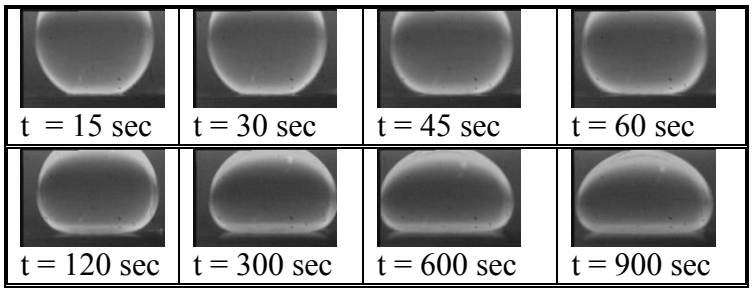

Time (sec)	Contact angle (degree)
15	145
30	146
45	157
60	160
120	162
300	164
600	164
900	164

Figure 5-17 Behaviour and contact angle of a 2µl droplet of water in contact with Glass in lipid and decane solution over the period of 900 seconds.

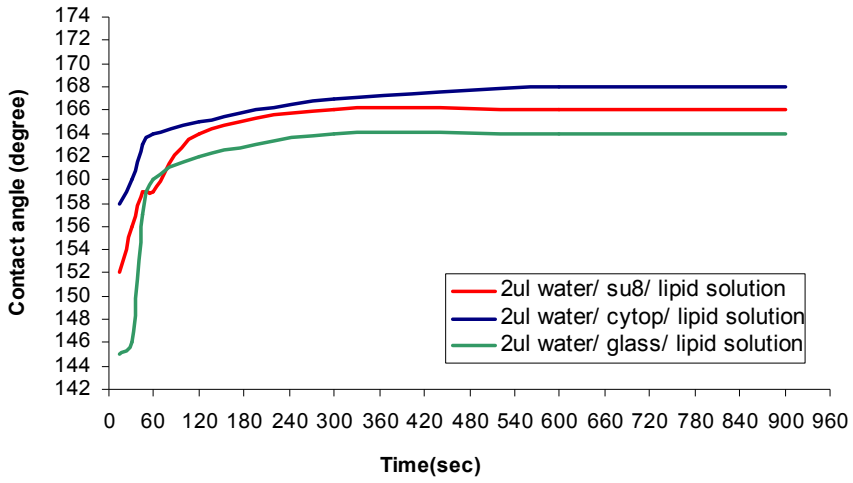

Figure 5-18 Variation of contact angle over time for 2 µl droplet of water in contact with three different surfaces in lipid-decane solution.

These results may be attributable to intermolecular forces i.e. van der Waals forces pulling the lipid molecules together with the surfactant governing the behaviour of the whole system. As well as clearly illustrating the strong effect of the surfactant, these results show that it is not necessary to use a highly hydrophobic surface for the manipulation of aqueous droplets within an alkane-lipid phase, a hydrophobic surface is

normally required for the movement of aqueous droplets in air. Additionally after dispensing the droplets, it is best to wait for a few minutes in order for the droplet shape to stabilise sufficiently.

5.2.2 Bilayer formation device

The device that was fabricated to study bilayer formation is show in Figure 5-19a. As depicted in Figure 5-19b, this device consists of six pairs of individually addressable electrodes that are used to produce the desired electrostatic field. The electrodes were coated with a 0.7 µm insulating layer of SU8. A plastic reservoir was bonded to the surface of the device to contain the lipid-decane solution and the electrodes were connected to an AC frequency generator and amplifier via an electronic switching circuit. By immersing a droplet of water in point A and applying a potential between the outer and inner electrode pairs (4-4', 3-3'), a non-uniform electric field is established inside the liquid body. This, results in a pressure difference between the right and left boundaries and the electrified pressure difference generates a fluid flow towards point B.

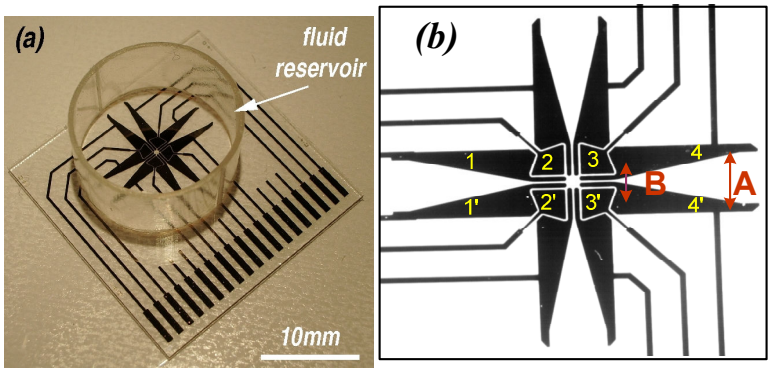

Figure 5-19 a) the device for producing BLMs. b) Top view of the electrowetting device. Points A and B are the regions with the lowest and highest capacitance per unit area respectively.

5.2.2.1 Electric field simulation

A finite element model of the device is simulated using Comsol Multiphysics to obtain the electric field distribution around the electrodes. Since the design is symmetric with respect to two in plane axes, a 3D quarter model is used to save computation effort and time. In order to solve the model, a stationary time-harmonic analysis is carried out with

the frequency set to 2 kHz. The environment of the electrodes is defined as air with relative permittivity of 1. As for the boundary conditions, an AC electric potential of 20 V is set on the actuation electrode and 0 V for the ground electrode. All external boundaries are defined to be electrically insulated. The inner symmetry planes are defined as port variables and set to have constant voltage so that the model is defined to be symmetric with respect to these planes. Figure 5-20a,b show the electric field distribution obtained with the parameters and conditions stated above. These results are obtained when (a) a voltage is applied between the electrode pairs 3-3' and 4-4' (Figure 5-19) and (b) a voltage is applied between the electrode pair 3-3'. The colour bar shows electric field intensity in Vm^{-1}(minimum (blue), maximum (red)).

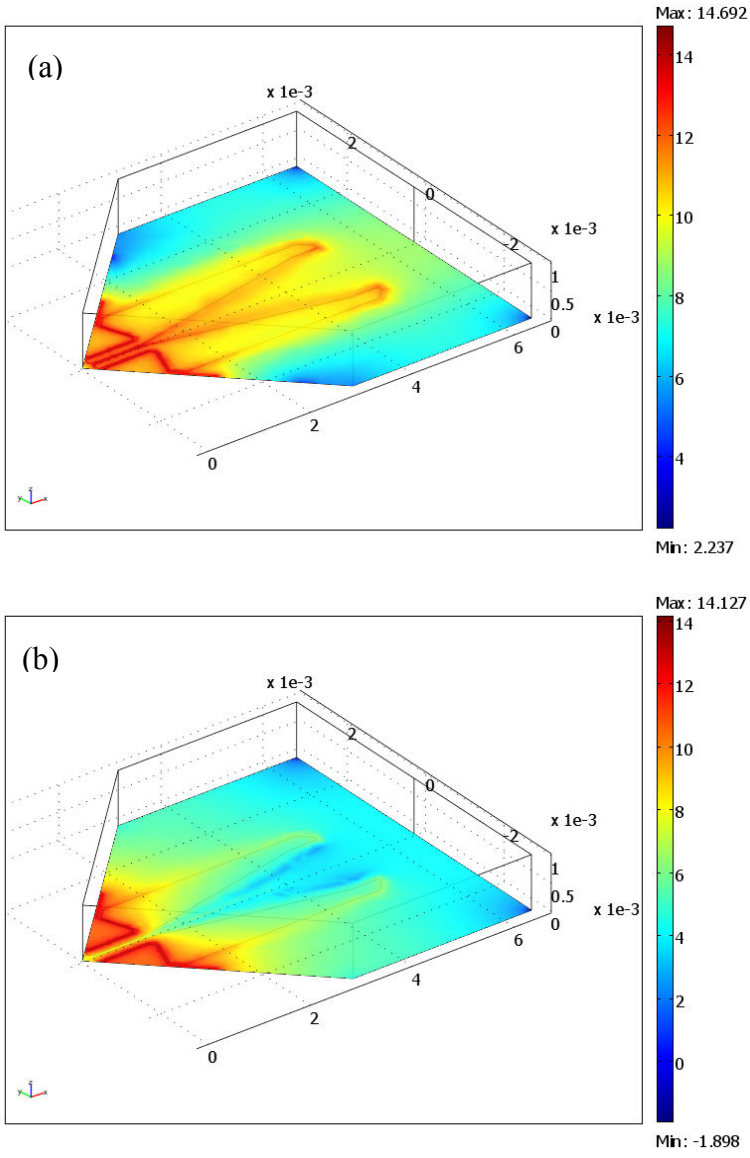

Figure 5-20 The electric field magnitude when the voltage is applied between the electrode pairs 3-3' and 4-4'from Figure 5-19. The regions between the inner and outer electrode pairs have the high electric field. b) Electric field distribution when the voltage is removed from the electrode pair 4-4'. The highest electric field strength moves to the centre of the device.

By applying a potential between electrode pairs 4-4' and 3-3', the highest field strength is located in the region between the inner and outer electrode pairs (Figure 5-20a). Then by holding the voltage between the electrode pairs 3-3' and removing the voltage from electrode pair 4-4', the region of highest field strength moves to the centre of the device (Figure 5-20b). Therefore in the first case if a droplet is placed at the far end of the wedge shape electrodes, after applying a voltage the droplet experiences a positive DEP and moves to the region between the inner and outer electrode pairs. At this point the force induced from inner and outer electrodes to the droplet is in balance and for further droplet movement the voltage must be removed from the outer electrodes and the droplets will move to the centre of the device. These two electric field distributions were employed to form a BLM by manipulating the aqueous droplets.

5.2.2.2 BLM formation protocol

After filling the plastic reservoir with asolectin in n-decane (20 mg mL^{-1}), two 2 μL droplets of 100 mM KCl were injected onto the outer electrodes, as illustrated in Figure 5-21a. The phospholipids self-assemble at the interface between the two phases to form a monolayer. The KCl droplets were then moved towards one another by applying a potential between the four electrode pairs 1-1', 2-2', 3-3'and 4-4' (Figure 5-21a). This positioned the droplets at the regions between the inner (2-2' and 3-3') and outer (1-1' and 4-4') electrode pairs, where the electric field is strongest (Figure 5-21b).

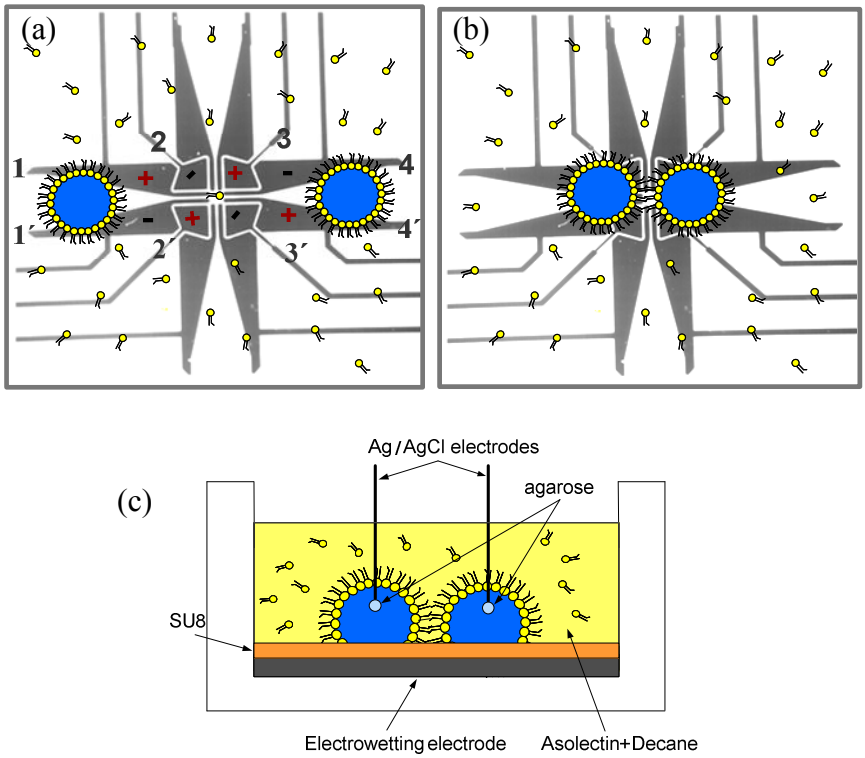

Figure 5-21 The device employed comprised six pairs of individually-addressable, thin-film microelectrodes, patterned on a glass substrate. a) Top view of the initial and final position of the droplets on the device. b) Lipid bilayers were formed by contacting the lipid monolayers at the interface of two aqueous droplets. c) Side view of the experimental set up, showing the electrode and dielectric (SU8) layers. Ag/AgCl electrodes are immersed into the droplets for measuring the capacitance and current across the interface.

Before the two droplets were brought into contact, Ag/AgCl electrodes were inserted into each droplet, so as to measure the capacitance between the two droplets. A lower potential was then applied to the electrode pairs 2-2' and 3-3'only (so that the strongest electric field region was then in the centre of the device, Figure 5-20b) to bring the droplets slowly into contact (Figure 5-21b). The applied voltage was then gradually decreased to zero.

5.2.3 Experimental Set up

The experimental set up which was used for formation of droplet interface bilayer is shown in Figure 5-22. The set up consists of a microscope, the electrowetting device, a camera, an amplifier connected to a high voltage to provide the required voltage for the electrodes, a switch box for turning the electrodes on and off and Ag/AgCl electrodes

for measuring the capacitance and current across the droplet interface (where the bilayer is formed). The Ag/AgCl electrodes were connected to the head stage of a patch clamp amplifier through which a DC voltage is applied to the bilayer. To reduce the external noise on measurements, the microscope, camera and the head stage were kept in a faraday cage. The measurement data was produced by recording the voltage at the output of the amplifier via a DAQ card. The program to record the data was written in Labview.

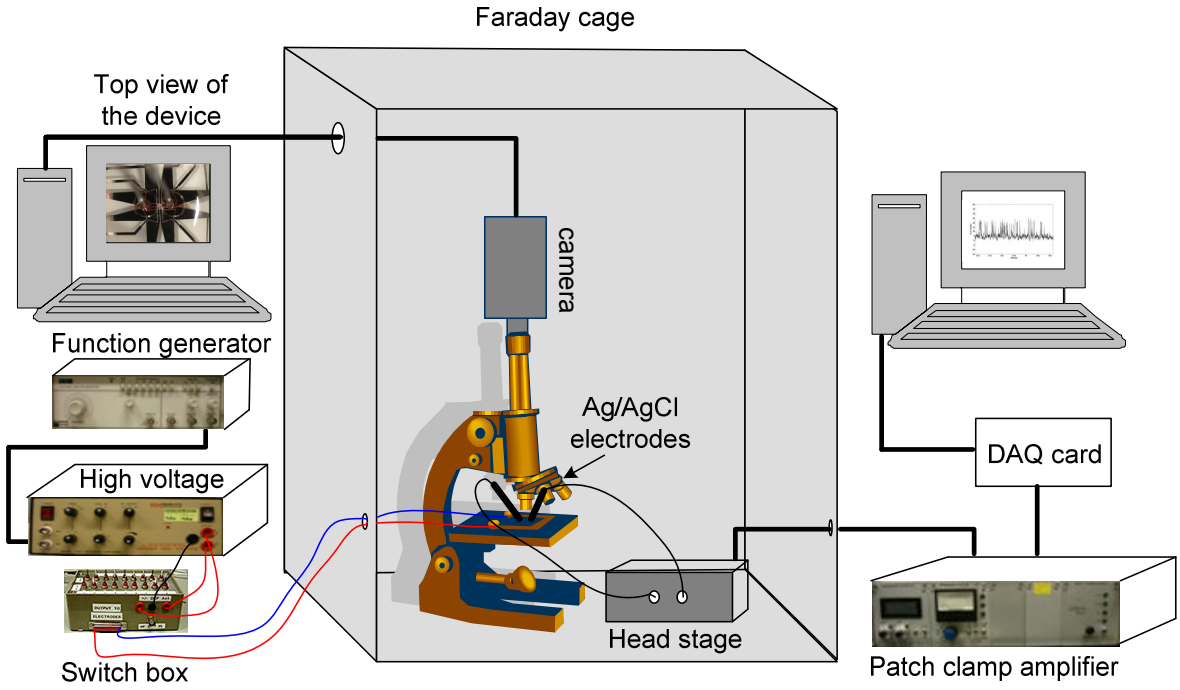

Figure 5-22 The experimental set up that comprises: a microscope and camera; a high voltage power supply and amplifier (Krohn-Hite Corporation, USA) that are connected to the EWOD electrodes via a switching circuit that enables the electrode pairs to be individually addressed; and a high sensitivity BLM amplifier and headstage (Industrial Developments Bangor, Bangor, UK) that were connected to the Ag/AgCl electrodes. The EWOD device, headstage, microscope and camera were placed within a Faraday cage.

5.2.4 Droplet manipulation

5.2.4.1 Effect of voltage and frequency on droplet movement

A number of experiments were performed in order to find the optimal voltage and frequency ranges for moving a droplet from point 1 to point 4 (see Figure 5-23) in the

lipid decane environment. It was observed that at low frequencies (in the range of Hz), the voltage required for moving a droplet was highest and by increasing the frequency threshold voltage is decreased. The movement of droplets were more controllable in the frequency range of 1-10 kHz where droplets moved from position 1 to position 4 in three steps.

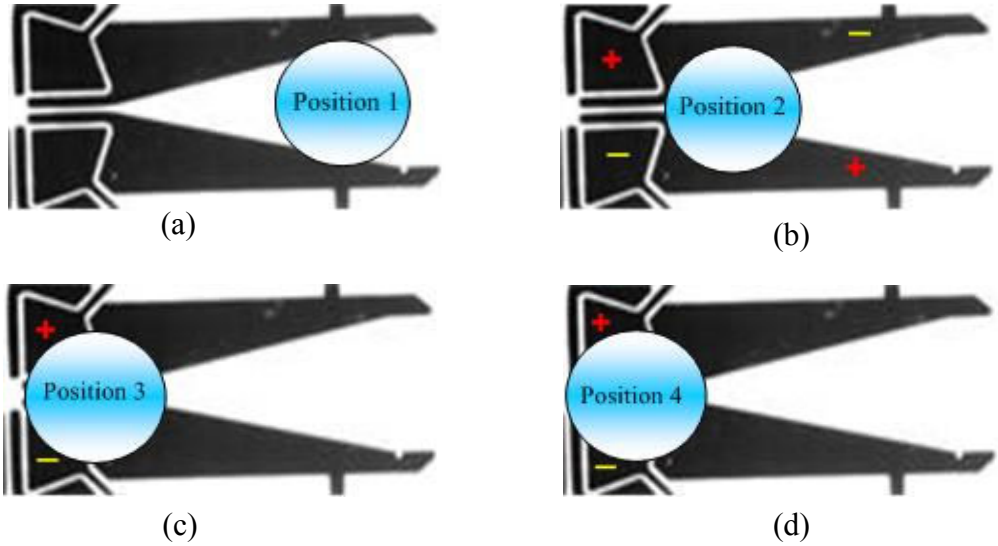

Figure 5-23 (a) Initial position of the droplet. By apply a potential between outer and inner electrodes droplet moves to position 2 (b) and by removing the potential from outer electrodes and applying a lower voltage into the inner electrodes droplet moves to position 3 (c). Then by stopping the droplets and applying even a low voltage into inner electrodes droplets moved slowly to the centre of the device (position4).

In the first step, a voltage is applied between the outer electrodes (4-4') in order to move the droplets from position 1 to position 2. The voltages required for droplet movement were measured at different frequencies and the results are plotted in Figure 5-24. When the droplet reached the second position, the voltage was removed from the electrodes (4-4'). In step 2, lower voltages were applied to the inner electrodes (the average voltage at 2 kHz was 8 V_{rms}) and the droplet moved to position 3. Finally in step 3, the required voltage for droplet movement from third position to fourth was even lower (about 3 V_{rms}).

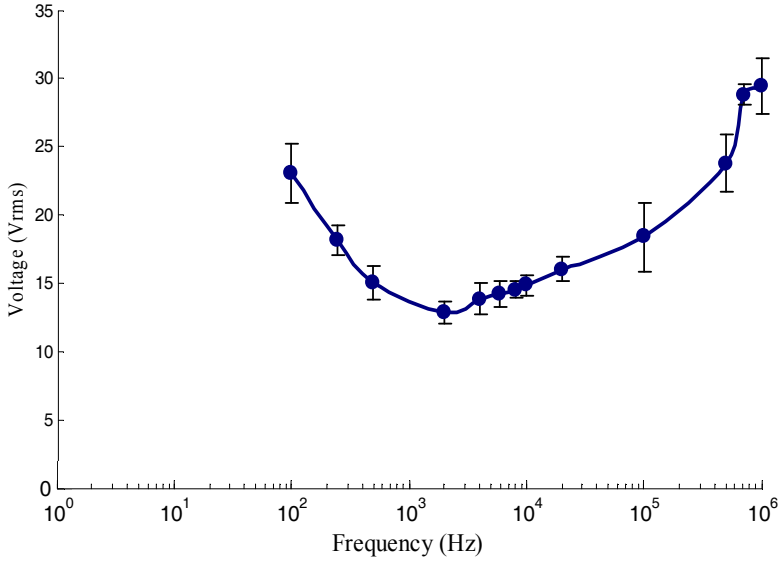

Figure 5-24 The voltages required for droplet movement from position 1 to position 2 versus frequency in the case of water droplet in lipid solution

The voltage required to move a droplet was frequency-dependent. Over the frequency range 100 Hz to 1 MHz, it was found that the lowest voltages required for droplet movement were in the range 1-10 kHz and a value of 2 kHz was chosen for all experiments.

5.2.5 Formation of droplet interface bilayer

Figure 5-25 shows the initial position of the droplets. As suggested in the Holden papers [74, 76], the droplets were left in the lipid solution for 30 minutes to stabilise. Surprisingly, it was observed that after 15 minutes a white layer started to grow from the bottom of the droplets (Figure 5-25) and completely covered the droplet. Inserting the Ag/AgCl electrodes to measure the capacitance of the lipid bilayer was necessary but the droplets were free in the lipid bath and it was difficult to immerse the electrodes into the droplets. This was made possible by increasing the stabilisation time for about another hour. Figure 5-25b shows the position of the droplets after applying the voltage to move the droplets closer and stabilise them for an hour. At this time it was obvious that the thick white layer had covered the droplets (Figure 5-25b). By inserting the Ag/AgCl electrodes into the droplets, the white layer was broken (Figure 5-25c) but it self repaired after about 5-10 minutes. While these electrodes were inside the droplets a

voltage was applied to the electrodes in order to bring the two droplets into contact (Figure 5-25d). The bilayer was monitored by measuring the capacitance, but as shown in Figure 5-26, the capacitance values were much smaller than expected (around 5 pF). This low capacitance could be due to the lipid itself, because asolectin lipid is a mixture of different lipids not a pure lipid. Another possible explanation is due to the long stabilisation time after which, a multi layer may be created instead of the monolayer at the interface of the droplet.

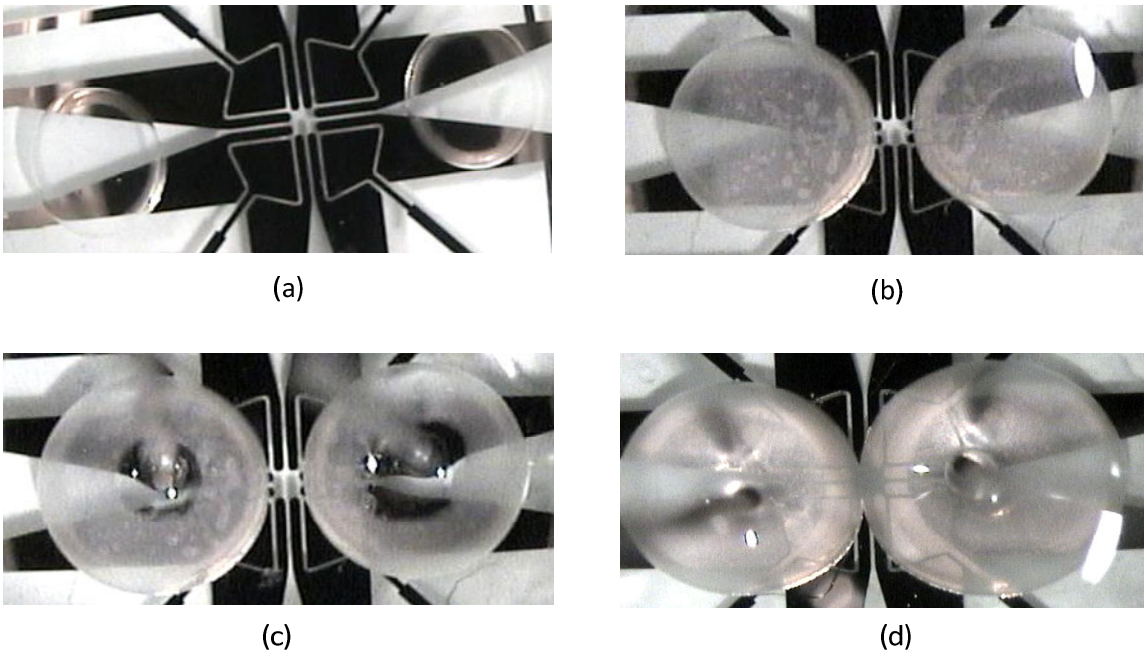

Figure 5-25 a) Initial position of 3 µl water droplets in an asolectin in n-decane solution b) After 30 minutes the droplets were brought closer and stayed at this position for another hour. The thick white layer covered the droplets. c) Ag/AgCl electrodes inserted to the droplets, resulting the broken white layer. d) After 5-10 minutes the broken layers were rebuilt and two droplets were brought into contact.

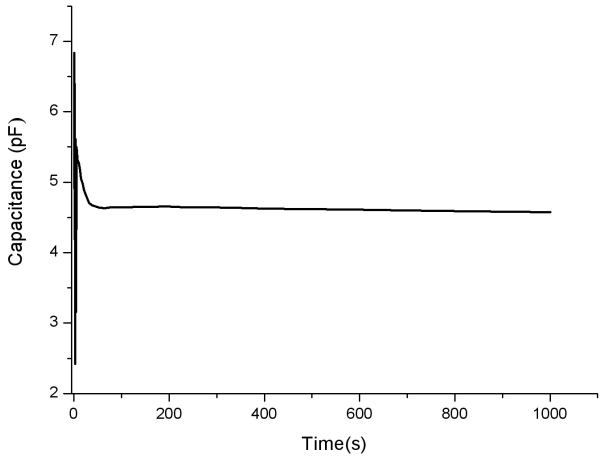

Figure 5-26 Capacitance traces showing the formation of a droplet interface bilayer. In these experiments droplets stabilised for more than 90 minutes before bringing the two droplets into contact.

To ensure that the asolectin lipid had not degraded, the double well device was fabricated in 5 mm PTFE. The diameter of the wells was 3 mm with 2 mm depth and the overlapped area was 1.5 mm. Then the chambers were filled with asolectin lipid-decane solution (20 mg/ml) and two droplets of water which were mixed with two different food dyes injected into each chamber. Interface of the two droplets made contact (Figure 5-28) and the bilayer formed spontaneously. The capacitance of the bilayer was monitored by inserting the Ag/AgCl electrodes into each droplet. The schematic of the device and the bilayer area is shown in Figure 5-27.

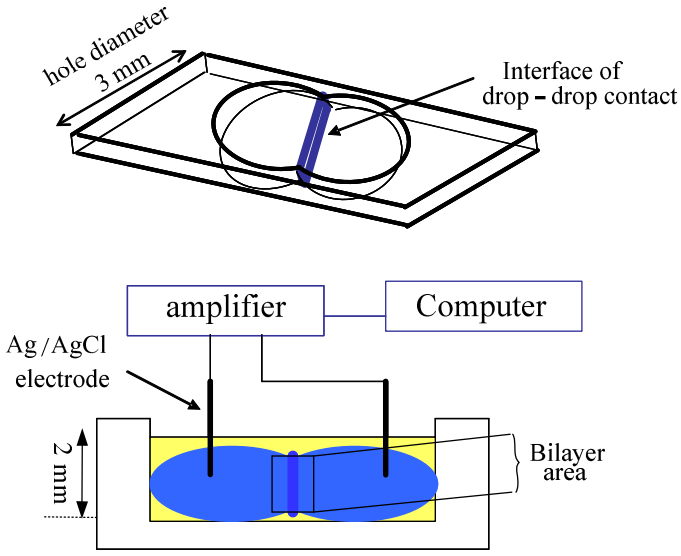

Figure 5-27 Schematic diagram of the double well device. Two water droplets were injected into each chamber filled with lipid-decane solution and the lipid bilayer was formed at the interface of two droplets. Adapted from [73].

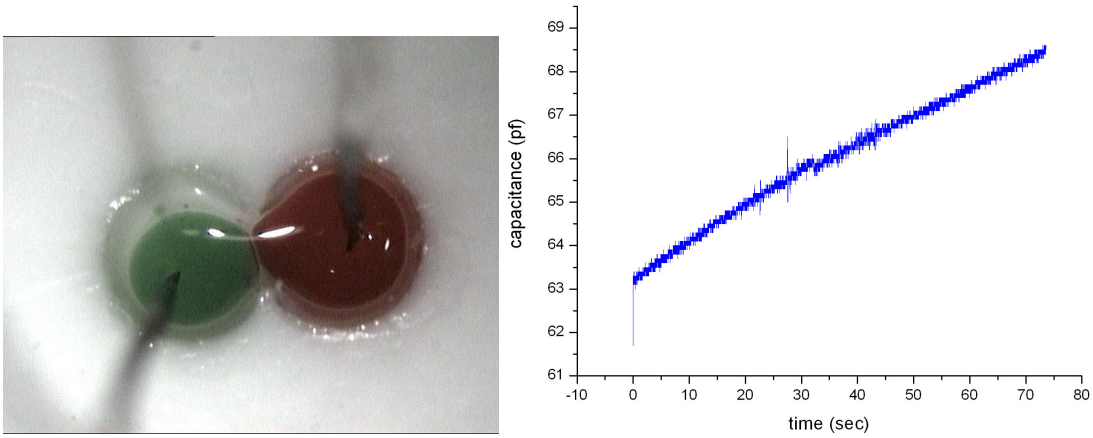

Figure 5-28 Two droplets of water injected into the chamber filled with asolectin-decane solution. Ag/AgCl electrodes are immersed into each droplet for recording the capacitance and current of the bilayer. After two droplet came in contact the bilayer formed and the capacitanvce started to increase.

In order to confirm that the bilayer had been produced, the current through the bilayer was recorded. Since the bilayer operates as an insulating dielectric, the voltage at which a typical BLM ruptures was determined. This breakdown causes the droplets to merge, and is in the range of 300-350 mV, a value similar to that obtained when using classical BLM apparatus (Figure 5-29).

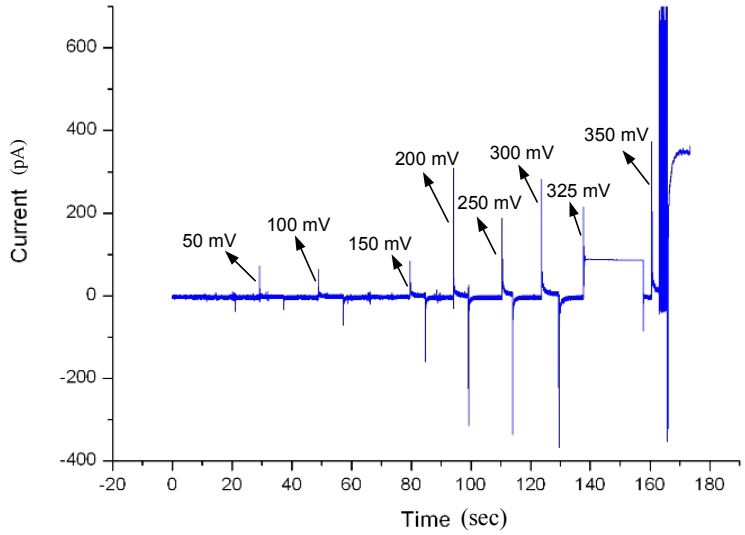

Figure 5-29 By applying a sequence of increasing DC voltage steps to a bilayer, the breakdown voltage can be estimated. In this example, the bilayer ruptured at 350 mV and the two droplets could be seen to merge.

As a result of the experiment with the double well device it was confirmed that using asolectin lipid to form the bilayer at the interface of two droplets is possible and a

bilayer will form immediately after contact. Furthermore, it was observed that there is no need to leave the droplets to stabilise in the lipid solution and that the only problem in the electrowetting protocol was inserting the Ag/AgCl into the free droplets in the lipid bath. To solve this problem, the electrodes ends were made as sharp as possible and coated with a thin layer of hydrophilic agarose gel.

The results of a typical BLM formation experiment, where the droplets were manipulated electrically, are shown in Figure 5-30. Here, two 2 µL droplets of 100 mM KCl mixed with food dyes were dispensed onto the outer electrodes of the device and then brought into contact, as described before. In all experiments the bilayer was monitored by measuring the electrical capacitance during formation. When the droplets were brought into contact, the capacitance began to rise, reaching a stable value after a few minutes.

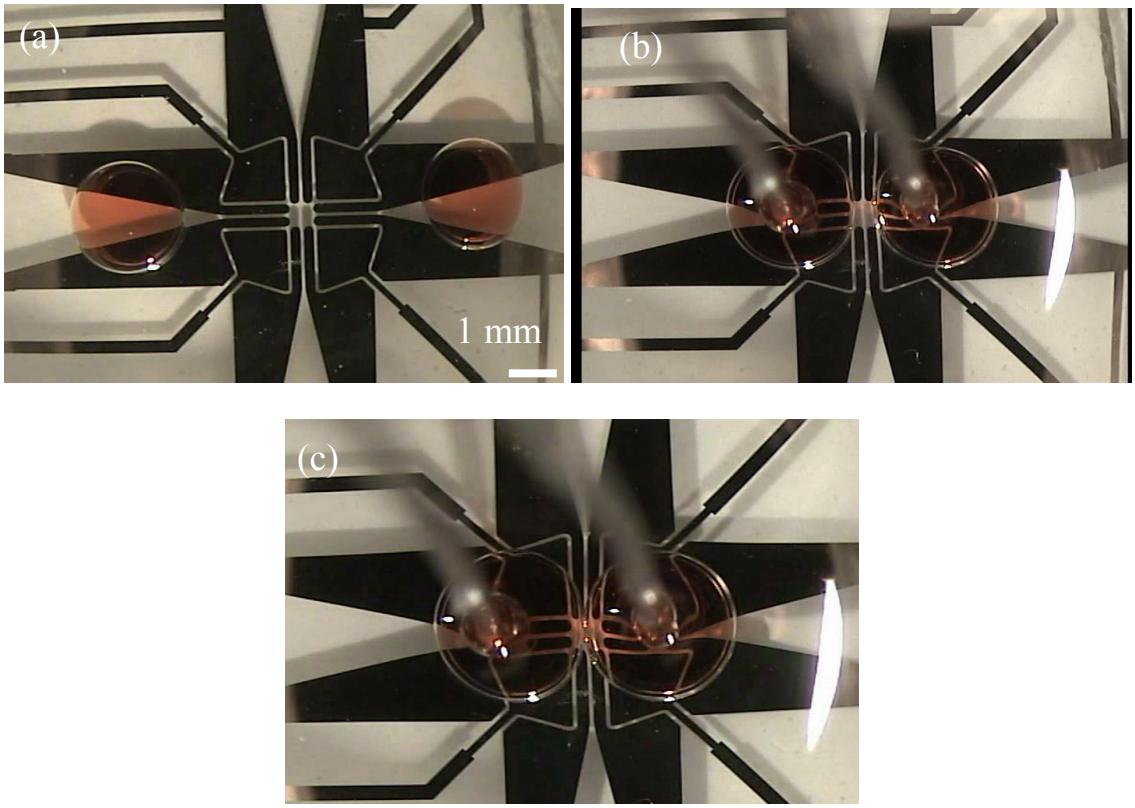

Figure 5-30 a) Initial position of two 2 µl 100 mM KCL onto the electrowetting device. b) By applying 12 V at 2 kHz to the outer and inner electrodes, droplets were moved towards each other when the two droplets were brought close enough the Ag/AgCl electrodes were inserted into each droplet to record the capacitance and current of the bilayer. c) Two droplets came into contact by applying 2 V into inner electrodes. e) A BLM is formed by two contacting lipid monolayers at the droplet-droplet interface.

Typical capacitance traces of the droplet interface bilayer without droplet stabilisation in lipid solution are presented in Figure 5-31. From sixteen experiments the mean capacitance of the bilayers obtained was 335±180 pF. By assuming a typical two droplets specific capacitance of 0.5 μF/cm^2 for a bilayer [56], this value corresponds to a bilayer corresponding to 283±74 μm in diameter. In these experiments the droplets were brought into contact within 5 minutes of dispensing. In their previous work, Holden et al. [74] found that in order to prevent the droplets from merging, it was necessary to wait for 30 minutes before bringing them into contact. However, when using the EWOD approach described, despite making the droplets contact shortly after dispensing, droplet merging was not observed.

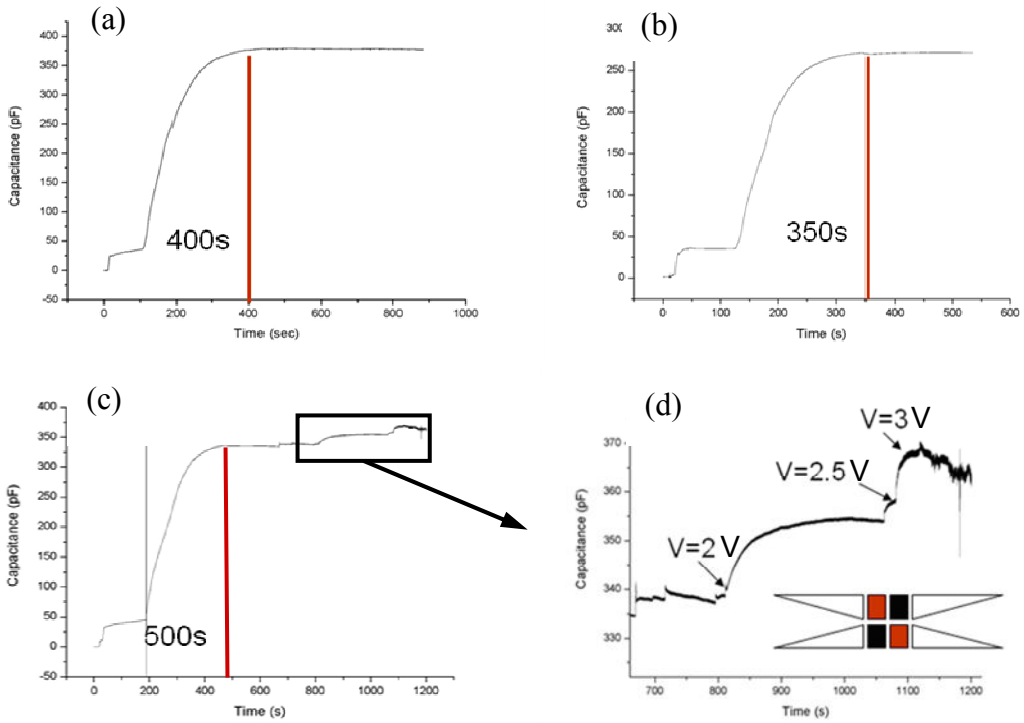

Figure 5-31 Capacitance traces (a-c) showing the spontaneous formation of a droplet interface bilayer. In these experiments there was no droplet stabilisation period prior to bringing the two droplets into contact and the time required to reach a stable capacitance value varied from experiment to experiment. d) By applying a voltage to the central electrodes, an increase in capacitance was observed.

The BLMs remained stable both with and without a voltage applied to the EWOD electrodes. The stable values of the BLM were obtained while the voltage at the

electrodes was zero (Figure 5-31). It was observed that by applying the voltage on the central electrodes, (where the droplets were in contact) and increasing it from 0 to 3 V, the capacitance increased from 330 pF to 365 pF. Furthermore it was observed that the longer the droplets were left in the lipid-decane solution before BLM formation, the smaller the capacitance. This could be due to the formation of multi layer around the droplets. From five experiments the mean capacitance of the BLM after leaving the droplets to stabilise for 15 minutes was 67 pF. The results of the droplet interface bilayer capacitance measurements are plotted in Figure 5-32.

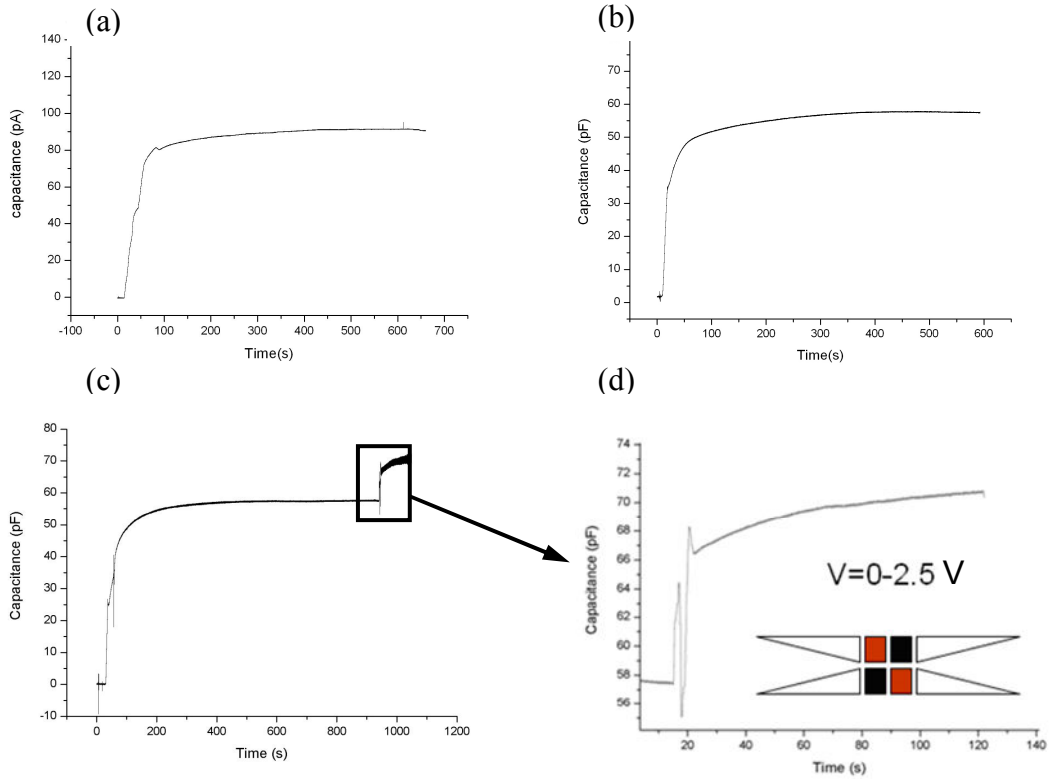

Figure 5-32 Capacitance traces (a-c) showing the spontaneous formation of a droplet interface bilayer. In these experiments droplets stabilised for 15 minutes before bringing the two droplets into contact. By applying a voltage to the central electrodes, an increase in capacitance was observed.

The mean capacitance of the BLM after leaving the droplets to stabilise for 30 minutes was 34 pF. The results of the droplet interface bilayer capacitance measurements from five experiments are shown in Figure 5-33.

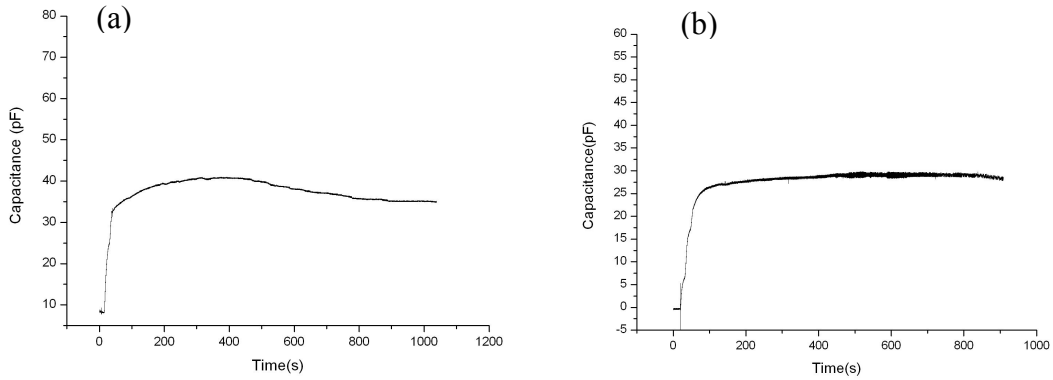

Figure 5-33 Capacitance traces (a,b) showing the spontaneous formation of a droplet interface bilayer. In these experiments droplets stabilised for 30 minutes before bringing the two droplets into contact.

The mean capacitance of the BLM after leaving the droplets to stabilise for 60 minutes was 15 pF. The results of the droplet interface bilayer capacitance measurements from five experiments are shown in Figure 5-34

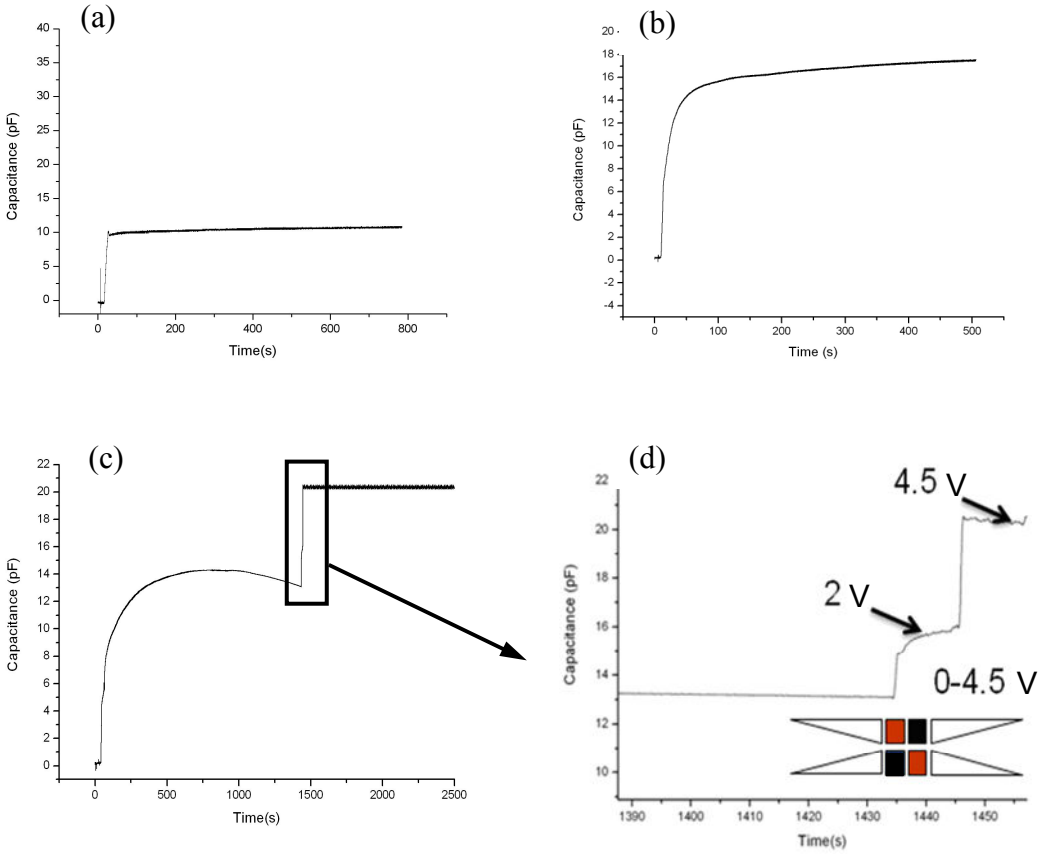

Figure 5-34 Capacitance traces (a-c) showing the spontaneous formation of a droplet interface bilayer. In these experiments droplets stabilised for 60 minutes before bringing the two droplets into contact. By applying a voltage to the central electrodes, an increase in capacitance was observed (13.2 pF to 20.5 pF)

The average BLM lifetime (when the capacitance remained above 20 pF and the membrane leakage current below 5 pA) was about 20 hours. The capacitance trace in Figure 5-35 is showing the life time of a BLM.

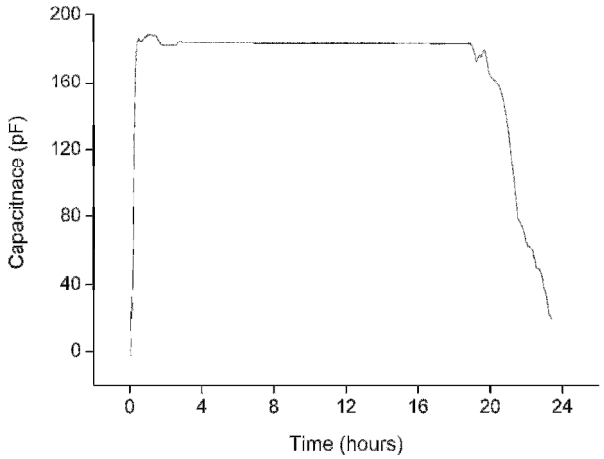

Figure 5-35 After approximately 20 hours, the capacitance begins to drops sharply as the BLM shrinks.

Additionally, when controlling droplet movement with EWOD, the separation of droplets and the subsequent re-formation of BLMs proved to be straightforward. By applying a potential (3 V at 2 kHz) to the outer electrode pairs (1-1' and 4-4') two BLM-forming droplets could be broken apart and a BLM then reformed using the protocol described previously. This is illustrated in Figure 5-36 where the variation of the capacitance with the position of the droplets (depending upon whether a BLM or a thick insulating decane layer is present between the droplets) is shown.

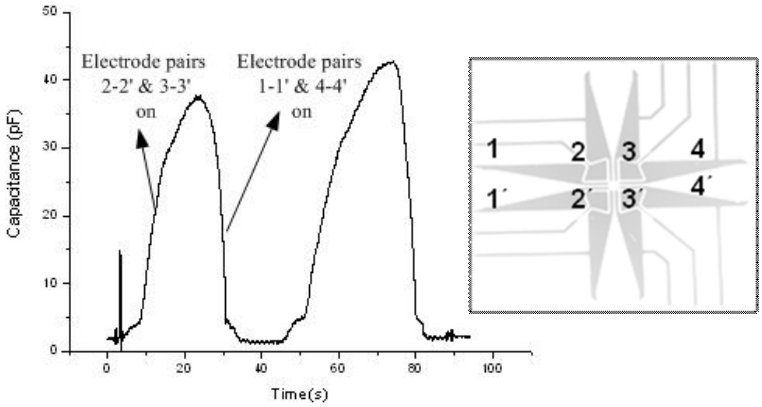

Figure 5-36 By applying an appropriate sequence of voltages to the electrodes, the two droplets can be moved back and forth. The capacitance varies according to the position of the droplets, depending upon whether a BLM (when electrode pairs 2-2' and 3-3' were on) or a thick insulating decane layer (when electrode pairs 1-1' and 4-4' were on) is present between the droplets.

In addition to measuring the capacitance between the two droplets, two other factors were assessed in order to confirm that a stable BLM had indeed been produced. Firstly, the BLM rupture voltage, which caused the droplets to merge was established at 290±30 mV, a value similar to that obtained when using classical BLM apparatus.

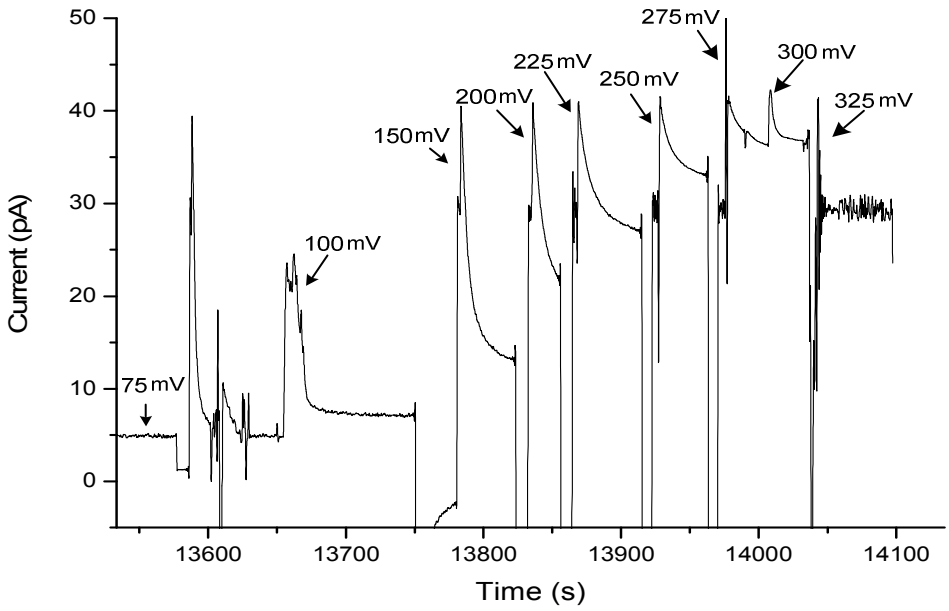

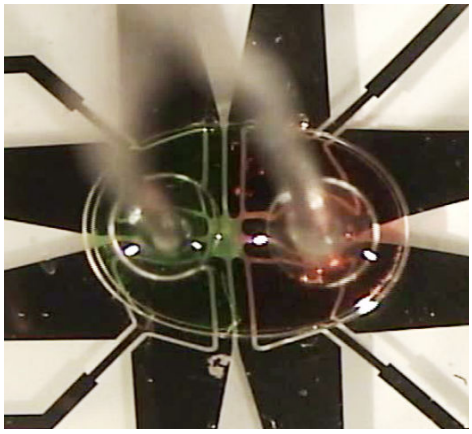

Figure 5-37 By applying a sequence of increasing DC voltage steps to a bilayer, the breakdown voltage can be estimated. In this example, the bilayer ruptured at 325 mV and the two droplets could be seen to merge.

Secondly, single channel recordings were acquired for both gramicidin A (10-20 pg ml^{-1}) and α-hemolysin (both obtained from Sigma Aldrich, UK).

5.2.6 Ion channel recording and delivery of the proteins into bilayer lipid membrane

Ion channels are pore-forming proteins that control the flow of ions across membranes of nerve, muscle and other living cells [50]. Ion channels may be classified as gating, i.e. the mechanism by which the channels are opened or closed. Voltage-gated ion channels activate/inactivate depending on the voltage gradient across the plasma membrane, whereas in ligand-gated ion channels the activation/inactivation depends on binding of ligands to the channel [77]. Furthermore, ion channels exhibit a number of distinctive characteristics, including highly specific, ion-selective filtering, where control and activation is through a variety of mechanisms, depending upon the function and nature of the cell [78, 79]. Therefore ion channels have a potential for use as particular sensitive biosensors and also for use in drug screening technologies [80] by taking advantage of transmembrane ion movement in an artificial and controlled environment [81]. If channels could be integrated into a lipid bilayer membrane system, it is possible to reproduce the natural environment of the protein and then electronic recording [82, 83]. In recent decades several investigations on ion channel behaviour have been reported, like studies on gating mechanisms and channel selectivity [84, 85]. For this purpose two main techniques were used: patch-clamp [50, 86, 87] and artificial black lipid membrane (BLM). Most channels are insoluble in water and do not reliably self insert into membranes [88, 89] Therefore, a reliable method for controlled delivery and fusion of active proteins into bilayer membranes is required. Some ion channels such as the peptide gramicidin A and α-hemolysin are water soluble and spontaneously insert in the bilayer [90, 91].

5.2.6.1 Gramicidin monomer

Gramicidin channels are mini-proteins composed of two tryptophan-rich subunits. These channels are selective for monovalent cation, with no measurable permeability to anions or polyvalent cations. Gramicidin channels supplied an important insight into the microphysics of ion permeation through bilayer-spanning channels [92]. Side and end views of the bilayer-spanning gramicidin A channel is shown in Figure 5-38. Gramicidin monomers diffuse in opposite leaflets of the lipid bilayer.

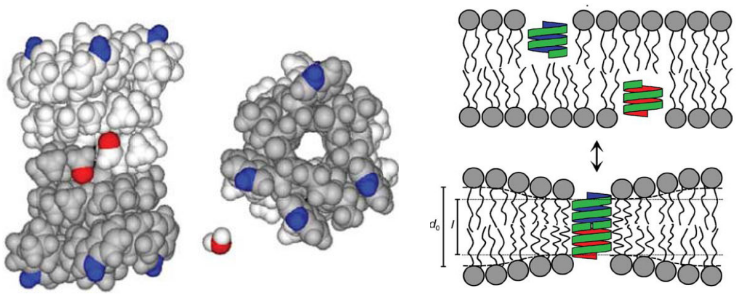

Figure 5-38 Side and end views of the bilayer-spanning gramicidin A channel. Taken from [92].

The gramicidin ion channel activities when mixed in droplets buffer (100 mM KCl) is shown in Figure 5-39. When the gramicidin monomer temporarily come together to form a dimer, an ion channel is formed across the bilayer and the K^+ can pass through the bilayer. Each jump in the gramicidin ion channel activity shown in Figure 5-39, indicates a single channel formation across the droplet interface bilayer.

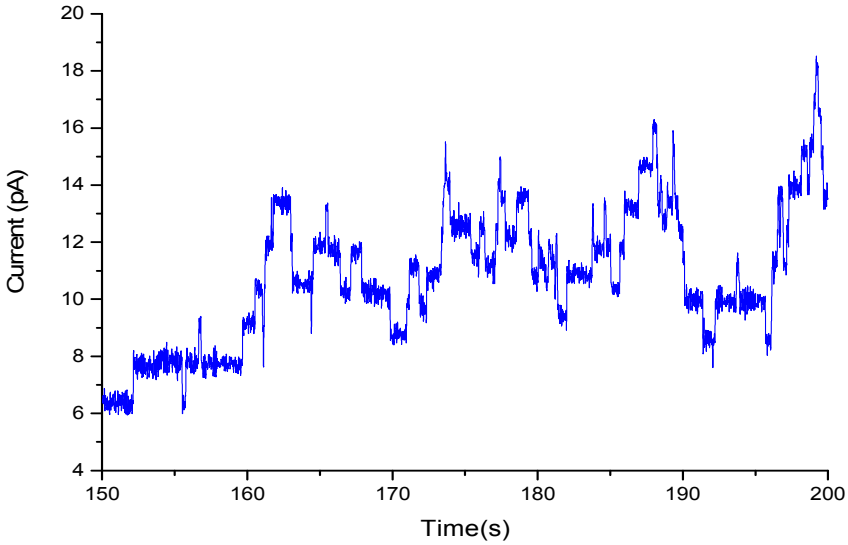

Figure 5-39 A current-time trace illustrating ion conduction through single gramicidin dimers in the BLM. Gramicidin was mixed into one droplet. The gramicidin monomers diffuse in opposite leaflets of the lipid bilayer and when they temporarily come together by diffusion to form a dimer, an ion channel forms. The ion current across the membrane was recorded under an applied voltage of 75 mV.

5.2.6.2 α -hemolysin

α-HL has a mushroom like structure with the stem crossing the lipid bilayer and a large transmembrane domain. It has been modified by other groups [73, 91] to act as

biosensor for specific analysis. α-HL heptamer with each protomer in a different colour is shown in Figure 5-40. The size of the mushroom shaped complex is estimated 100 Å in length and up to 100 Å in diameter and the size of the stem domain is about 52 Å in height and 26 Å in diameter [93].

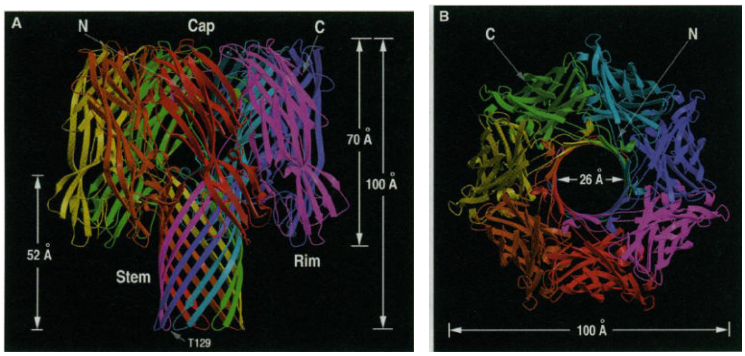

Figure 5-40 Side and top view of α-hemolysin structure. Taken from [93].

A recording of the single channel current activity of α-hemolysin nanopores is shown in Figure 5-41. One droplet is made of 100 mM KCl buffer and the other is made of the same buffer mixed with α-HL. The ion current across the membrane was recorded under an applied voltage of 50 mV. A few minutes after droplet contacting and bilayer formation, the stem crossed the lipid bilayer, and the current steps that corresponded to the integration of single α-HL pores into the lipid bilayer were detected.

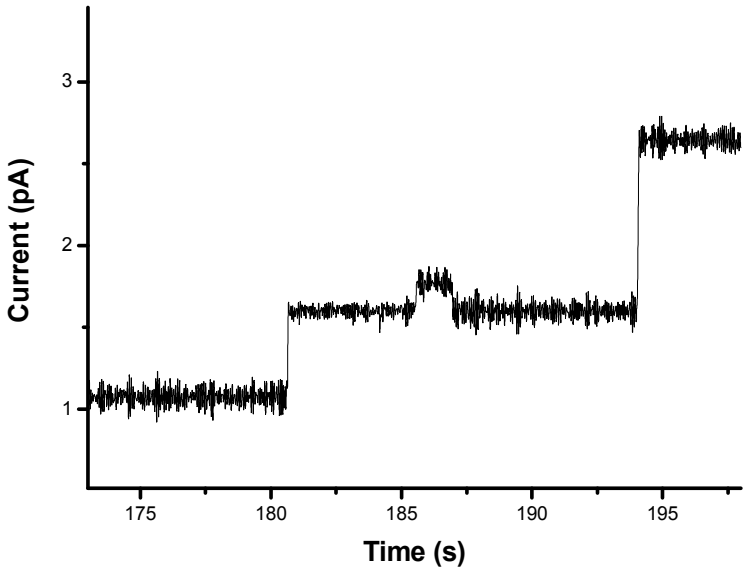

Figure 5-41 A current-time trace of α-hemolysin reconstituted into the lipid bilayer formed at the droplet interface. The voltage clamped at 50 mV.

These results show that the functional lipid bilayer was formed at the interface of two droplets using electrodynamics technique and indicates that this membrane can be used for the functional study of reconstituted membrane protein.

5.2.6.3 Protein delivery

Since most ion channels are not water soluble and cannot insert in the bilayer spontaneously, a reliable method for delivery and reconstitution of active proteins into bilayer membranes is required. A proteoliposome is a unilamellar lipid vesicle into which membrane proteins have been reconstituted. These vesicles have been used for ion channel delivery into bilayer membranes [94]. The basic method of preparation of the vesicle and the delivery to the BLM is explained in literature [95] [72, 96-98]. It was observed that the delivery of larger membrane proteins to a droplet-interface bilayer was also possible. Figure 5-42 shows a recording of the activity of the K^+ channel KcsA (M.W. 67 kDa for the tetram eric form) that was delivered to a 1:1 POPG:POPC bilayer (Palmitoyl – 2 – Oleoyl – sn – Glycero – 3 – Phospho – rac – 1 – glycerol (POPG): 1 – Palmitoyl – 2 – Oleoyl – sn – Glycero – 3 - Phosphatidylcholine (POPC) were obtained from Avanti Polar Lipids, Alabama, USA). This was achieved by mixing lipid vesicles containing KcsA (obtained from Dr. P. Marius and Prof. A.G. Lee, who purified and reconstituted the KcsA) into one of the droplet buffers. This buffer contained 600 mM KCl, 10 mM Hepes with pH = 7.4, whilst the second droplet buffer contained 150 mM KCl, 10 mM Hepes at pH of 4, an acidic pH being required in order for KcsA to open. Therefore, when the droplets were brought into contact, the salt gradient across the resulting BLM caused the fusion of a number of vesicles with the droplet-interface bilayer and KcsA activity was subsequently observed.

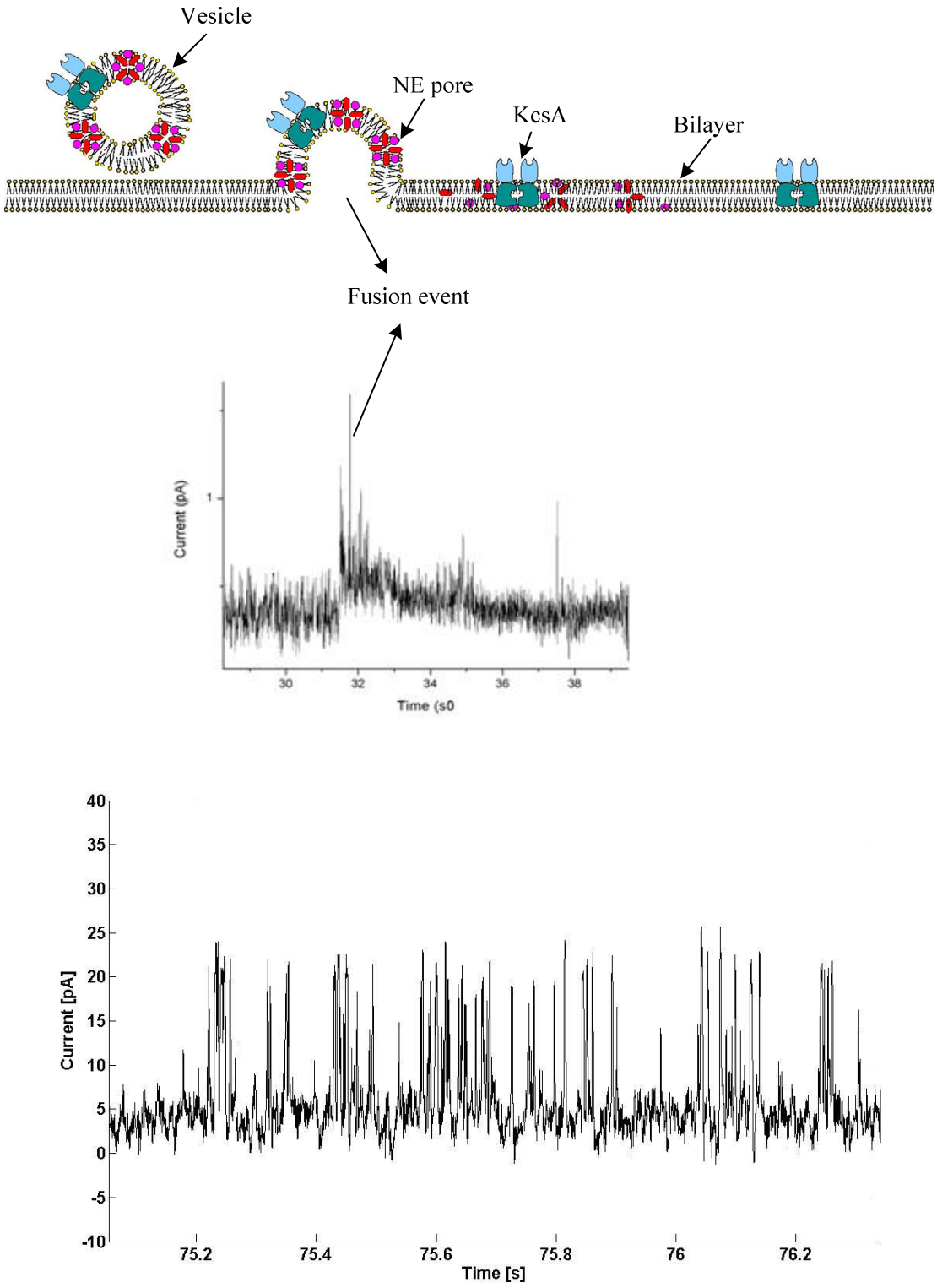

Figure 5-42 Nystatin ergosterol pore disassembles, the fusion happened by a large transient current spike. Current trace shows a recording of the activity of the K^+ channel KcsA that was delivered to a 1:1 POPG: POPC bilayer.

5.2.7 Droplet interface bilayer network

In addition to forming single BLMs, networks of bilayers may be formed using EWOD. Preliminary results showing the formation of two linked BLMs are shown in Figure 5-43. Three droplets were used, with droplet A containing 10 pg ml^{-1} Gramicidin in 100 mM KCl and droplets B and C containing only 100 mM KCl. To form a BLM network from the three droplets, a voltage (12 V at 2 kHz) was first applied between the electrode pairs 5-5', 2-2'and 3-3' to guide droplet A towards the centre of the device, by removing the voltage from 5-5' so that the droplet remained between electrode pairs 2-2'and 3-3' (Figure 5-43b). Then, by applying a voltage to electrode pairs 1-1' and 4-4', the two droplets B and C moved towards the droplet A. Before the three droplets were brought into contact, Ag/AgCl electrodes were inserted into droplets B and C. Finally, after removing the voltage from electrodes 1-1' and 4-4', the three droplets were brought into contact (Figure 5-43c)

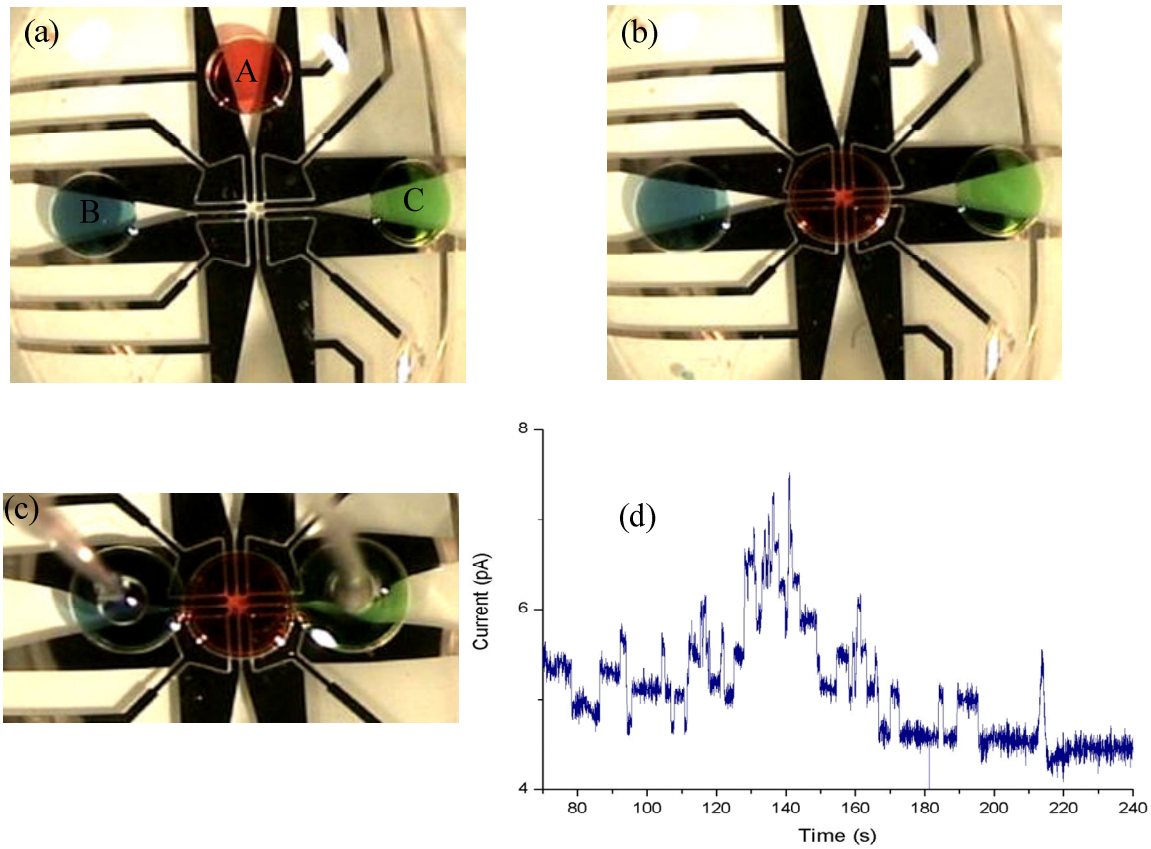

Figure 5-43 a) The initial position of the three droplets used to create a droplet-interface bilayer network. b) After applying the appropriate sequence of voltages, droplet A is placed in the centre of the device. c) The droplet network is formed by bringing the droplets B and C into contact with droplet A then the multiple bilayer were formed at the interface of the droplets A-B and A-C. d) Recording the ion channel activity of gramicidin through the multiple bilayer.

When the three droplets came into contact the multiple bilayer were formed at the interface of the droplets A-B and A-C. Gramicidin monomers diffuse in the lipid bilayer leaflets and in some cases they were flipped over and came together to form a single ion channel. While the two single channels formed across the two interfaces at the same time, the K^+ could pass through these channels. Recording the ion channel activity of gramicidin through the multiple bilayers is shown in Figure 5-43d.

5.2.8 Conclusion

In this section, we described the formation of artificial BLMs at the interface of aqueous droplets submerged in an organic solvent-lipid phase, with the movement of the aqueous droplets controlled by DEP. Previous methods for forming droplet BLMs used micromanipulators/manual dispensing or fluidic channels. Increasing the scale (i.e. arrays) or having flexible control with these methods is difficult. Instead, using electrodynamic droplet control provides a flexible, reconfigurable method for forming (and also disassembling and reforming) BLMs within a microsystem under simple electronic control. This approach is particularly well suited to the development of automated array platforms and programmable biological assays that can be integrated with previously demonstrated on-chip fluidic operations (such as droplet dispensing, mixing and splitting). In comparison to typical EWOD droplet applications, the use of surfactants meant that low potential (less than 15 V) could be used for droplet manipulation. BLM formation was extremely reliable using this method and the BLMs formed were stable (with lifetime of 20 hours) and suitable for electrophysiology analysis. Single channel recordings were acquired for both gramicidin, alpha hemolysin and the membrane protein KcsA reconstituted into droplet BLMs, showing that these droplet BLMs are highly suitable for membrane protein analysis. In addition, we have demonstrated that this approach can be used to manipulate a series of droplets to form a BLM network, allowing for the development of functional biological networks.

.

6 Nanoparticle-Biomembrane Interactions Studied with Droplet-on-Chip System

6.1 Introduction

Nanoparticles are currently employed (or in development) for a wide variety of products and applications, including medical, but there is a concern that nanoparticles may have harmful or even toxic effects [99, 100]. A major determinant for toxicity, as well as for the success of drug-delivery applications, is the interaction of nanoparticles with cell membranes [101]. A wide variety of nanoparticles have been shown to translocate across cell membranes into the cytosol [100, 101] but it is unknown whether this induces membrane damage. Protein-free model membranes (bilayer lipid membranes) are an ideal system to systematically address the interactions of nanoparticles with cell membranes. Recently, it has been shown that a wide variety of cationic nanoparticles are able to perturb supported BLMs [102], thus demonstrating the important contributions of BLMs to nanotoxicity studies. At a cellular level, nanoparticles will first interact with the cell membrane, after which uptake into the cell and subcellular structures can occur. To assess whether nanoparticle-membrane contact leads to perturbation of the membrane structure, we measure the conductance of artificial membranes (lipid bilayer) exposed to nanoparticles. In this work, it is demonstrated that the presence of nanoparticles with diameters between 50 and 500 nm can damage protein-free membranes at particle concentrations in the femtomolar range. The effects of particle size and surface chemistry are investigated. It is shown that a large number of nanoparticles can translocate across a membrane, even when the surface coverage is relatively low, indicating that nanoparticles can exhibit significant cytotoxic effects.

6.1.1 Nanoparticles

The use of nanoparticles, generally regarded as particle with dimensions in the 10^{-7} m to 10^{-9} m range, is rapidly expanding. One important example is the use of nanospheres in drug delivery systems, which is advantageous over alternative mechanisms. Due to the increasing use of nanoparticles in various applications, it is important to consider and investigate their negative effects; a science known as nanotoxicity.

For living organisms, the effect of nanotoxicity can be partly characterized by its effect on the cell membrane. A defect in the membrane could lead to it not being able to withhold the cell structure, hence losing its ability to maintain cell potential. An investigation into such possible effects would help identify the circumstances under which nanoparticle drug delivery and other uses of such particles could pose a hazard.
The nanoparticles used in our investigation are formed of silicon dioxide (SiO_2 – also known as silica) with two different surface chemistries: plain, and aminated (NH_2).

6.1.2 Nanotoxicity

Applications for engineered nanomaterials are wide-ranging; they include clothing, sports equipment, sunscreens, cosmetics and electronics. Due to their small size, the physical and chemical properties of these materials are somewhat unusual. Particularly, the very high proportion of atoms on the surface of a molecule of nanomaterials gives rise to effects not observed with the bulk material. Research suggests that properties of nanomaterials may affect biological response at cellular, sub-cellular and protein scales. It is believed that nanomaterials can travel through the human body. Upon entering the body, they can attach to some organs, penetrate cell membranes and induce hazardous responses [97].
Copper nanoparticles, which are used at the nano-level in additive and metallic coatings, are just one example of a nanomaterial proven to have grave toxicological effects. Whilst micro-scale copper particles are inherently non-toxic, nano-scale particles (23.5 nm) have been found to cause severe harm to otherwise healthy mice.
Significant damage to the kidneys, liver and spleen was observed as well as deaths due to renal damage caused by a built-up concentration of deposits [103].
Some of the mechanisms causing nanotoxicity have been revealed by experimental work investigating the damage caused by polar nanoparticles of different sizes to bilayer membranes. Results show that for particles smaller than 22 nm in diameter, membrane pores appear around the location of the particle. For particles in the 22-100 nm size range, the membrane tends to fully envelope the particle. Among these larger nanoparticles, those with a non-smooth surface have membrane pores near rough, rather than smooth, regions. Such preliminary results suggest that investigating the effects of nanoparticles of different sizes can reveal information on the effects of nanotoxicity [104].

There have been attempts to incorporate hydrophobic silver nanoparticles (5.7 nm diameter) into the lipid bilayer structure. As the bilayer imitates natural cell membrane behaviour, it is beneficial to stabilize functional nanoparticles by incorporating them into the lipid bilayer structure. Results obtained so far indicate the capability of bilayers to deform in order to encompass nanoparticles larger than the width of the bilayer. Similarities have been observed between nanoparticles contained within bilayers and the membrane's ability to encompass large transmembrane proteins in the real world. Results also suggest, however, that there may be a significant difference in bilayer stability as a result of lipid ordering being affected by the inclusion of nanoparticles [105].

Investigations show the formation of holes in the bilayer when nanoparticles in the 1.2 nm – 22 nm size range translocate across the lipid structure of plasma biological membranes [106]. Findings support the focus of this work by suggesting that the main characteristics affecting the formation of pores are size and charge. With scanning probe microscopy, used for direct imaging of the pores, a number of structural differences were detected. The different pore types are schematically depicted in Figure 6-1.

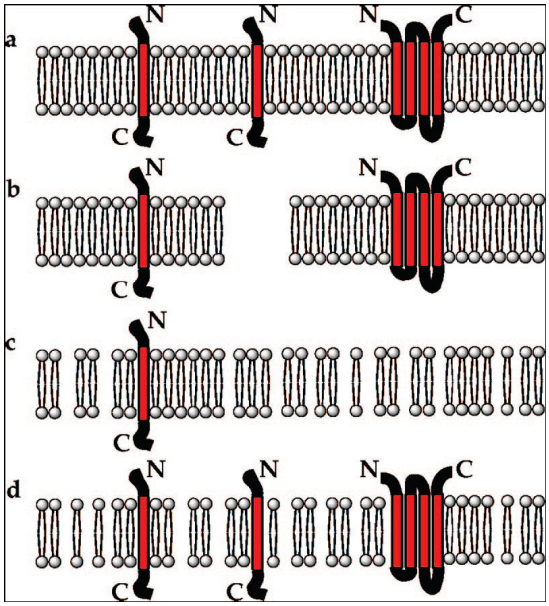

Figure 6-1 Different pore types in cell plasma membranes; (a) intact membrane containing lipid and protein, (b) membrane with pore, (c) membrane including low-density areas where the lipid and protein concentration is reduced, (d) membrane containing a lipid-poor area. Taken from [106].

Results in the literature obtained with similar experiments suggest three different mechanisms for nanotoxicity: physical disruption to the bilayer membrane, electron transfer of reduction-oxidation mechanisms, and the emancipation of nanoparticles that include toxic elements. The size of the nanoparticles affects the physical contact between them and the bilayer membrane and therefore supports the idea of bilayer properties being dependent upon nanoparticle dimensions [107].

6.2 Silica nanosphere characterization

Dynamic light scattering, using a Zetasizer Nano ZS system (Malvern Instruments, UK) with a 633 nm source, was used to investigate the hydrodynamic size distribution of four batches of commercially-acquired silica nanosphere. The four batches had the following properties:

i. 50 nm nominal diameter, non-functionalized
ii. 50 nm nominal diameter, aminated (functionalized with NH_2)
iii. 500 nm nominal diameter, non-functionalized
iv. 500 nm nominal diameter, aminated

Three solutions were prepared for each batch by dispersing the nanoparticles in water, 10 mM KCl, and 100 mM KCl and transferring to polystyrene cuvettes. Measurements were conducted at room temperature with a backscattered angle of 173° and several 60-70 seconds runs were performed for each measurement to obtain average distributions.
The dynamic light scattering results indicate that the technique is capable of rapidly identifying size differences and potentially the varying degree of agglomeration between sample formulations. For example, dispersing the plain 50 nm nanospheres in 100 mM KCl, instead of 10 mM KCl or deionised water, coincided with a trend towards larger diameters in the resulting size distribution, thus suggesting possible agglomeration. Figure 6-2 illustrates a comparison of the averaged results obtained for 50 nm silica samples in water, 10 mM and 100 mM KCl.

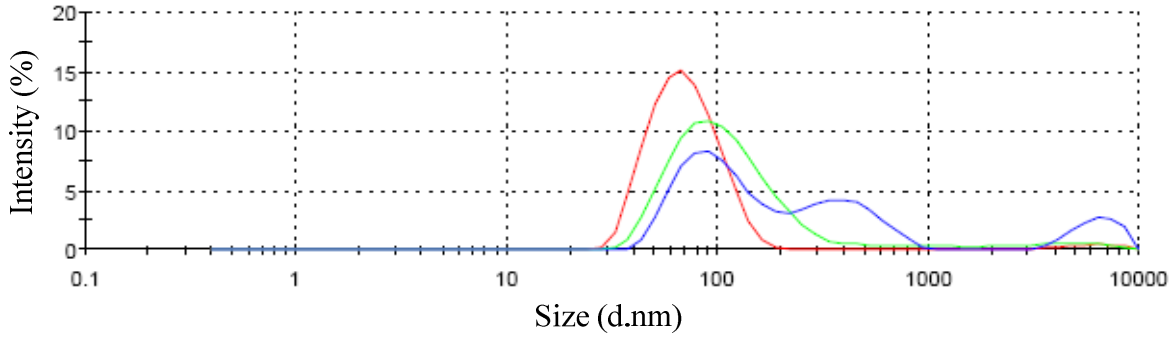

Figure 6-2 Overlay of averaged intensity size distribution results obtained for the plain 50 nm silica sphere suspensions in deionised water (Red line), 10mM (Green line) and 100mM KCl (Blue line).

The nanoparticle distribution can also be visualised with fluorescence microscopy. For this purpose, 1 μL droplets of 10 mM KCl and 100 mM KCl dispersions containing fluorescently labeled nanoparticles were immersed in a 1,2-dioleoyl-*sn*-3-phosphatidylcholine (DOPC), a synthetic lipid widely used for permeability studies of membrane-degrading compounds such as bacterial toxins and anti-microbial peptides [108]. Confocal fluorescence images of the centre of the droplet were taken with a Zeiss LSM5 Exciter microscope. A 488 nm laser was used as the excitation source. Figure 6-3 shows that 500 nm fluorescent nanospheres were concentrated at the bottom of the droplet when using a high salt concentration medium.

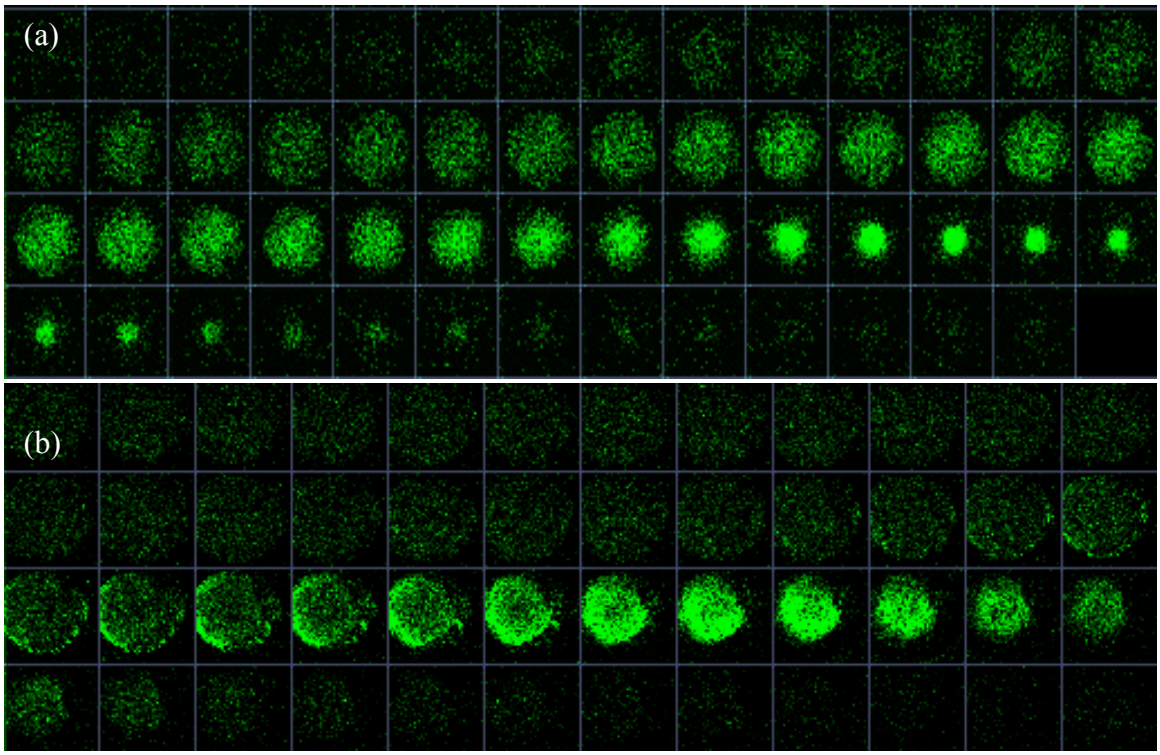

Figure 6-3 Confocal fluorescence images of a droplet of 500 nm diameter fluorescently labeled aminated silica nanospheres in DOPC-decane. a) droplet of nanoparticles in 10 mM KCl. b) droplet of nanospheres in 100 mM KCl. Confocal microscopy provided images of planes at various depths within the droplet (each set of images is known as a z-stack). Each image shows the nanoparticle distribution at a particular z-plane within the droplet. The separation between planes is 20.45 μm.

This variation in particle distribution for different salt concentrations may be explained by Derjaguin-Landau-Verwey-Overbeek (DLVO) theory, which states that the stability of a colloidal system is determined by the sum of attractive van der Waals and repulsive electrical double layer forces that exist between particles as they approach each other due to Brownian motion. By increasing the salt concentration the surface potential decreases and the double layer is contracted, therefore the electrostatic repulsion force between the particles will decrease. This allows the attractive force to dominate and pull them into contact, resulting in particle aggregation [9]. To minimize this effect that could lead to particle clustering, in most of our electrophysiology experiments the nanospheres were diluted in 10 mM KCl.

Using the Zetasizer Nano ZS, the intensity size distributions reported z-averages of 60.7 nm and 462.2 nm for the plain nanospheres, and 61.1 and 489.7 nm for the two aminated samples, all in 10 mM KCl. These values are close to the quoted 50 nm and

500 nm sizes. Polydispersity results for these samples were also relatively low (below 0.1), indicating that the samples were fairly well dispersed. Figure 6-4 shows the size distribution graphs of these four particles. The Z-average size is listed in Table 1.

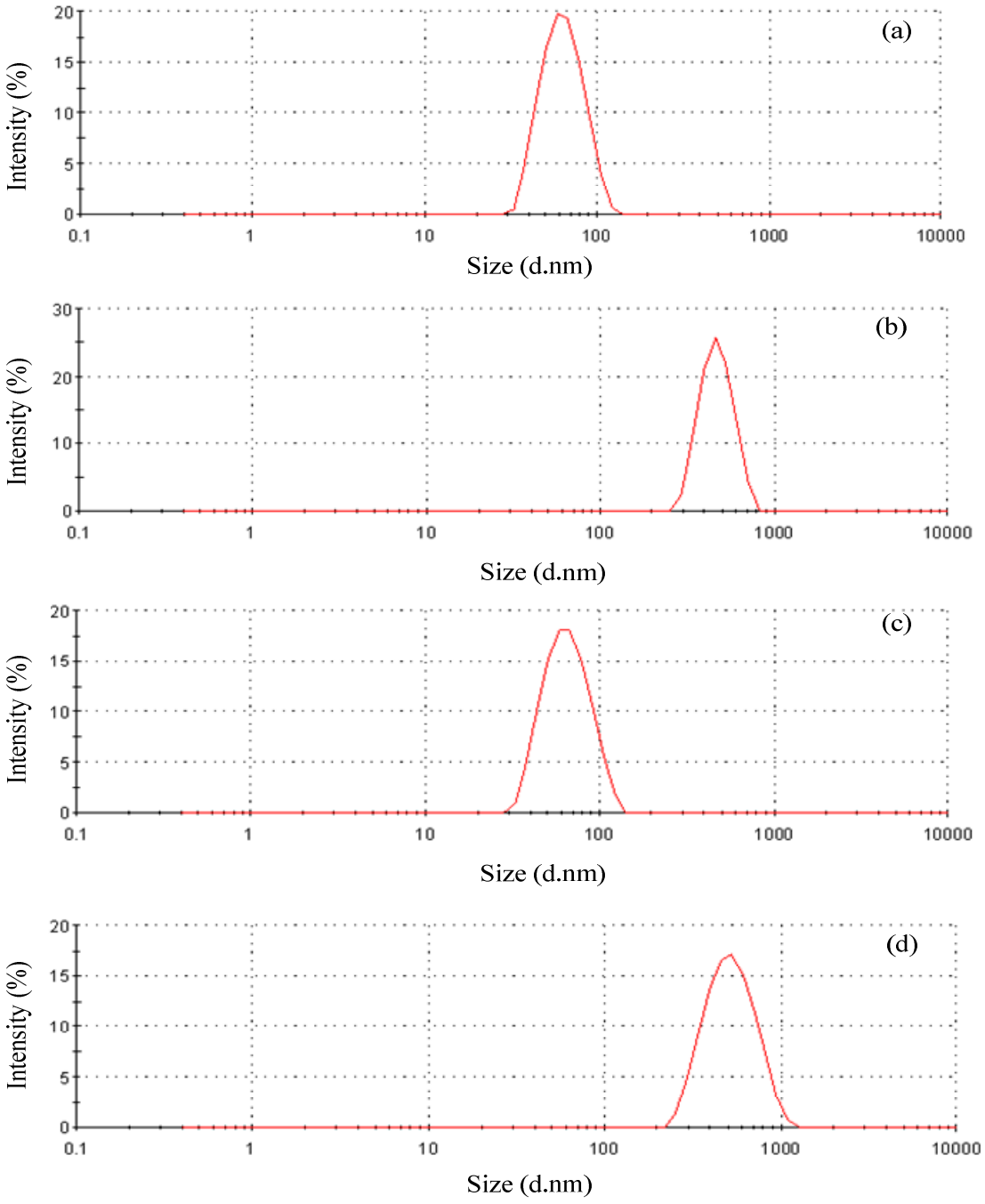

Figure 6-4 Overlay of averaged intensity size distribution results obtained for a) 50 nm plain silica nanosphere. b) 500 nm plain silica nanosphere. c) 50 nm aminated silica nanosphere. d) 500 nm aminated silica nanosphere suspension in 10 mM KCl.

Surface chemistry	Nominal particle diameter [nm]	Z-average diameter [nm]
Plain silica	50	60.7
	500	462.2
Aminated silica	50	61.1
	500	489.7

Table 1 Characterization of nanoparticle size

The relationship between particle size, concentration and surface area is given in Table 2.

Surface chemistry	Nominal particle diameter [nm]	Particle concentration [μL^{-1}]	Particle molar concentration [M]	Weight/volume concentration [$\mu g/mL$]	Total particle surface area [$\mu m^2/\mu L$]
plain silica	50	5,000	$8.3 \cdot 10^{-15}$	$1.2 \cdot 10^{-3}$	$5.8 \cdot 10^{1}$
Plain silica	500	5,000	$8.3 \cdot 10^{-15}$	$5.2 \cdot 10^{-1}$	$3.4 \cdot 10^{3}$
Aminated silica		5,000	$8.3 \cdot 10^{-15}$	$6.2 \cdot 10^{-1}$	$3.8 \cdot 10^{3}$
plain silica	50	500,000	$8.3 \cdot 10^{-13}$	$1.2 \cdot 10^{-1}$	$5.8 \cdot 10^{3}$
plain silica	50	5,000,000	$8.3 \cdot 10^{-12}$	1.2	$5.8 \cdot 10^{4}$
Plain silica	500	5,000,000	$8.3 \cdot 10^{-12}$	$5.2 \cdot 10^{2}$	$3.4 \cdot 10^{6}$
Aminated silica		5,000,000	$8.3 \cdot 10^{-12}$	$6.2 \cdot 10^{2}$	$3.8 \cdot 10^{6}$

Table 2 Concentration and total surface area of silica nanospheres. The calculations are based on an ideal spherical geometry and a silica density of 2.0 g/cm^3.

6.3 Experiment set up

In this study protein-free model membranes (lipid bilayers) were made using either DOPC, a synthetic lipid, or asolectin, which is a natural lipid extract. For both lipid compositions, bilayers were formed between a droplet of pure 10 or 100 mM KCl solution and a droplet containing the desired concentration of nanospheres to imitate the intracellular and extracellular environments, respectively. The position of each droplet, and the contact force between them, was controlled electrodynamically using a planar microelectrode structure (see chapter 5 for more details). A schematic of this set up is shown in Figure 6-5.

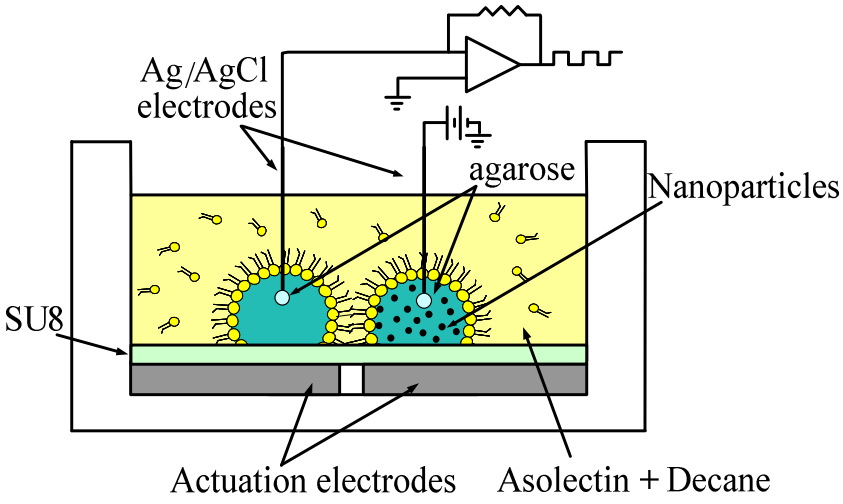

Figure 6-5 Aqueous droplets that are submerged into an oil phase containing lipids become coated with a lipid monolayer. A pair of AgA/gCl electrode inserted into each droplet from the top. Two lipid-coated droplets are brought into contact by dielectrophoretic means and a stable lipid bilayer is formed at the interface of the two droplets (details are explained in the chapter 5). The bilayer is then voltage-clamped at +100 mV and the current is monitored with single ion-channel sensitivity, in the presence of nanoparticles.

The voltage was clamped at +100 mV and a bilayer current monitoring rate of 10 kHz was used for each experiment. Several measurements were taken between 5 and 20 minutes after the droplets were brought into contact with each other for each sample. The example traces shown are representative of at least three of these.

6.4 Data analysis

The experimental set up is extremely sensitive to electrical noise from external sources, which negatively affects the recorded bilayer current signals. To identify and eliminate the noise signal from the time series data, the power spectral density (PSD) of the signals was analysed. The PSD shows the strength of the signals as a function of frequency. In other words, it reveals frequencies that are strong or weak sources of noise. A segment of the current trace of pure asolectin lipid bilayer shows in Figure 6-6a and its corresponding power spectral density is presented in Figure 6-6b. By zooming into the low frequency region (Figure 6-6c) it is found that the first noise peak occurs at 50 Hz, with similar noise peaks appearing periodically at 50 Hz intervals. Therefore, the noise components at every 50 Hz play a significant part in the total noise of the system.

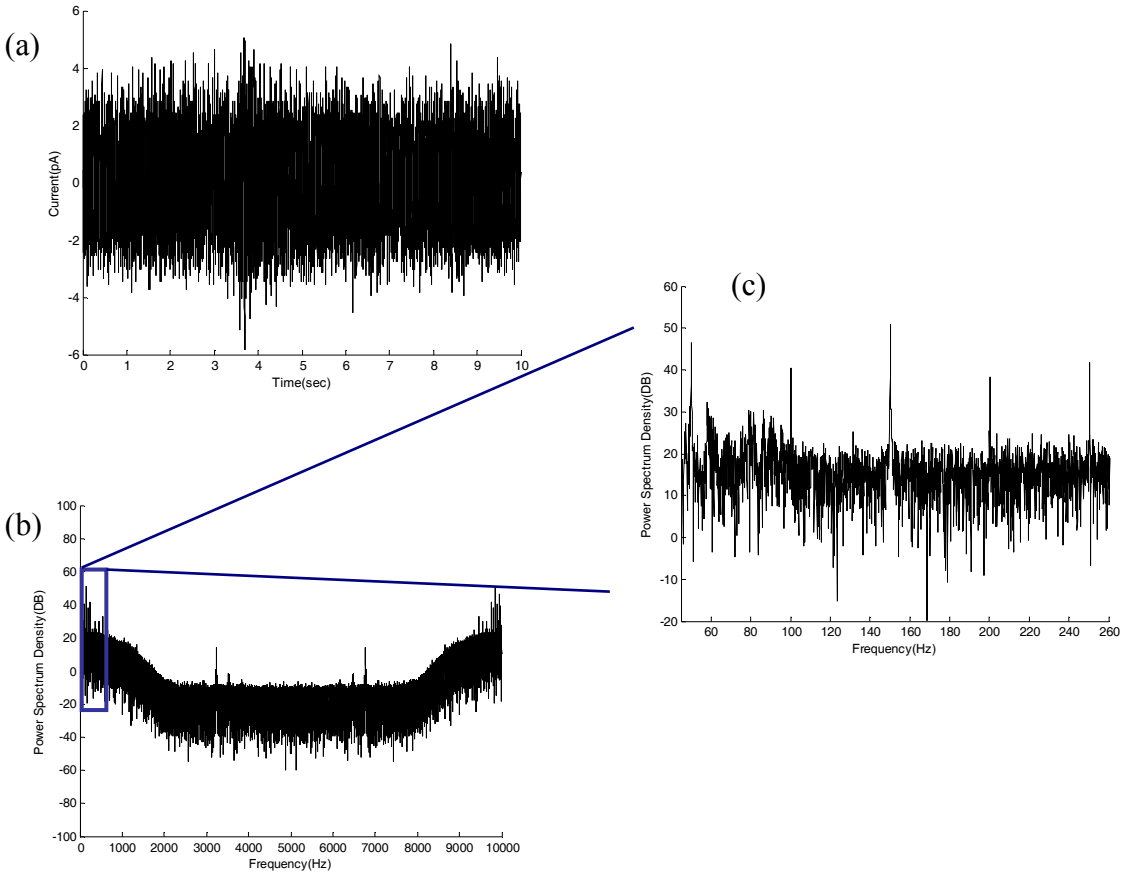

Figure 6-6 a) A current trace of the pure asolectin bilayer. b) The power spectrum of the current segment that is used to analyse the strength of the noise. c) The first noise peak appears at 50 Hz, and then the similar noise peaks repeated for every 50 Hz.

The same analysis has been performed for when the 500 nm NH_2 particles are introduced to the membrane. Figure 6-7 illustrates a segment of the current trace for the 500 nm aminated particles. Similarly, by considering the low frequency region of the current trace power spectral density (Figure 6-7b) the repetition of a 50 Hz noise frequency were observed, which is most likely caused by the power supply (Figure 6-7c). Based on these analyses a 50 Hz low pass filter was used to eliminate noise from the power supply.

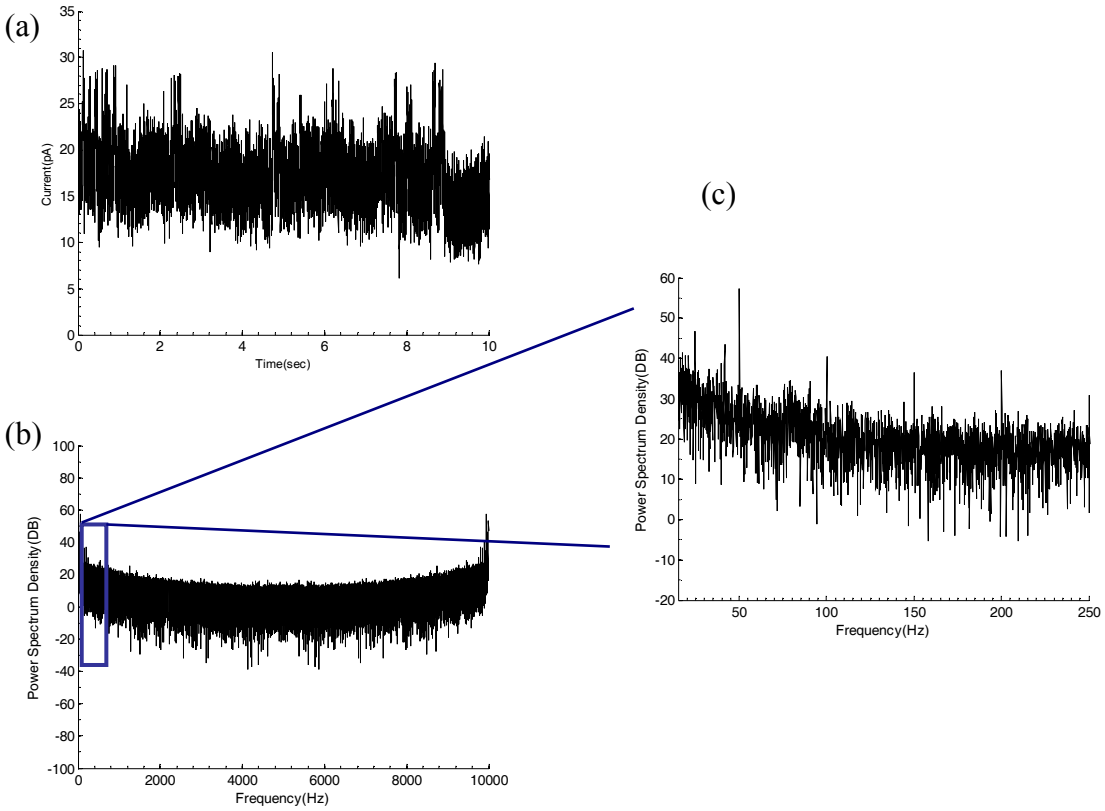

Figure 6-7 a) A current trace of asolectin bilayer while it was exposed to 500 nm aminated silica nanoparticles. b) The power spectrum of the current trace that is used to analyse the strength of the noise c) By zooming into the low frequency it is indicated that the first noise peak appears at 50 Hz, and then the similar noise peaks repeated for every 50 Hz.

6.5 Results

To investigate the effect of silica nanospheres on a cell membrane, the bilayer current was measured in the absence of nanoparticles and compared with the bilayer current after introducing the nanoparticles to the membrane. By including silica samples of two different diameters and two different surface chemistries, the effects of these parameters on the nanosphere/bilayer interaction behavior could be investigated. A steady bilayer current of 5 pA, with a peak-to-peak noise of 4 pA, was measured for both the DOPC and asolectin preparations without nanoparticles at 100 mV (Figure 6-8a). This indicates that an electrically insulating membrane with a resistance in the GHz Ω range is formed for the pure lipid bilayer. When one of the droplets is replaced by one containing 500 nm diameter aminated nanospheres (Figure 6-8b), the bilayer current rises rapidly to 50 pA, then more gradually increases to 100 pA over 3 minutes. There is then a spike to more than 300 pA, indicating disintegration of the membrane. This behavior is evidence of nanoparticles inducing the formation of holes in the DOPC bilayer and causing disintegration within only 3 minutes despite being present at a relatively low concentration of about 8 fM (0.62 μg/mL). Increasing the particle concentration by a factor of 1000 causes a more rapid disintegration of the bilayer, with more than 300 pA current spike appearing after only 90 seconds (Figure 6-8c). The current profile for this sample until disintegration is also markedly different, consisting of a series of sharp spikes in the 200-250 pA range, rather than the steady increase observed for the low concentration sample.

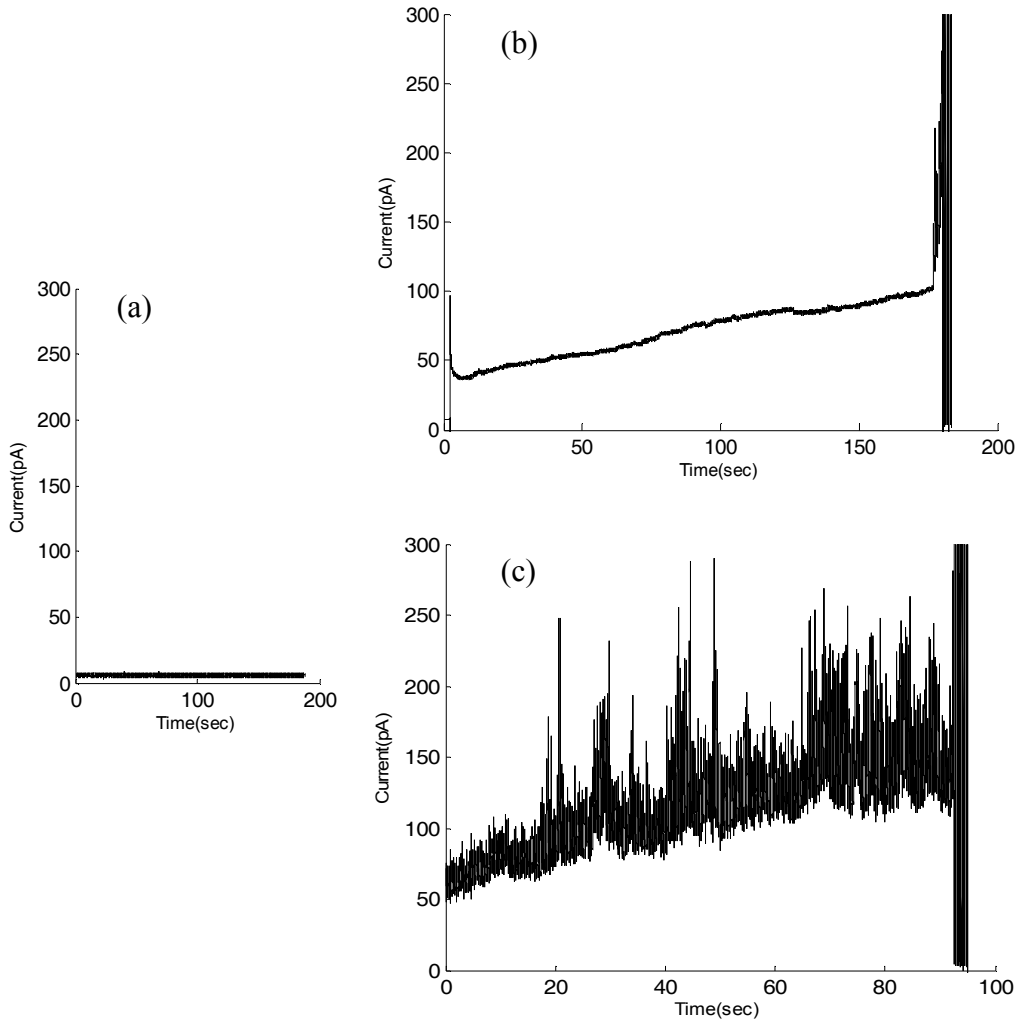

Figure 6-8 Current measurements of voltage-clamped bilayers of DOPC in the absence and presence of nanoparticles. a-c) DOPC bilayer exposed to 500 nm aminated silica nanospheres: 0 fM (a), 8 fM (b), 8 pM (c).

As mentioned in chapter 5, the inter-droplet bilayers are stable for several hours without any changes in the bilayer current, when using asolectin in the absence of nanoparticles. The presence of 500 nm aminated silica nanospheres at different concentrations causes a consistent increase in the bilayer current. Figure 6-9b,c shows the influence of 500 nm aminated silica nanoparticles, diluted in 100 mM KCl, on the bilayer current. Current spikes of up to about 35 pA are seen at the higher nanoparticle concentration. Unlike the DOPC bilayers, the baseline current for asolectin bilayers remains constant for about 15-30 minutes, which is long enough for electrophysiology measurements. Asolectin bilayers are therefore used for the rest of our experiments.

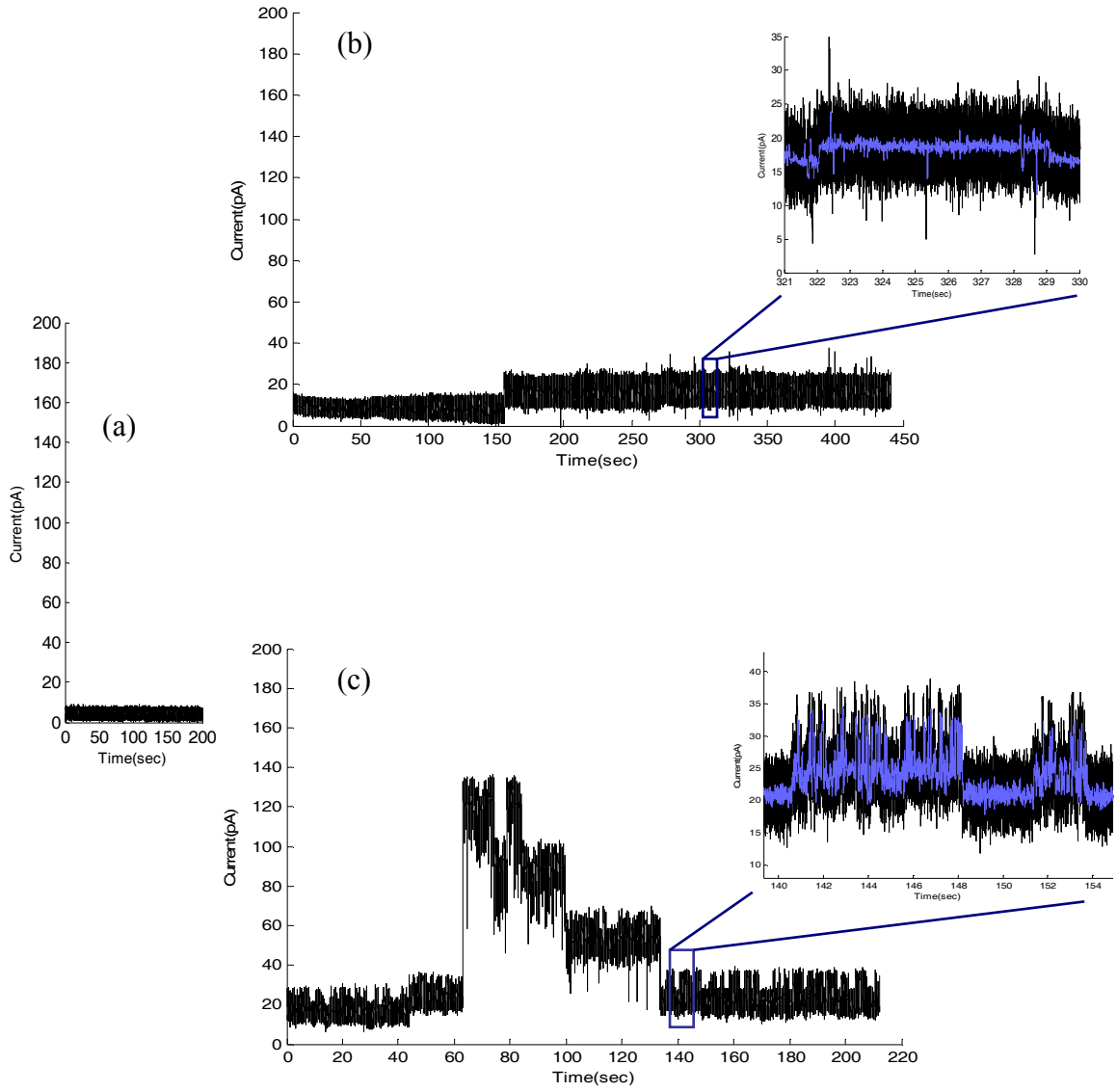

Figure 6-9 Current measurements of voltage-clamped bilayers of asolectin in the absence and presence of nanoparticles. Asolectin bilayer exposed to 500 nm aminated silica nanospheres: 0 fM (a), 8 fM (b), 8 pM (c). A 50 Hz low-pass filter (blue traces) was applied to emphasize the well-defined amplitude of the current steps in the un-filtered data (black traces).

The results show that aminated nanospheres cause the rapid disintegration of both DOPC and asolectin bilayer membranes. Ohmic behavior, evidenced by the linear nature of the I-V results in Figure 6-10, indicates an ion channelling conduction mechanism with pore diameters exceeding 2 nm. This demonstrates nanoparticle-induced damage at concentrations 100 times lower than that previously reported in the literature, for example by Tao et al. who reported a decrease in the viability of cell cultures for 500 nm aminated silica concentrations down to about 50 µg/mL [109]. In

another example of electrophysiological studies of the effects inorganic nanoparticles on bilayers, Ramachandran et al. showed that the incorporation of CdSe quantum dots, 3-15 nm in diameter, into DOPC bilayers, caused current bursts of up to 800 pA [110]. In the only other study of this type (to my knowledge), 30 pA current spikes were observed in DOPC bilayers with CdSe quantum dots [111].

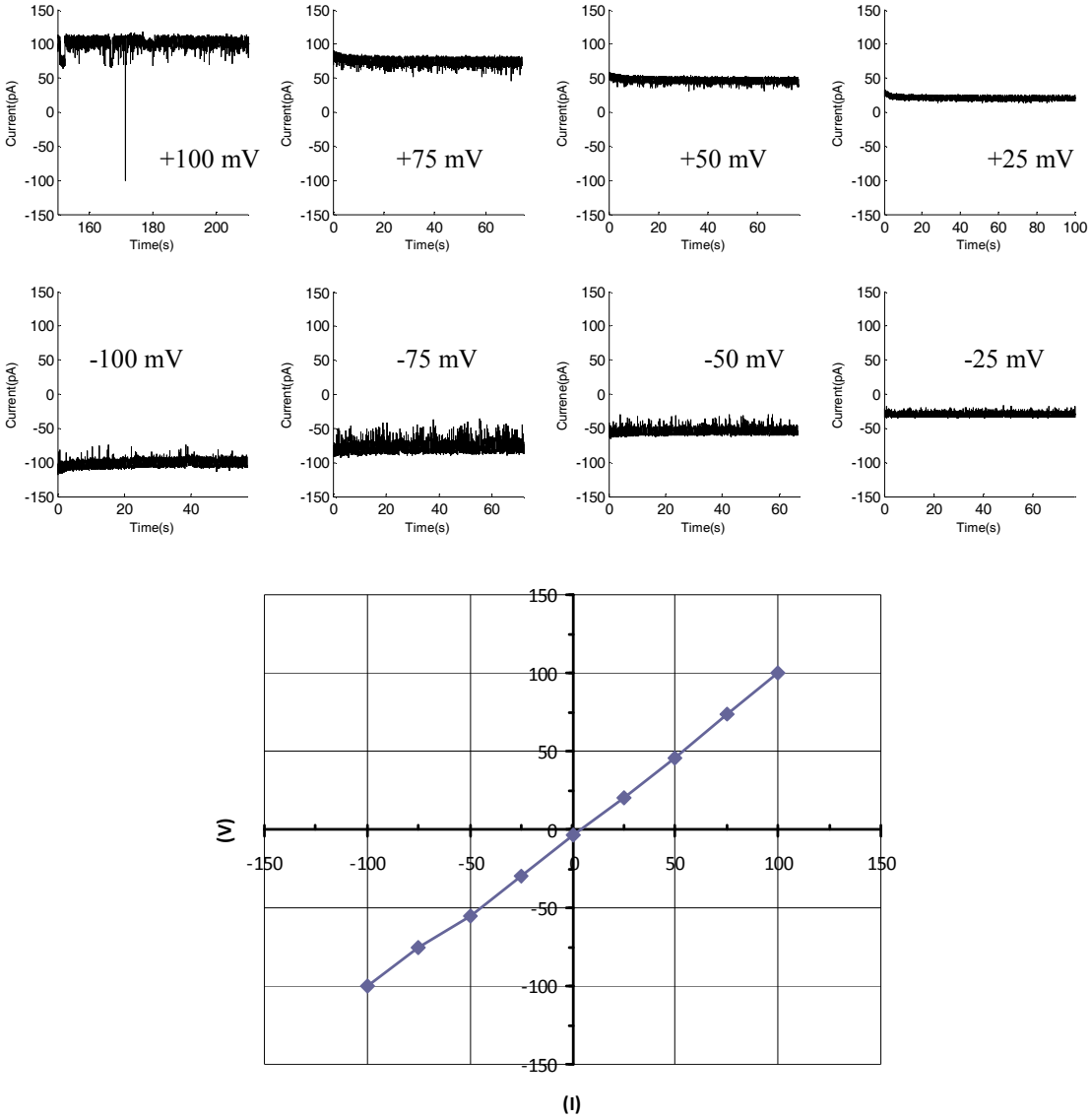

Figure 6-10 Current measurements of different voltage-clamped bilayers of asolectin in the presence of 500 nm aminated nanoparticles. The voltage was varied between +100 mV and -100 mV. The chart represents a linear relationship between an electric current and a corresponding voltage which implies the presence of pores, i.e. channel-like structures.

Moving to the non-functionalised silica nanoparticles, it is observed that those with a diameter of 500 nm produce a similar increase in bilayer current (Figure 6-11a) compared to their aminated counterparts at the same concentration of 5000 particles/μL (8 fM) (Figure 6-9b). However, the 50 nm non-functionalised nanoparticles, when applied at 100 times the concentration so that the total particle surface area is equivalent, at ~4 mm^2/mL, to the 500 nm samples, cause the bilayer current to increase to ~100 pA (Figure 6-11c). This suggests that comparisons between differently-sized nanoparticles should be made at the same molar concentration rather than the same total surface area.

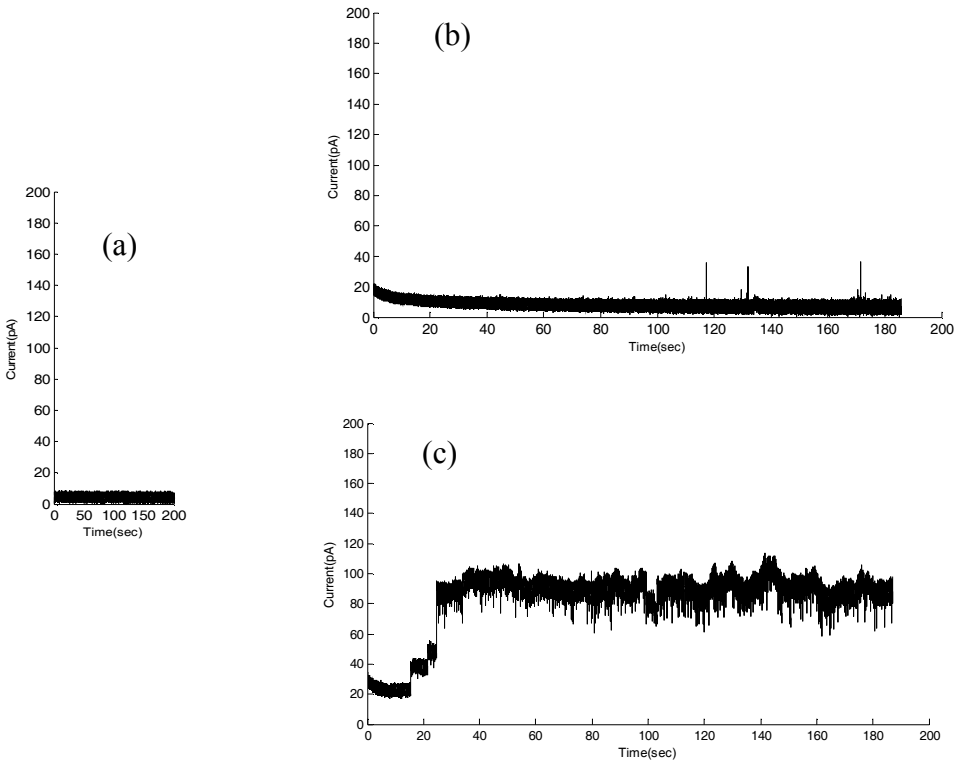

Figure 6-11 Asolectin bilayer in the presence of different un-functionalised silica nanospheres with the same total surface area: a) no nanoparticles b) 500 nm silica nanospheres at 8 fM concentration and c) 50 nm silica nanospheres at 1 pM concentration. The droplets were approximately 2 μL of 100 mM KCl solution.

Results from experiments with picomolar nanoparticle concentrations are shown in Figure 6-12. The bilayer current is observed to be significantly higher (often exceeding 20 pA) when nanospheres are present, compared to when they are absent, for all four

types of nanoparticle tested. Current spikes lasting more than 1 millisecond and current steps lasting more than 20 milliseconds, with a 1-10 per second event frequency, are observed for all samples with the exception of the 500 nm, non-functionalised nanoparticle sample. The expanded views of the current traces (Figure 6-13) reveal the existence of two levels between which the current fluctuates. This is indicative of "ion channel-like" modulation of the bilayer current, as observed previously in cytotoxic β-amyloid oligomers [112]. From Figure 6-12, we can order the nanoparticle types in terms of how deleterious they are to bilayer membrane structural integrity (from most to least destructive):

i. 500 nm, aminated
ii. 50 nm, unfunctionalised
iii. 50 nm aminated
iv. 500 nm, unfunctionalised

It is unclear from these four samples whether size or surface chemistry dominates the interaction between nanoparticles and negatively-charged asolectin bilayers and so further experiments are required on a wider range of nanoparticles and charged bilayers to determine this.

The results presented here demonstrate asolectin bilayer perturbation with 50 and 500 nm plain silica nanospheres at a concentration of only 8 pM, a much lower concentration than a recent report demonstrating 50% hemolysis with nanoparticles of diameters of 37, 142 and 263 nm at concentrations of 18 μg/ml (515 pM), 94 μg/ml (47 pM) and 307 μg/ml (25 pM), respectively [113].

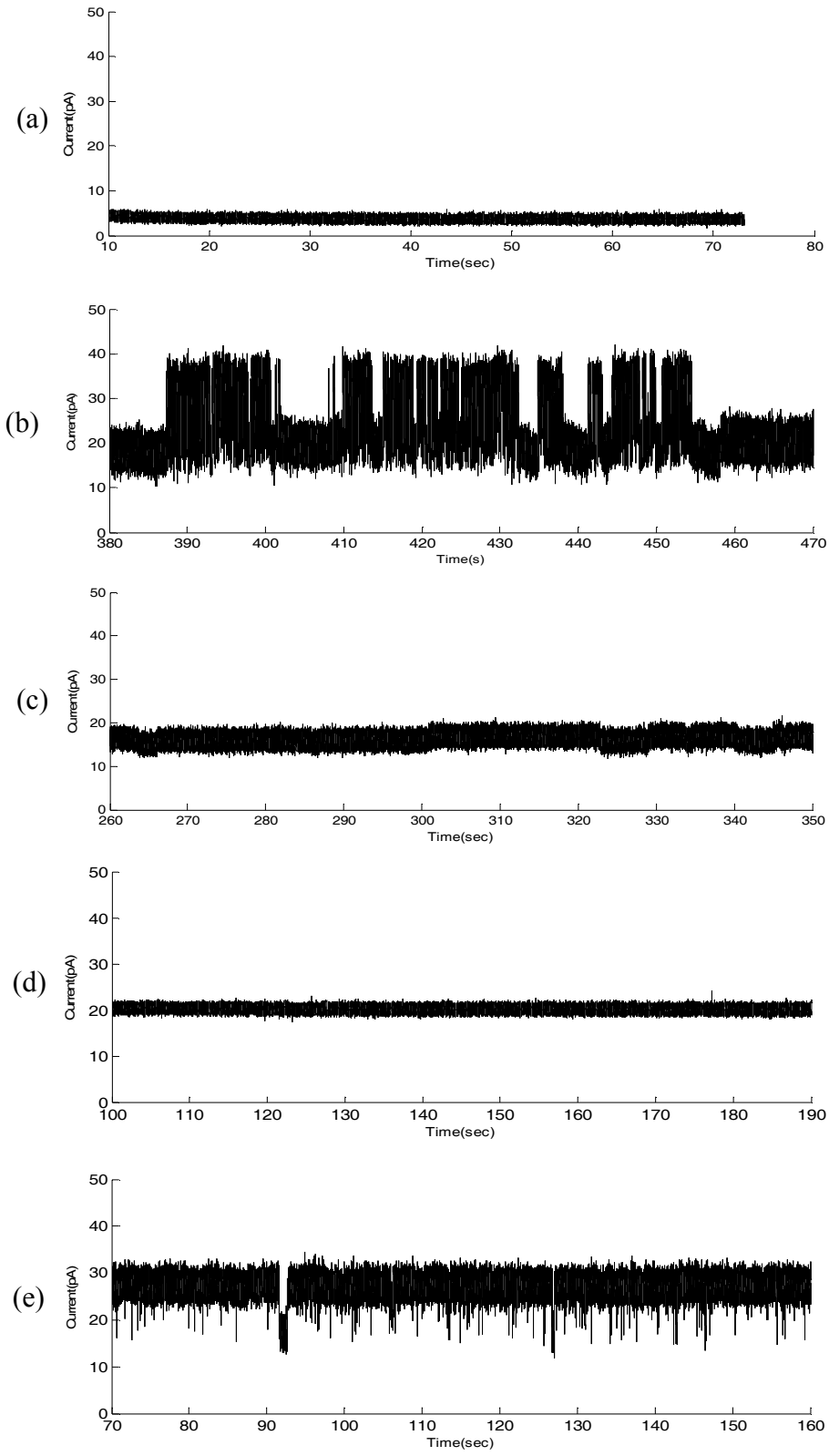

Figure 6-12 Current measurements of voltage-clamped bilayers of asolectin in the presence of: a) non nanoparticles b) 500 nm diameter aminated silica nanospheres, c) 50 nm aminated nanospheres, d) 500 nm non-functionalised silica nanospheres, e) 50 nm non-functionalised nanospheres . The silica nanospheres were present at a concentration of 5 million particles per microlitre (8 pM) in 10 mM KCl. The grey traces in each panel depict the bilayer current in the absence of nanoparticles.

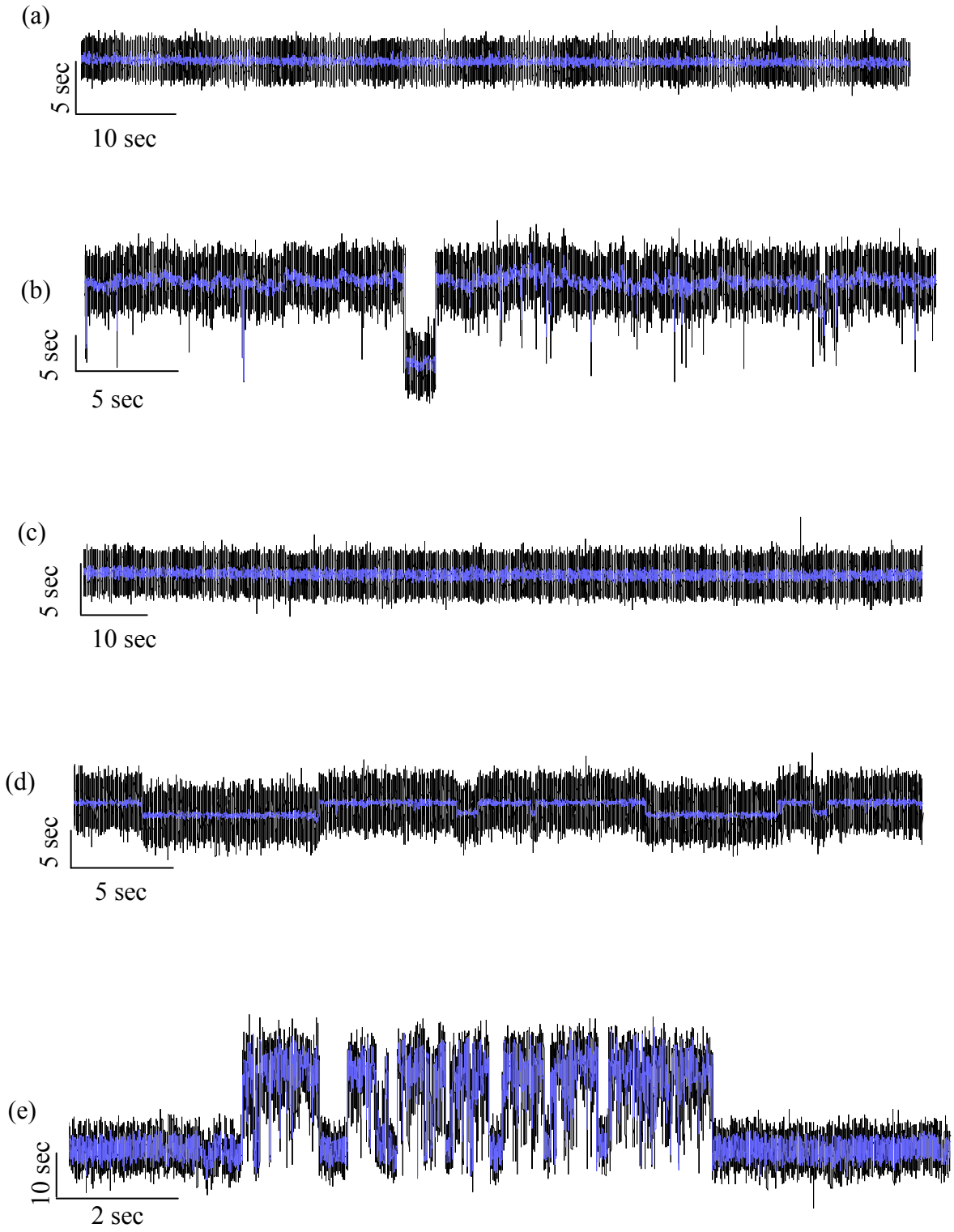

Figure 6-13 Expanded view of asolectin bilayer current trace for the following silica nanospheres: a) no nanoparticles, b) 50 nm non-functionalized particles, c) 500 nm non-functionalized particles, d) 50 nm aminated particles, e) 500 nm aminated particles. The nanosphere concentration is 8.3 pM in 10 mM KCl. A 50 Hz low-pass filter (blue traces) was applied to emphasize the well-defined amplitude of the current steps in the un-filtered data (black traces).

Confocal microscopy of a droplet of fluorescently-labeled nanosphere solution (500 nm, aminated) demonstrates an accumulation of the nanospheres around the perimeter of the droplet (Figure 6-14). Assuming a 0.06 mm^2 thick bilayer and estimating from the fluorescence intensity profile (Figure 6-14) that about 5% of the spheres have collected at the droplet surface, leads to an estimate that about 4000 particles contribute to the currents shown in Figure 6-12. This represents only 2% and 0.02% surface coverage for the 500 nm and 50 nm diameter nanoparticles, respectively, indicating that bilayer interactions of a large number of particles are collectively contributing to the increases in bilayer current observed in Figure 6-13. However, single particle interactions are likely to be responsible for the observed channel-like current transitions.

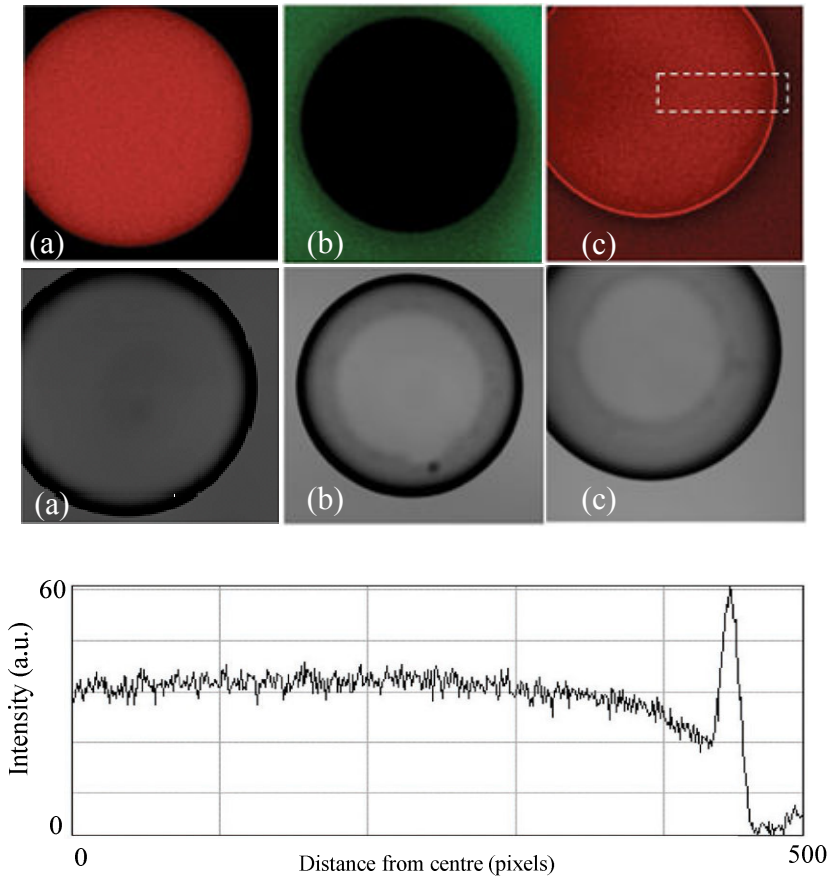

Figure 6-14 Confocal fluorescence images of a droplet of: a) 500 nm diameter fluorescently labeled aminated silica nanospheres in pure decane, b) droplet of 10 mM KCl solution in decane with asolectin lipids, c) droplet of nanospheres (58 pM in 10 mM KCl) in decane/asolectin with fluorescence intensity profile from boxed area. Asolectin has some fluorescent components which have the same false colour in panel (c) as the fluorescent nanospheres. The nanospheres are distributed homogeneously throughout the droplet when it is immersed in pure decane but accumulate at the droplet-decane interface when asolectin lipids are present. Top panels are fluorescence images and bottom panels are transmitted light images.

A top-down schematic of the elecrodynamic experimental set-up is presented in Figure 6-15a. Droplet 1 consists of KCl solution formed in the asolectin/decane support material and impregnated with the 500 nm aminated nanoparticles to a concentration of 5 million particles per μL. Droplet 2, consisting of KCl solution only, is formed in the support medium and then brought into contact with droplet 1 by application of an electric field as described in Chapter 5. The experiment is then allowed to proceed for 15 minutes.

To assess whether lipid association of the nanospheres leads to translocation across the inter-droplet bilayer, droplet 2 was extracted from the reservoir after the experiment and deposited onto a microscope slide and allowed to dry. A similar sample was prepared from the solution used for droplet 1. In addition, a sample was prepared from a droplet of KCl extracted from the asolectin /decane medium. This was representative of droplet 2 prior to contact with droplet 1. Optical micrographs (Figure 6-15b,c,d) were then obtained of the dried deposits from both droplets and from the support medium. Optical micrographs of droplet 1 are shown in Figure 6-15b, in bright field mode (i), illustrating the presence of KCl salt crystals, and in fluorescent mode (ii), showing fluorescent nanoparticles. The fluorescence image of the dried deposit from droplet 2 after the experiment (Figure 6-15c), also clearly shows the presence of fluorescent nanoparticles and so provides evidence for translocation of nanoparticles from droplet 1, across the bilayer membrane, into droplet 2.

To estimate the fraction of nanoparticles transferred from droplet 1 to droplet 2 during the experiment, the whole of the dried deposit of droplet 2 was imaged as a series of fluorescent micrographs at a magnification of ×60 (an example of one of these images is presented in Figure 6-15c). A micrograph was also acquired from the dried deposit of the droplet of KCl taken from asolectin solution (this droplet did not contain nanoparticles) (Figure 6-15d) to determine the background fluorescence due to the lipids. The maximum background lipid fluorescence was then used as a threshold value enabling the subtraction of all pixels with values below this to isolate the fluorescence due to the nanoparticles (Figure 6-15e). Following thresholding, the calculated fluorescent area was divided by the area of a single particle to estimate the number of particles in each image. By knowing the area of the images, the number of particles in each image and the area of the droplet deposit on the microscope slide, the total number of particles in droplet 2 could be calculated and expressed as a fraction of the number of particles originally present in droplet 1 (estimated from the original nanoparticle

concentration). Using this method, it is estimated that a small fraction of the particles, ~0.01-0.05%, translocated across the bilayer from the droplet 1 to droplet 2.

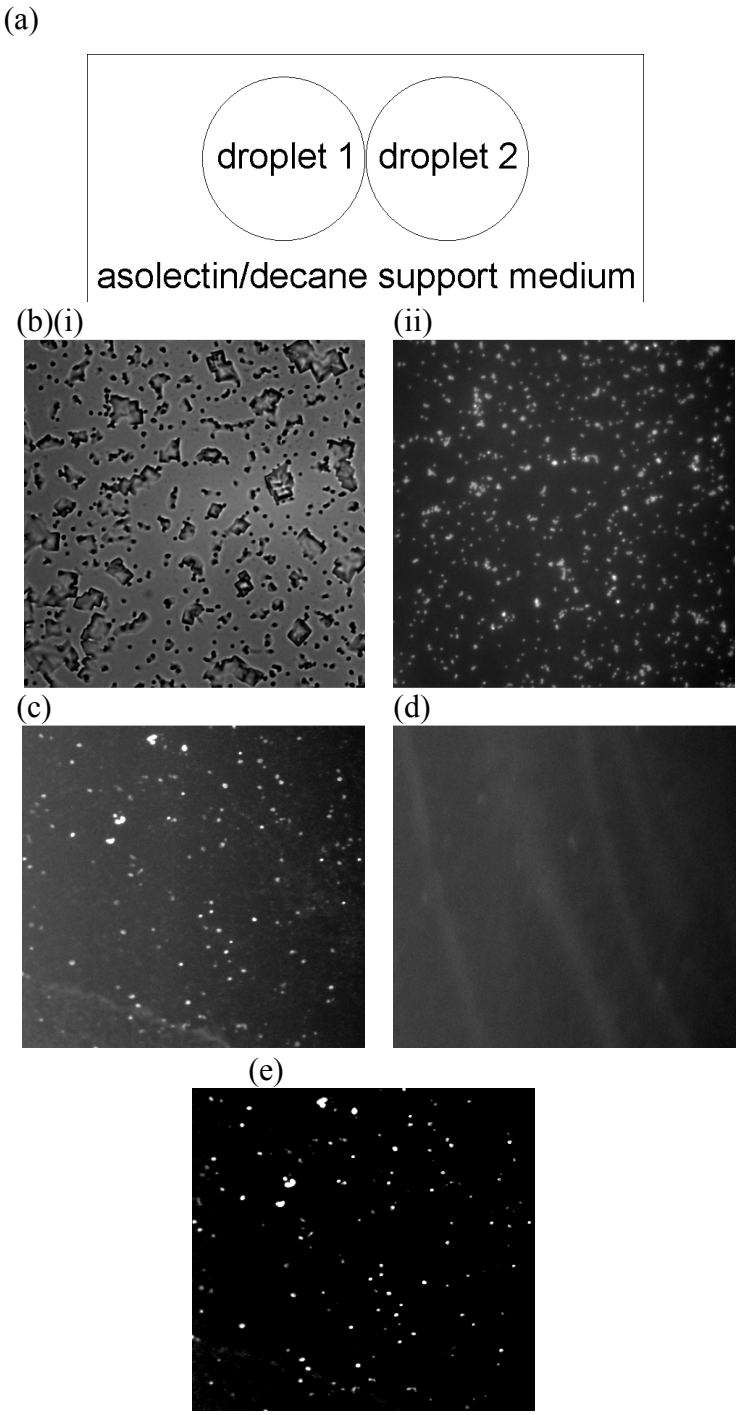

Figure 6-15 a) Schematic of experimental set-up, top down view, b) Optical micrographs of KCl solution droplet after (droplet 1 in (a)) containing nanoparticles in (i) bright field, (ii) fluorescent mode. c) Fluorescent image of droplet 2 after experiment showing nanoparticles have transferred from droplet 1 to droplet 2, through the bilayer membrane, d) Fluorescent image of KCl droplet extracted from asolectin in decane support medium (identical to droplet 2 prior to contact with droplet 1) showing background fluorescence from lipids, e) Fluorescent image from (c) after thresholding with background lipid fluorescent level determined from (d).

Passive interactions between the nanospheres and the lipids must be solely responsible for translocation because active transport mechanisms are impossible in protein-free bilayer membranes [99]. The translocation of silica nanospheres passively has also been reported in pure DOPC vesicles, in which the nanospheres were unfunctionalised and 100 nm in diameter [114].

6.6 Conclusion

The electrophysiological and fluorescence results presented in this chapter reveal that silica nanospheres can cause holes to form in bilayer lipid membranes at particle concentrations well below those previously reported to have induced cytotoxicity. Increasing the nanoparticle concentration induces a higher degree of membrane degradation, as evidenced by the observed increase in bilayer current. This link between nanoparticle concentration and level of membrane disruption raises the possibility that other reports of plasma membrane disintegration following exposure to various nanoparticles [98] could be directly due to nanoparticle association rather than the previously suggested secondary effect connected to the interaction of ingested particles with intracellular molecules. The droplet-based bilayer system, along with other biophysical assays, is a crucial tool for the exploration of nanotoxic effects. It also has the potential to become a high-throughput prescreening technique for nanoparticles suspected of causing membrane disruption.

7 Conclusion

Electrowetting and liquid dielectrophoresis, achieved through several techniques, can enable droplet actuation in flexible, scalable and dynamically configurable structures and thus are potentially useful techniques for several applications in lab-on-a-chip as well as other areas such as displays and focal lenses. In this work, these two mechanisms have been used to develop a system for droplet handling including mixing, forming an artificial lipid bilayer membrane to analyse the effect of silica nanospheres on membrane.

Analysing the behaviour of a droplet in the presence of an AC electric field verified that at high frequencies, applying a non-uniform AC electric field induces a dielectrophoretic force which can be used to move and manipulate liquids and to create linear arrays of very small droplets. In contrast, at low frequencies, electrowetting takes place. It is observed that at high frequencies (about 250 kHz) the DEP force draws out a liquid finger from a parent droplet when an AC voltage is applied. At low frequencies, the electrowetting force balances the three line interfacial energies and a subsequent change of contact angle occurs.

7.1 Electrodynamics droplet actuation achievements

7.1.1 Mixing

A new design of an electrowetting based mixer was presented to demonstrate a method for rapidly bringing together two droplets and mixing them. The movement of the droplets in a controlled manner from the dispensing position to the centre of the device and the subsequent mixing by altering the applied potentials in the central interdigitated area was demonstrated. The results show that the rate of mixing by electrowetting can be greatly increased through active manipulation of the droplets. The effect of varying voltage and frequency on droplet mixing was examined. The highest efficiency mixing was achieved at 1 kHz and 110 V where the time taken to mix two 2 µl droplets was about 0.55 seconds.

7.1.2 Artificial bilayer lipid membrane formation

A new method for the formation of artificial bilayer lipid membranes by the controlled, electrical manipulation of aqueous droplets immersed in a lipid-alkane solution was demonstrated. In this technique, droplet movement was generated using dielectrophoresis on planar microelectrodes covered in a thin insulator. Droplets, surrounded by lipid monolayers, were brought into contact and spontaneously formed a lipid bilayer. The method produced BLMs suitable for single-channel recording of membrane protein activity and the technique can be extended to create programmable BLM arrays and networks. DEP control of droplets provides a flexible method for forming BLMs within a microsystem under simple electronic control at low electrical potentials (~10 V). The BLMs have long lifetimes and are suitable for the acquisition of electrophysiological data from membrane proteins. The approach is particularly well suited to the development of programmable biological assays, integrated with micro-chip fluidic operations, and could be used for large-scale, automated, microarray platforms for membrane protein analysis.

7.1.3 Nanotoxicity

Since nanoparticles are currently employed for a wide variety of products and applications, including drug delivery. There is concern that some of these nanoparticles may have harmful or even toxic effects. The droplet BLM system, along with other biophysical assays, is a crucial tool for the exploration of nanotoxic effects. To assess whether nanoparticle-membrane contact leads to perturbation of the membrane structure, the conductance of artificial membranes exposed to silica nanospheres was measured. It was demonstrated that the presence of silica nanoparticles with diameters between 50 and 500 nm can damage protein-free membranes at particle concentrations in the femtomolar range. It was also found that the measured increase in membrane permeability depends on nanosphere concentration, surface chemistry and size. Fluorescence microscopy showed that the nanospheres are enriched at the lipid-water interface and a large number of nanoparticles can translocate across a membrane, even

when the surface coverage is relatively low, indicating that nanoparticles can exhibit significant cytotoxic effects.

7.2 Future potential

1. In addition to the work described in chapter 4 for two droplet mixing, the device was designed for the mixing of **four** droplets. The mixing process was initially examined by placing four DI water droplets onto each of the outer electrode pairs. As mentioned before, the wedge-shaped electrodes were used to create a field gradient and accelerate the droplets towards the highest field intensity. By applying an AC electric field at 2 kHz and 150 V, while all the electrodes (outer and inner) were kept on, the four droplets could be moved to the centre of the device and mixed together (Figure 7-1 (a) to (c)).

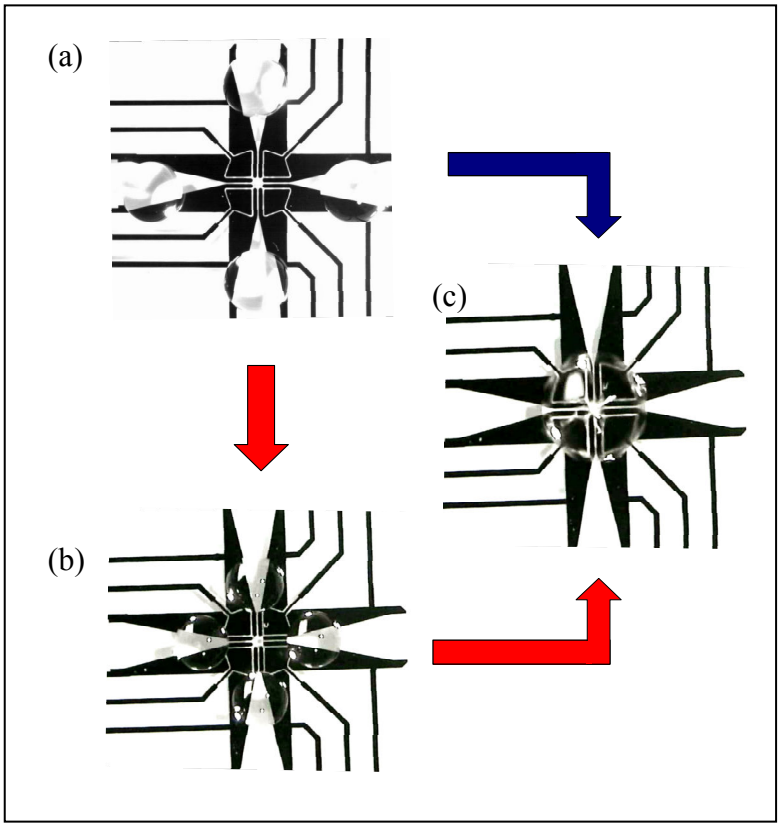

Figure 7-1 Two processes for the mixing of four aqueous droplets. Following the application of a potential of 150 V at 2 kHz to all the electrodes (outer and inner), four droplets moved to the centre of the device for mixing ((a) to (c)). In a more controlled manner, droplets can be moved and held at the end of wedge-shaped electrodes under the application of an electrical potential between the outer electrodes ((a) to (b)) and then by applying the voltage between the inner electrodes, droplets can be moved to the centre of the device and mixed ((b) to (c)).

2. It is also observed that this device is capable of controlling the movement of droplets in the electrical field. Hence, in a more controllable manner, if a low voltage is applied only to the outer electrodes, droplets can be moved toward the centre of the device and when they reach the end of the wedge-shaped electrodes (outer electrodes), the movement can be stopped by removing the voltage (Figure 7-1b). By then applying the voltage just to the inner electrodes, droplets can be forced to coalesce. This process is shown in Figure 7-1 ((a) to (b) then (b) to (c)). It is also possible to mix two droplets first, and then bring the third and forth droplet in to continue the mixing process. This feature is applicable for mixing of chemical solutions which are required to be mixed in two or three steps. This device is compatible with existing EWOD and could be easily integrated as a mixing component in a large device. Possible future work could include analysis of the efficiency of mixing with respect to different voltages and frequencies. Experiments using fluorescent dyes and involving critical analysis based on intensity, velocity, viscosity and volume of the droplet can be designed.

3. With the current Droplet BLM set-up it is difficult to capture side-view movies and photographs of droplets as they come into contact to form a bilayer. There is therefore potential to improve the set-up by incorporating a camera to enable the acquisition of movies in order to analyse capacitance traces. In these experiments, the droplet behaviour must be observed with respect to the stabilisation time and to the two-stage formation of bilayers (assuming the resolution will be sufficient). Also, taking photographs of the BLM area in the BLM plane with respect to the stabilisation time and to the two-stage formation will provide additional information, allowing speculation or explanation of the BLM formation mechanism.

4. Another area for future work is the development of a droplet dispensing experiment, which would involve the design of many different layouts of finger-railed devices. This would involve analysing the behaviour of the droplet subjected to non-uniform electric fields with different frequencies for an aqueous droplet in different mediums such as air, decane and lipid solutions.

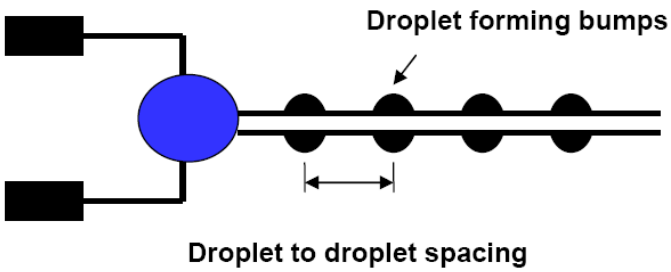

Figure 7-2 Coplanar electrode with periodic semicircular bumps designed for fixing the position of the droplets that form when the voltage is removed.

Figure 7-2 shows an example of a device which Ahmed et al used to control the droplet formation, size and space between the droplets. The periodic semicircular bumps are patterned on the co-planar electrodes.

7.3 Publications originating from this work

Sara Aghdaei, Mairi E. Sandison, Michele Zagnoni, Nicolas G. Green and Hywel Morgan, "Formation of artificial lipid bilayers using droplet dielectrophoresis", Lab on chip,vol.8, pp 1617-1620,2008.

Sara Aghdaei, Nicolas G Green, Thomas B Jones, Hywel Morgan, "Droplet mixer based on electrowetting", Electrostatic 2007, Journal of Physics: Conference Series voll.142, pp. 12071, 2008.

S. Aghdaei, T. Heslington, N. Rogers, H. Morgan and M.R.R. de Planque, "Assessment of nanoparticle cytotoxicity with on-chip suspended bilayers", Proceedings of the 14th International Conference on Miniaturized Systems for Chemistry and Life Sciences (MicroTAS 2010), pp. 298-300.

Maurits R. R. de Planque, Sara Aghdaei, Tiina Roose and Hywel Morgan, "Electrophysiological characterization of membrane disruption by nanoparticles" ACS nano, Submitted.

8 Appendix

8.1 LabView program for microfluid DEP and particle DEP

A program was developed in Labview environment for National Instrument's DAQ Card in order to control the relay board which was previously controlled by a switch box. Using the programme facilitates experimenting with chips with two different designs which are currently used in the lab. Each design requires 9 electrode pairs and can be used for microfluid DEP (electrowetting) and particle DEP. As shown in Figure 8-1, there are two switches in the front panel that allow for selecting the design and the DEP mode (Micro-fluid or particle).

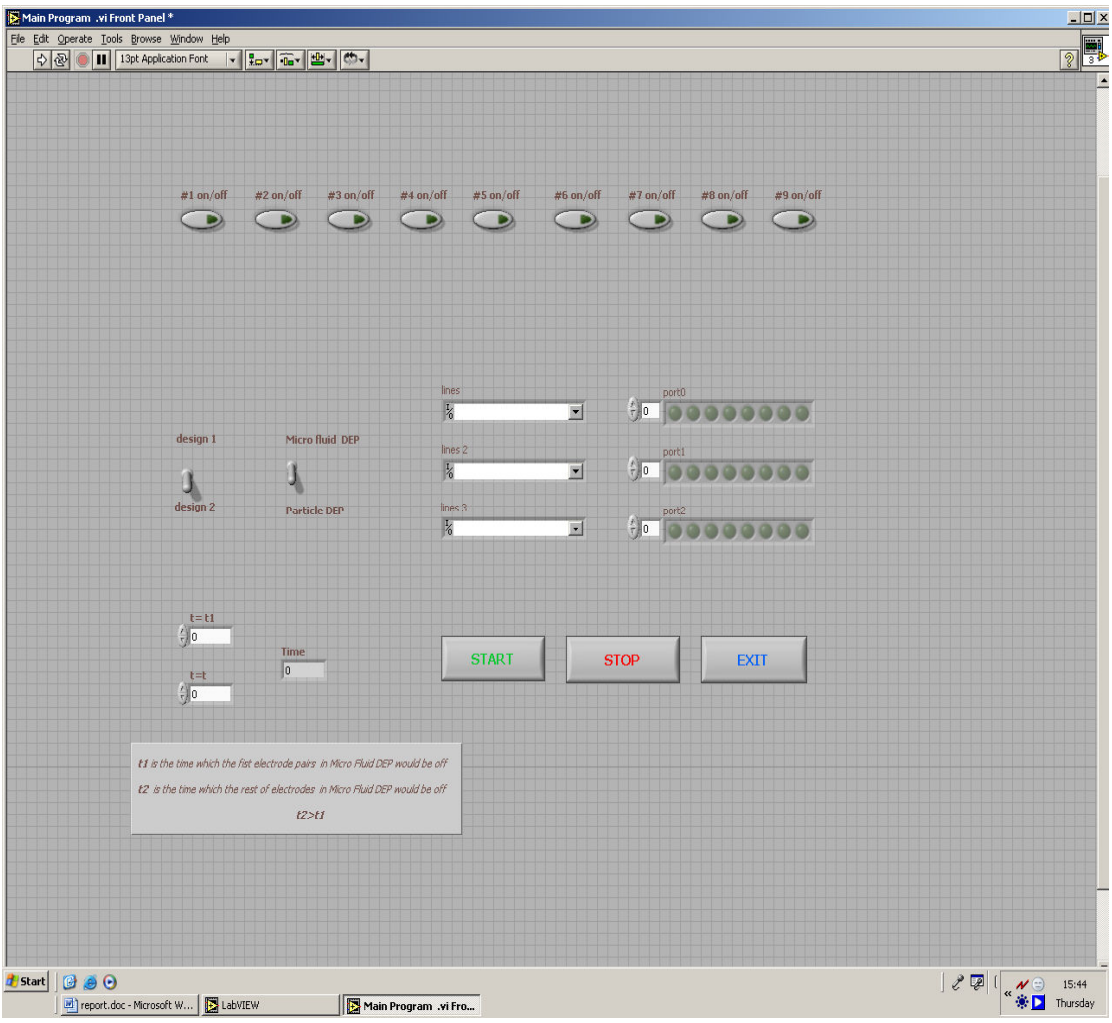

Figure 8-1 Front panel of LabView program to control the relay board for the chips with two different electrode designs to do microfluid DEP and particle DEP.

For both micro fluid DEP and particle DEP in each design, the polarity is preset and cannot be changed throughout the program execution. The “Time” box is simply to show the time in milliseconds from the start point. “Lines” boxes are for choosing the output port of the respective DAQ card. Since there may be more than one card installed on the PC, the device (card) and the corresponding port should be chosen. In the case of the card with three output ports, the line corresponding to the output in front of it should be selected. The port boxes simply show the bitwise status of each output port of the card. The Start and Stop buttons are obviously to start and stop the program at any time and the Exit button is for exiting the program.

When the switch is on Micro Fluid DEP, the user has to define the time t_1 and t_2 in milliseconds .In both designs when the program runs (at $t = 0$) the high voltage and low frequency are applied to all electrodes and the liquid actuation will start and finger will reach to the end, then at $t = t_1$ the voltage of the first electrode pair are turned off (electrode 1&1’ off) to trap the liquid. After $t = t_2 > t_1$ the other electrode pairs are turned off.In this case after $t_2 + t_1$ the program will stop automatically.

At this stage the small droplets are formed in each bump. If a particle DEP is desired, by changing the switch to particle DEP mode and running the program, the low voltage and high frequency are applied in some electrodes to be selected by the user. This can be done by clicking on the buttons #1 to #9 at the top of the screen. Pressing each button activates the corresponding electrode pair. The program execution may be stopped at any time by pressing the stop button.

8.2 LabView program for mixing chip

This program is developed for the chip that requires 2 electrode pairs and can be used for mixing by electrowetting. The program is manual and it works exactly like a manual switch box. As shown in Figure 8-2, the front panel depicts the schematic of a device with two pairs of electrodes. Therefore, there are two switches for turning the electrodes on and off and two switches for changing the polarity. The polarity can be changed throughout the program execution.

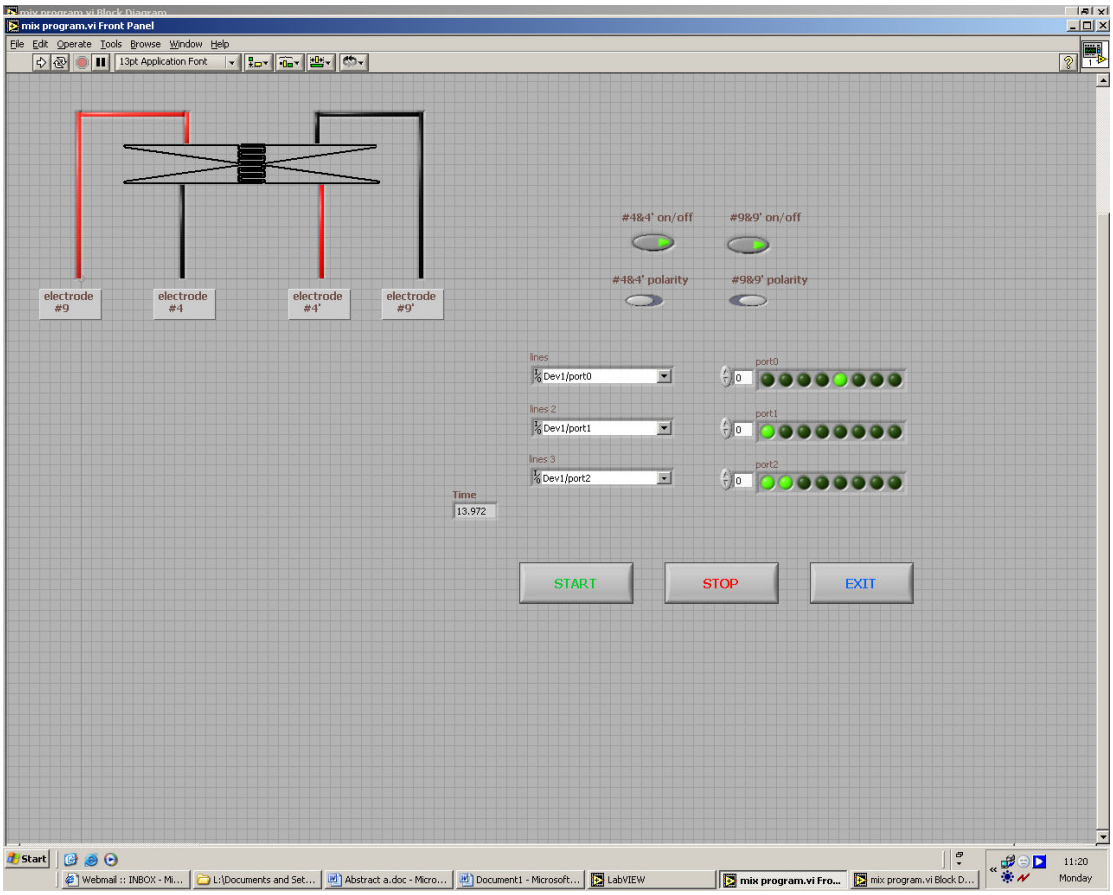

Figure 8-2 Manual Labview program front panel for mixing two droplets.

By turning the electrodes on, their polarity position is visible in the front panel. The red and the black electrodes show the positive and negative polarities respectively. The user can change the polarity by clicking on the Polarity buttons. So the device schematic shown in the front panel can be used to control and observe the polarity of electrodes through the experiment. The time box in the front panel is simply to show the time in milliseconds from the start point. Start and Stop buttons are obviously for starting and stoping the program. By pressing the Exit button user can completely exit from the Labview program.

One more program is developed for controlling the droplets throughout the mixing experiment. This program is different in that the polarity is preset and cannot be changed throughout the program execution (it is changed automatically). When the program runs (at $t = 0$) the high voltage and low frequency are applied to electrodes and droplets will start to move towards the interdigitate electrodes in the centre of the device. $t = t_1$ is the time which is taken for the two droplets to reach the interdigitate area. In addition at $t = t_1$ the polarity is reversed and droplets will enter the centre of the

chip and coalescence occurs. At this stage, the user should stop the program by pushing the stop button.

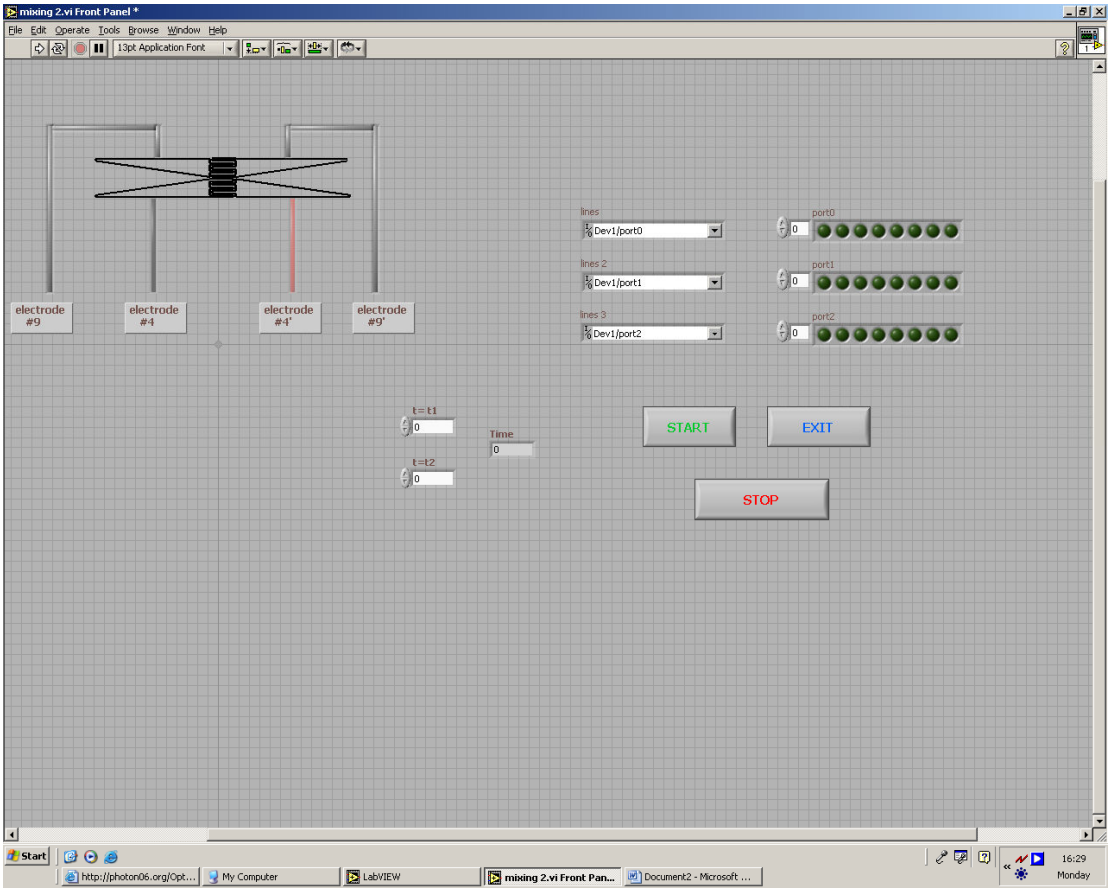

Figure 8-3 Non manual Labview program front panel for using mixing of two droplets.

Before starting the program the user should enter the time in milliseconds for t_1 and t_2.

9 References

[1] F. Mugele, J. C. Baret, and D. Steinhauser, "Microfluidic mixing through electrowetting-induced droplet oscillations," *Applied Physics Letters,* vol. 88, 2006.

[2] S. C. Jacobson, T. E. McKnight, and J. M. Ramsey, "Microfluidic devices for electrokinetically driven parallel and serial mixing," *Analytical Chemistry,* vol. 71, pp. 4455-4459, 1999.

[3] P. Paik, V. K. Pamula, M. G. Pollack, and R. B. Fair, "Electrowetting-based droplet mixers for microfluidic systems," *Lab on a Chip,* vol. 3, pp. 28-33, 2003.

[4] T. S. Sammarco and M. A. Burns, "Heat-transfer analysis of microfabricated thermocapillary pumping and reaction devices," *Journal of Micromechanics and Microengineering,* vol. 10, pp. 42-55, 2000.

[5] B. S. Gallardo, V. K. Gupta, F. D. Eagerton, L. I. Jong, V. S. Craig, R. R. Shah, and N. L. Abbott, "ELectrochemical principles for active control of liquids on submillimeter scales," *Science,* vol. 283, pp. 57-60, 1999.

[6] H.A.Pohl, "Dielectrophoresis," *Cambridge University Press,* 1978.

[7] M. Washizu, "Electrostatic actuation of liquid droplets for microreactor applications," *Ieee Transactions on Industry Applications,* vol. 34, pp. 732-737, 1998.

[8] F. F. Ruess, *Mem.Soc.Imperiale Naturalistes de Moscow,* vol. 2, p. 327, 1809.

[9] H. Morgan and N.G. Green, "AC Electrokinetics: colloids and nanoparticles," *Research Studies Press LTD,* 2003.

[10] Y. Huang and R. Pethig, "Electrode Design for Negative Dielectrophoresis," *Measurement Science & Technology,* vol. 2, pp. 1142-1146, 1991.

[11] L. G, "Relations entre les ph´enom`enes ´electriques et capillaires," *Ann. Chim. Phys,* vol. 5, p. 494, 1875.

[12] G. Beni and S. Hackwood, "Electrowetting Displays," *Bulletin of the American Physical Society,* vol. 26, pp. 445-446, 1981.

[13] B. Berge, "Electrocapillarity and Wetting of Insulator Films by Water," *Comptes Rendus De L Academie Des Sciences Serie Ii,* vol. 317, pp. 157-163,1993.

[14] http://en.wikipedia.org/wiki/Electrowetting.

[15] R. A. Hayes and B. J. Feenstra, "Video-speed electronic paper based on electrowetting," *Nature,* vol. 425, pp. 383-385, 2003.

[16] T. Roques-Carmes, R. A. Hayes, B. J. Feenstra, and L. J. M. Schlangen, "Liquid behavior inside a reflective display pixel based on electrowetting," *Journal of Applied Physics,* vol. 95, pp. 4389-4396, 2004.

[17] http://www.research.philips.com/newscenter/archive/2004/fluidlenses.html.

[18] P. Paik, V. K. Pamula, and R. B. Fair, "Rapid droplet mixers for digital microfluidic systems," *Lab on a Chip,* vol. 3, pp. 253-259, 2003.

[19] F. Mugele and J. C. Baret, "Electrowetting: From basics to applications," *Journal of Physics-Condensed Matter,* vol. 17, pp. R705-R774, 2005.

[20] J. Lienemann, A. Greiner, and J. G. Korvink, "Modeling, simulation, and optimization of electrowetting," *Ieee Transactions on Computer-Aided Design of Integrated Circuits and Systems,* vol. 25, pp. 234-247, 2006.

[21] http://en.wikipedia.org/wiki/Wetting.

[22] D. Langbein, "Capillary surfaces," *Capillary Surfaces,* vol. 178, pp. 1-20, 2002.

[23] P. G. Genne, F. Brochard-Wyart and D. Quere, "Capillarity and Wetting Phenomena," 2004.

[24] J. A. M. Sondaghuethorst and L. G. J. Fokkink, "Potential-Dependent Wetting of Electroactive Ferrocene-Terminated Alkanethiolate Monolayers on Gold," *Langmuir,* vol. 10, pp. 4380-4387, Nov 1994.

[25] W. J. J. Welters and L. G. J. Fokkink, "Fast electrically switchable capillary effects," *Langmuir,* vol. 14, pp. 1535-1538,1998.

[26] T. B. Jones, "On the relationship of dielectrophoresis and electrowetting," *Langmuir,* vol. 18, pp. 4437-4443, 2002.

[27] T. B. Jones, "An electromechanical interpretation of electrowetting," *Journal of Micromechanics and Microengineering,* vol. 15, pp. 1184-1187, 2005.

[28] K. H. Kang, "How electrostatic fields change contact angle in electrowetting," *Langmuir,* vol. 18, pp. 10318-10322, 2002.

[29] Pellat, "H. Mesure de la force agissant sur les die´lectriques liquides non e´lectrise´s place´s dans un champ e´litrique," *C. R. Acad. Sci. Paris* vol. 119, pp. 691-694, 1895

[30] T. B. Jones and J. R. Melcher, "Dynamics of Electromechanical Flow Structures," *Physics of Fluids,* vol. 16, pp. 393-400, 1973.

[31] T. B. Jones, "Hydrostatics and Steady Dynamics of Spatially Varying Electromechanical Flow Structures," *Journal of Applied Physics,* vol. 45, pp. 1487-1491, 1974.

[32] T. B. Jones, K. L. Wang, and D. J. Yao, "Frequency-dependent electromechanics of aqueous liquids: Electrowetting and dielectrophoresis," *Langmuir,* vol. 20, pp. 2813-2818, 2004.

[33] R. Becker, "*Electromagnetic fields and interactions,*" *Section 35,* NewYork 1982.

[34] T. B. Jones, J. D. Fowler, Y. S. Chang, and C. J. Kim, "Frequency-based relationship of electrowetting and dielectrophoretic liquid microactuation," *Langmuir,* vol. 19, pp. 7646-7651, 2003.

[35] T. B. Jones, M. Gunji, M. Washizu, and M. J. Feldman, "Dielectrophoretic liquid actuation and nanodroplet formation," *Journal of Applied Physics,* vol. 89, pp. 1441-1448, 2001.

[36] R. Ahmed and T. B. Jones, "Dispensing picoliter droplets on substrates using dielectrophoresis," *Journal of Electrostatics,* vol. 64, pp. 543-549, 2006.

[37] R. Ahmed, D. Hsu, C. Bailey, and T. B. Jones, "Dispensing picoliter droplets using dielectrophoretic (DEP) microactuation," *Microscale Thermophysical Engineering,* vol. 8, pp. 271-283, 2004.

[38] M. Gunji and M. Washizu, "Self-propulsion of a water droplet in an electric field," *Journal of Physics D-Applied Physics,* vol. 38, pp. 2417-2423,2005.

[39] A. F. Stalder, G. Kulik, D. Sage, L. Barbieri, and P. Hoffmann, "A snake-based approach to accurate determination of both contact points and contact angles," *Colloids and Surfaces a-Physicochemical and Engineering Aspects,* vol. 286, pp. 92-103, 2006.

[40] A. Quinn, R. Sedev, and J. Ralston, "Contact angle saturation in electrowetting," *Journal of Physical Chemistry B,* vol. 109, pp. 6268-6275, 2005.

[41] V. Peykov, A. Quinn, and J. Ralston, "Electrowetting: a model for contact-angle saturation," *Colloid and Polymer Science,* vol. 278, pp. 789-793, 2000.

[42] O. Raccurt, J. Berthier, P. Clementz, M. Borella, and M. Plissonnier, "On the influence of surfactants in electrowetting systems," *Journal of Micromechanics and Microengineering,* vol. 17, pp. 2217-2223, 2007.

[43] U. Domanska, M. K. Kozlowska, and M. Rogalski, "Solubilities, partition coefficients, density, and surface tension for imidazoles plus octan-1-ol or plus water or plus n-decane," *Journal of Chemical and Engineering Data,* vol. 47, pp. 456-466, 2002.

[44] J. Heikenfeld, "Flat electrowetting optics based on arrayed light valves and microprisms," *2007 Ieee Leos Annual Meeting Conference Proceedings,* Vol 1, pp. 206-207, 2007.

[45] J. H. Chang, D. Y. Choi, S. Han, and J. J. Pak, "Driving characteristics of the electrowetting-on-dielectric device using atomic-layer-deposited aluminum oxide as the dielectric," *Microfluidics and Nanofluidics,* vol. 8, pp. 269-273, 2010.

[46] B.Razavi, "Design of Analog CMOS Integrated Circuits," pp. 626, 2000.

[47] Alberts, *Molecular Biology of The Cell*, third edition ed.: Garland publishin, N.Y, 1994.

[48] http://www.micronit.com/en/about_microfluidics/labonachip.php.

[49] B. A. Lodish H, Zipursky LS, *Molecular Cell Biology,*, 4th ed., 2004.

[50] G. M. Berg, J. L. Tymoczko and,S. Lubert, *biochemistry*, 6th edition, 2006.

[51] http://kentsimmons.uwinnipeg.ca/cm1504/Image78.gif.

[52] http://virtualcuriosityshop.blogspot.com/2007/06/on-micelles-vesicles-and-artificial.html.

[53] Mueller P Rudin D. O Tien H. T. Wescott W. C, " Reconstitution of cell membrane structure in vitro and its transformation into an excitable system" *Nature* pp. 194,979, 1962.

[54] Mueller et al, " Reconstitution of excitable cell membrane structure in vitro," *Circulation,* vol. 26, pp. 1167-1177, 1962.

[55] D. P. Nikolelis and U. J. Krull, "Reliable and Facile Method for Preparation of Solventless Bilayer Lipid-Membranes for Electroanalytical Investigations," *Talanta,* vol. 39, pp. 1045-1049, 1992.

[56] M. E. Sandison, M. Zagnoni, and H. Morgan, "Air-exposure technique for the formation of artificial lipid bilayers in microsystems," *Langmuir,* vol. 23, pp. 8277-8284, 2007.

[57] Tien H. T. Dawidowicz E. A, "Black lipid films in aqueous media: Anew type of interfacial phenomenon Experimental techniques and thickness measurements," *Colloid Interface Sci,* vol. 22, pp. 438-453, 1966.

[58] Tien H. T Dawidowicz E. A, " Black lipid films in aqueous media: A new type of interfacial phenomenon. Experimental techniques and thickness measurements," *Colloid Interface Sci,* vol. 22, pp. 438-453, 1966.

[59] Montal M. Mueller P, "Formation of Bimolecular Membranes from Lipid Monolayers and a Study of Their Electrical Properties.," *Proc Natl Acad Sci U S A. ,* vol. 69(12), pp. 3561–3566, 1972.

[60] H. Schindler, "Formation of Planar Bilayers from Artificial or Native Membrane-Vesicles," *Febs Letters,* vol. 122, pp. 77-79, 1980.

[61] Y. X. Jiang, A. Lee, J. Y. Chen, M. Cadene, B. T. Chait, and R. MacKinnon, "Crystal structure and mechanism of a calcium-gated potassium channel," *Nature,* vol. 417, pp. 515-522, 2002.

[62] N. Malmstadt, M. A. Nash, R. F. Purnell, and J. J. Schmidt, "Automated formation of lipid-bilayer membranes in a microfluidic device," *Nano Letters,* vol. 6, pp. 1961-1965, 2006.

[63] T. D. Osborn and P. Yager, "Formation of Planar Solvent-Free Phospholipid-Bilayers by Langmuir-Blodgett Transfer of Monolayers to Micromachined Apertures in Silicon," *Langmuir,* vol. 11, pp. 8-12, 1995.

[64] Y. L. Cheng, R. J. Bushby, S. D. Evans, P. F. Knowles, R. E. Miles, and S. D. Ogier, "Single ion channel sensitivity in suspended bilayers on micromachined supports," *Langmuir,* vol. 17, pp. 1240-1242, 2001.

[65] N. Fertig, C. Meyer, R. H. Blick, C. Trautmann, and J. C. Behrends, "Microstructured glass chip for ion-channel electrophysiology," *Physical Review E,* vol. 6404, 2001.

[66] M. C. Peterman, J. M. Ziebarth, O. Braha, H. Bayley, H. A. Fishman, and D. M. Bloom, "Ion channels and lipid bilayer membranes under high potentials using microfabricated apertures," *Biomedical Microdevices,* vol. 4, pp. 231-236, 2002.

[67] M. E. Sandison, M. Zagnoni, M. Abu-Hantash, and H. Morgan, "Micromachined glass apertures for artificial lipid bilayer formation in a microfluidic system," *Journal of Micromechanics and Microengineering,* vol. 17, pp. S189-S196, 2007.

[68] C. Schmidt, M. Mayer, and H. Vogel, "A chip-based biosensor for the functional analysis of single ion channels," *Angewandte Chemie-International Edition,* vol. 39, pp. 3137-3140, 2000.

[69] H. T. Suzuki, K.; Kato-Yamada, Y.; Noji, H.; Takeuchi, S. . "Planar Lipid Bilayer Chip for Electrophysiological Analysis of Membrane Proteins," *In Proceedings of iTAS 2004, The 8th International Conference on Miniaturized Systems for Chemistry and Life Sciences,* vol. 2, pp. 246-248, 2004.

[70] M. E. Sandison and H. Morgan, "Rapid fabrication of polymer microfluidic systems for the production of artificial lipid bilayers," *Journal of Micromechanics and Microengineering,* vol. 15, pp. S139-S144, 2005.

[71] Le Pioufle B. Suzuki H. Tabata KV. Noji H. Takeuchi S, "Lipid bilayer microarray for parallel recording of transmembrane ion currents " *Anal Chem* vol. 80, pp. 328-332, 2008.

[72] M. Zagnoni, M. E. Sandison, P. Marius, A. G. Lee, and H. Morgan, "Controlled delivery of proteins into bilayer lipid membranes on chip," *Lab on a Chip,* vol. 7, pp. 1176-1183, 2007.

[73] K. Funakoshi, H. Suzuki, and S. Takeuchi, "Lipid bilayer formation by contacting monolayers in a microfluidic device for membrane protein analysis," *Analytical Chemistry,* vol. 78, pp. 8169-8174, 2006.

[74] M. A. Holden, D. Needham, and H. Bayley, "Functional bionetworks from nanoliter water droplets," *Journal of the American Chemical Society,* vol. 129, pp. 8650-8655, 2007.

[75] C. E. Stanley, K. S. Elvira, X. Z. Niu, A. D. Gee, O. Ces, J. B. Edel, and A. J. deMello, "A microfluidic approach for high-throughput droplet interface bilayer (DIB) formation," *Chemical Communications,* vol. 46, pp. 1620-1622, 2010.

[76] W. L. Hwang, M. A. Holden, S. White, and H. Bayley, "Electrical behavior of droplet interface bilayer networks: Experimental analysis and Modeling," *Journal of the American Chemical Society,* vol. 129, pp. 11854-11864, 2007.

[77] H.T. Tien. A. Ottova-Leitmannova, "*Planar Lipid Bilayers (BLMs) and their applications*" Membrane Sience and technology series 7, 2003.

[78] I. R. Booth, M. D. Edwards, and S. Miller, "Bacterial ion channels," *Biochemistry,* vol. 42, pp. 10045-10053, 2003.

[79] C. Kung and P. Blount, "Channels in microbes: so many holes to fill," *Molecular Microbiology,* vol. 53, pp. 373-380, 2004.

[80] K. Durick and P. Negulescu, "Cellular biosensors for drug discovery," *Biosensors & Bioelectronics,* vol. 16, pp. 587-592, 2001.

[81] M. Tanaka and E. Sackmann, "Polymer-supported membranes as models of the cell surface," *Nature,* vol. 437, pp. 656-663, 2005.

[82] M. E. Sandison, M. Zagnoni, R.J. Wood, P. L. Roach, H. Morgan, " On chip formation of lipid bilayers using an air-exposure technique", *μTAS, Proceedings of the 10th international Conference on Miniaturized system for Chemistry and Life Sciences* Tokyo, 2006.

[83] Y. L. Zhang, J. Dunlop, and J. E. Dalziel, "Recombinant human voltage-gated skeletal muscle sodium channels are pharmacologically functional in planar lipid bilayers," *Biosensors & Bioelectronics,* vol. 22, pp. 1006-1012, 2007.

[84] S. Terrettaz, M. Mayer, and H. Vogel, "Highly electrically insulating tethered lipid bilayers for probing the function of ion channel proteins," *Langmuir,* vol. 19, pp. 5567-5569, 2003.

[85] K. Atsuta, H. Noji, and S. Takeuchi, "Micro patterning of active proteins with perforated PDMS sheets (PDMS sheets)," *Lab on a Chip,* vol. 4, pp. 333-336, 2004.

[86] F. J. Sigworth and K.G. Klemic "patch clamp on a chip," *biophysical,* vol. 82, pp. 2831-2832, 2002.

[87] N. Fertig, R. H. Blick, and J. C. Behrends, "Whole cell patch clamp recording performed on a planar glass chip," *Biophysical Journal,* vol. 82, pp. 3056-3062, 2002.

[88] E. K. Schmitt, M. Vrouenraets, and C. Steinem, "Channel activity of OmpF monitored in nano-BLMs," *Biophysical Journal,* vol. 91, pp. 2163-2171, 2006.

[89] H. Suzuki, K. V. Tabata, H. Noji, and S. Takeuchi, "Electrophysiological recordings of single ion channels in planar lipid bilayers using a polymethyl methacrylate microfluidic chip," *Biosensors & Bioelectronics,* vol. 22, pp. 1111-1115, 2007.

[90] H. Suzuki, K. V. Tabata, H. Noji, and S. Takeuchi, "Highly reproducible method of planar lipid bilayer reconstitution in polymethyl methacrylate microfluidic chip," *Langmuir,* vol. 22, pp. 1937-1942, 2006.

[91] J. A. Maurer, V. E. White, D. A. Dougherty, and J. L. Nadeau, "Reconstitution of ion channels in agarose-supported silicon orifices," *Biosensors & Bioelectronics,* vol. 22, pp. 2577-2584, 2007.

[92] O. S. Andersen, R. E. Koeppe, and B. Roux, "Gramicidin channels," *Ieee Transactions on Nanobioscience,* vol. 4, pp. 10-20, 2005.

[93] L. Z. Song, M. R. Hobaugh, C. Shustak, S. Cheley, H. Bayley, and J. E. Gouaux, "Structure of staphylococcal alpha-hemolysin, a heptameric transmembrane pore," *Science,* vol. 274, pp. 1859-1866, 1996.

[94] T. D. Ingolia and D. E. Koshland, "Role of Calcium in Fusion of Artificial Vesicles," *Journal of Biological Chemistry,* vol. 253, pp. 3821-3829, 1978.

[95] D. J. Woodbury and C. Miller, "Nystatin-Induced Liposome Fusion - a Versatile Approach to Ion Channel Reconstitution into Planar Bilayers," *Biophysical Journal,* vol. 58, pp. 833-839,1990.

[96] M. R. R. de Planque, G. P. Mendes, M. Zagnoni, M. E. Sandison, K. H. Fisher, R. M. Berry, A. Watts, and H. Morgan, "Controlled delivery of membrane proteins to artificial lipid bilayers by nystatin-ergosterol modulated vesicle fusion," *Iee Proceedings-Nanobiotechnology,* vol. 153, pp. 21-30, 2006.

[97] M. R. R. de Planque, V. Raussens, S. Antoranz Contera, D. T. S. Rijkers, R. M. J. Liskamp, J. M. Ruysschaert, J. F. Ryan, F. Separovic and A. Watts, "β-Sheet Structured β-Amyloid Perturbs Phosphatidylcholine Model Membranes," *J. Mol. Biol,* vol. 368, pp.982–997, 2007

[98] D. J. Woodbury and K. Rognlien, "The t-SNARE syntaxin is sufficient for spontaneous fusion of synaptic vesicles to planar membranes," *Cell Biology International,* vol. 24, pp. 809-818, 2000.

[99] A. Nel, T. Xia, L. Madler, and N. Li, "Toxic potential of materials at the nanolevel," *Science,* vol. 311, pp. 622-627, 2006.

[100] N. Lewinski, V. Colvin, and R. Drezek, "Cytotoxicity of nanoparticles," *Small,* vol. 4, pp. 26-49, 2008.

[101] K. Unfried, C. Albrecht, L. O. Klotz, A. Von Mikecz, S. Grether-Beck, and R. P. F. Schins, "Cellular responses to nanoparticles: Target structures and mechanisms," *Nanotoxicology,* vol. 1, pp. 52-71, 2007.

[102] P. R. Leroueil, S. A. Berry, K. Duthie, G. Han, V. M. Rotello, D. Q. McNerny, J. R. Baker, B. G. Orr, and M. M. B. Holl, "Wide varieties of cationic nanoparticles induce defects in supported lipid bilayers," *Nano Letters,* vol. 8, pp. 420-424, 2008.

[103] H. Meng, Z. Chen, G. M. Xing, H. Yuan, C. Y. Chen, F. Zhao, C. C. Zhang, Y. Wang, and Y. L. Zhao, "Ultrahigh reactivity and grave nanotoxicity of copper nanoparticles," *Journal of Radioanalytical and Nuclear Chemistry,* vol. 272, pp. 595-598, 2007.

[104] Y. Roiter, M. Ornatska, A. R. Rammohan, J. Balakrishnan, D. R. Heine, and S. Minko, "Interaction of nanoparticles with lipid membrane," *Nano Letters,* vol. 8, pp. 941-944, 2008.

[105] G.Bothun, "Hydrophobic silver nanoparticles trapped in lipid bilayers: Size distribution, bilayer phase behavior, and optical properties," *Journal of Nanobiotechnology,* vol. 6:13, 2008.

[106] P. R. Leroueil, S. Y. Hong, A. Mecke, J. R. Baker, B. G. Orr, and M. M. B. Holl, "Nanoparticle interaction with biological membranes: Does nanotechnology present a janus face?," *Accounts of Chemical Research,* vol. 40, pp. 335-342, 2007.

[107] J. H. s.Hong, MM. Banaszak Holl, P.Leroueil, A. Mecke, BG. Orr, "Physical interactions of nanoparticles with biological Membranes: The observation of nanoscale hole formation," *Journal of chemical health & safty,* vol. 13, pp. 16-20, 2006.

[108] C. J. Arnusch, H. Branderhorst, B. De Kruijff, R. M. J. Liskamp, E. Breukink, and R. J. Pieters, "Enhanced membrane pore formation by Multimeric/Oligomeric antimicrobial peptides," *Biochemistry,* vol. 46, pp. 13437-13442, 2007.

[109] Z. M. Tao, B. B. Toms, J. Goodisman, and T. Asefa, "Mesoporosity and Functional Group Dependent Endocytosis and Cytotoxicity of Silica Nanomaterials," *Chemical Research in Toxicology,* vol. 22, pp. 1869-1880, 2009.

[110] S. Ramachandran, G. L. Kumar, R. H. Blick, and D. W. van der Weide, "Current bursts in lipid bilayers initiated by colloidal quantum dots," *Applied Physics Letters,* vol. 86, 2005.

[111] S. A. Klein, S. J. Wilk, T. J. Thornton, and J. D. Posner, "Formation of nanopores in suspended lipid bilayers using quantum dots - art. no. 012022," *International Symposium on Advanced Nanodevices and Nanotechnology,* vol. 109, pp. 12022-12022 110, 2008.

[112] M. R. R. de Planque, V. Raussens, S. A. Contera, D. T. S. Rijkers, R. M. J. Liskamp, J. M. Ruysschaert, J. F. Ryan, F. Separovic, and A. Watts, "beta-sheet structured beta-amyloid(1-40) perturbs phosphatidylcholine model membranes," *Journal of Molecular Biology,* vol. 368, pp. 982-997, 2007.

[113] Y. S. Lin and C. L. Haynes, "Impacts of Mesoporous Silica Nanoparticle Size, Pore Ordering, and Pore Integrity on Hemolytic Activity," *Journal of the American Chemical Society,* vol. 132, pp. 4834-4842, 2010.

[114] O. Le Bihan, P. Bonnafous, L. Marak, T. Bickel, S. Trepout, S. Mornet, F. De Haas, H. Talbot, J. C. Taveau, and O. Lambert, "Cryo-electron tomography of nanoparticle transmigration into liposome," *Journal of Structural Biology,* vol. 168, pp. 419-425, 2009.